THE ROLE OF THE AXON INITIAL SEGMENT AND TAU MODIFICATIONS IN AXOSOMATIC TAU DISTRIBUTION

By

Andrew Kneynsberg

A DISSERTATION

Submitted to
Michigan State University
in partial fulfillment of the requirements
for the degree of

Neuroscience – Doctor of Philosophy

2018

ABSTRACT

THE ROLE OF THE AXON INITIAL SEGMENT AND TAU MODIFICATIONS IN AXOSOMATIC TAU DISTRIBUTION

By

Andrew Kneynsberg

Tau is enriched in the axonal compartment in healthy neurons but is mislocalized to the somatodendritic compartment in disease. This process is thought to play an important role in tauopathy pathogenesis. The localization of tau in axons involves the axon initial segment (AIS), which is a specialized region of the proximal axon that acts as a retrograde diffusion barrier for tau. Here, we examined the timing of AIS development alongside the differential distribution of tau in axons of hippocampal neurons in culture. We also examined AIS morphology and levels of axonal and somatic tau in aging process of Fisher 344 rats. Using tau domains, pseudophosphorylation, and a familial tau mutation combined with a photoconvertible fluorescent construct, we analyzed the diffusion behavior of tau in living hippocampal neurons. We discovered that the microtubule binding region is necessary and sufficient to prevent diffusion from the axon to the soma, and that disease-related changes in tau such as phosphorylation and familial mutation of tau show enhanced axosomatic tau diffusion. Analysis of aged rat brains showed that the AIS-associated protein, Ankyrin G, remains largely unchanged during aging, and the axosomatic distribution of tau does not change in hippocampal neuron populations.

To further elucidate the mechanisms by which the AIS inhibits retrograde tau mislocalization we used shRNAs to knockdown the expression of AIS proteins: Ankyrin G (AnkG) and tripartite motif containing protein 46 (TRIM46). We show that TRIM46 plays a critical role in maintenance of the diffusion barrier in cultured hippocampal neurons.

Knockdown of TRIM46 is sufficient to allow somatic diffusion of axonal tau into the somata of neurons and reduce the relative axonal enrichment of tau. Knockdown of AnkG does not change tau localization or axosomatic distribution. Immunoprecipitation and mass spectrometry was used to characterize this connection between tau and TRIM46, but we conclude that tau and TRIM46 do not interact directly. Instead, we identified TRIM46 interactions with several microtubule-associated and actin-associated proteins supporting an integral role in maintenance of the AIS cytoarchitecture. We propose that the regulation of microtubule orientation and organization in the AIS by TRIM46 prevents somatic diffusion of tau, and tau modifications that disrupt its interactions with microtubules contribute to axosomatic mislocalization.

ACKNOWLEDGEMENTS

I thank Dr. Nicholas Kanaan for his guidance, inspiration, generosity, and unyielding standards. He encouraged me to follow my curiosities and allowed me to pursue scientific discovery without constraint or sacrifice. He is truly a mentor in science and in life and I am proud to have had the opportunity to learn from his example.

For their contributions to my education and scientific work, I also thank the members of my dissertation committee: Dr. Jack Lipton, Dr. Timothy Collier, and Dr. Scott Counts. I thank Dr. Cheryl Sisk and her laboratory for being exceptional colleagues and supportive friends.

Finally, I thank all members of the Kanaan laboratory for their hard work, support and friendship. Tessa has always made my life easier and for that I am grateful. Ben has challenged me to be a better scholar and I believe I am better for it.

PREFACE

At the time of writing this dissertation, one chapter is in preparation for publication and one chapter is published. Chapter 2, or a similar presentation of the data, will be submitted for publication. Chapter 3 was published by Kneynsberg and Kanaan in *eNeuro* (PMCID: PMC5520750). In addition, some portions of a review published by Kneynsberg and colleagues in Frontiers in Neuroscience are used for the introduction on tauopathies (PMCID: PMC5651019).

TABLE OF CONTENTS

LIST OF TABLES	ix
LIST OF FIGURES	X
KEY TO ABREVIATIONS	xi
CHAPTER 1	
Overall Introduction	1
INTRODUCTION	1
ALZHEIMER'S DISEASE	
NON-ALZHEIMER'S DISEASE TAUOPATHIES	5
Pick's disease	6
Progressive supranuclear palsy	7
Corticobasal degeneration	
Chronic traumatic encephalopathy	
Frontotemporal dementia with Parkinsonism linked to chromosome 17	
BIOLOGY OF TAU LOCALIZATION IN DISEASE	10
THE AXON INITIAL SEGMENT AS A RETROGRADE DIFFUSION BARRIER.	14
TAU MISLOCALIZATION OR AIS DYSFUNCTION IN NORMAL AGING	16
DISSERTATION OBJECTIVE	
TRIM46 Knockdown and Pathological Tau Modifications Increase the Axosomatic Diffusion Tau in Hippocampal Neurons	21
INTRODUCTION	21
METHODS	24
Antibodies and reagents	24
cDNA and shRNA constructs	25
Animals	26
Primary neurons	
Immunocytofluorescence	
Confocal imaging	
Axonal intensity measurements	29
Live-cell tracking	30
Retrograde diffusion	31
Dual-luciferase reporter assay	31
Proximity ligation assay	32
NanoBRET donor saturation assay	33
Tissue processing	
TRIM46 immunoprecipitation	
Mass spectrometry	
Immunoblotting	
Statistical analyses	40

RESULIS	41
Axonal tau enrichment occurs coincident with TRIM46 localization to during development	
Retrograde axonal diffusion of tau is inhibited in the proximal axon Disease-related tau modifications mislocalize to the somatodendritic	43
	15
compartment	
TRIM46 is required for axonal tau enrichment	
Tau is not a direct binding partner with TRIM46	
DISCUSSION	
Axonal protein distribution	48
The microtubule binding domain of tau exhibits impaired axosomatic diffusion	
Disease-related tau modifications disrupt tau diffusion barrier	50
TRIM46 maintains axosomatic tau diffusion barrier in neurons	51
TRIM46 interactions and mass spectrometry	52
Conclusions	
CHAPTER 3	
Aging Does Not Affect Axon Initial Segment Structure and Somatic Localization of T	'au Protein
in Hippocampal Neurons of Fischer 344 Rats	
INTRODUCTION	
METHODS	75
Animals	75
Tissue processing	
Immunoblotting	
Immunohistochemistry and immunofluorescence	
Stereology	
Cellular protein quantification	
Statistical analyses	
RESULTS	
Immunoblotting of AIS proteins and tau	
Stereological assessment of AIS length and morphology	
Optical density measurements of tau levels in the somata and axonal la	
hippocampus	
DISCUSSION	
ACKNOWLEDGEMENTS	
CHAPTER 4	
Overall Discussion	95
DISCUSSION	
Causes of tau mislocalization.	
Components of the axon initial segment modify tau enrichment	
Axosomatic tau and AnkG do not change in aged neurons	
Proposed mechanism of tau localization	
Future directions	

REFERENCES		
DEFEDENCES	 1-	٠
NEFERENCES	 J.	,

LIST OF TABLES

Table 2.1	An interaction between tau and TRIM46 was not detected with multiple methods of co-immunoprecipitations using HEK293 cells, primary hippocampal culture, and hippocampal brain lysates.	71
Table 2.2	TRIM46 immunoprecipitation mass spectrometry	72

LIST OF FIGURES

Figure 2.1	Axonal tau enrichment is coincident with TRIM46 localization to the axon initial segment in developing cultured hippocampal neurons.	55
Figure 2.2	Normalized axonal intensity profiles from DIV 2-9 show axonal tau distribution corresponds to development of TRIM46 in the AIS.	57
Figure 2.3	Intensity profiles from DIV 2-9 normalized to DIV9 levels show decrease in total tau expression and increase of TRIM46, AnkG, and MAP2.	59
Figure 2.4	Retrograde diffusion of tau is dependent on the microtubule binding region and increases with disease-related modifications.	61
Figure 2.5	shRNA knock-down of TRIM46, and not Ankyrin-G, reduced axonal tau enrichment and increase axosomatic tau diffusion.	63
Figure 2.6	Tau and TRIM46 do not exhibit a direct protein-protein interaction.	65
Figure 2.7	Positive identification of axonal processes and validation of retrograde diffusion potential.	67
Figure 2.8	TRIM46 mediates axonal tau enrichment and inhibits axosomatic diffusion.	69
Figure 3.1	Aging does not alter levels of axon initial segment proteins, total tau, and phosphorylated tau proteins.	90
Figure 3.2	Structural analysis of the AIS with Ankyrin G (AnkG) reveals regional changes in the hippocampus during aging.	92
Figure 3.3	Optical density measurement of tau immunofluorescence in the somata and axons of hippocampal neurons shows no changes across age.	94

KEY TO ABBREVIATIONS

AD Alzheimer's disease

APP amyloid precursor protein

AnkG ankyrin G

AIS axon initial segment

Aβ β-amyloid

CTE chronic traumatic encephalopathy

CBD corticobasal degeneration

DTI diffusion tensor imaging

FTD frontotemporal dementia

GFAP glial fibrillary acidic protein

GAPDH glyceraldehyde 3- phosphate dehydrogenase

HP hippocampus

MT microtubule

MAP microtubule associated protein

MCI mild cognitive impairment

MRI magnetic resonance imaging

NFT neurofibrillary tangle

NFDM-TBS nonfat dry milk in Tris-buffered saline

PC photoconverted

PiD Pick's disease

PET positron emission tomographic

PSP progressive supranuclear palsy

PLA proximity ligation assay

TRIM46 tripartite motif containing protein 46

TBS Tris-buffered saline

UC unconverted

CHAPTER 1

Overall Introduction

INTRODUCTION

The microtubule-associated protein tau is an important factor in the pathogenesis of several neurodegenerative diseases called tauopathies, the most prevalent of which is Alzheimer's disease (AD). Pathological accumulations of amyloid-β (Aβ) and tau are definitive markers for the diagnosis of AD. The spatiotemporal aggregation of tau within the brain correlates well with neuronal loss and symptomatic onset, making understanding tau protein functions critical to comprehending the disease (Braak & Braak, 1991; 1995). Yet, there are many unanswered questions regarding the full functions of tau, the regulatory mechanisms of tau, and the effects of tau modification on its involvement in disease pathologies. This dissertation focuses on the axonal localization of tau within neurons, specifically, what factors of neuronal cytoarchitecture maintain normal tau distribution and how modification of tau alters that localization. Here, the mechanisms that regulate axonal tau localization and prevent retrograde diffusion from the axon back into the somatodendritic compartment (here referred to as axosomatic diffusion) are examined with respect to the effects of aging, manipulation of the axon initial segment (AIS), and disease associated modifications of tau in rat brains.

ALZHEIMER'S DISEASE

Greco-Roman philosophers described mental decline with age over 2500 years ago and considered cognitive deterioration an inevitable event associated with the disease of aging (Halpert, 1983). Originally only describing the aged person, the word "senile" began to shift to

mean "demented" as the philosophers continued to described loss of mental ability with age.

Anatomist and physician Thomas Willis gave the first characterization of the causes of dementia in 1684, which included: age, head injury, and congenital factors, among others (Wilks, 1864).

Not until Bielschowsky's modification of Golgi's silver stain was it possible to visualize pathological structures in neurons, he called neurofibrils (Berchtold & Cotman, 1998). It was this staining method that Alois Alzheimer used to describe the pathology of Auguste Deter, a 51 year old patient who died after developing dementia in 1906 (Goedert & Ghetti, 2007). Only after 11 cases of disease were described with the same pathological hallmarks in the next 5 years did Emil Kraepelin's nomenclature of Alzheimer's disease become final (Torack, 1978).

Today, Alzheimer's disease is the 6th leading cause of death in the United States, affecting 5.7 million people (Alzheimer's, 2016). The number of Americans suffering from AD will grow to almost 14 million by the year 2050 (Hebert *et al.*, 2010). This will lead to 1 in 3 seniors dying with AD or another dementia, yet there is no cure or treatment that slows disease progression or symptom severity. Thus, it is imperative to scientifically investigate the pathophysiology of the disease in order to discover mechanistic causes and develop therapeutics that can help minimize or even avoid this major health crisis.

The early phases of AD are believed to be displayed in the clinical symptoms associated with mild cognitive impairment (MCI), which include memory complaints and slight impairment in cognition, but the ability to maintain daily functions remains relatively intact (Petersen *et al.*, 2001). MCI is viewed as a prodromal state for AD as one converts from normal aging to AD. As AD worsens, severe decline in memory and impairment of executive function, attention, language, mood and personality are observed (Perrin *et al.*, 2009). Cognitive decline continues in patients, who lose the ability to perform daily tasks and ultimately die of intercurrent illness

(Savonenko *et al.*, 2012). Several neuropsychological tests are used to assess dementia syndromes and define clinical phenotypes, such as the Mini-Mental State Examination, the Montreal Cognitive Assessment, and the Addenbrooke's cognitive examination. AD patients present with deficits in episodic memory, visuospatial ability and concentration, while language and social cognition remain largely intact (Burrell & Piguet, 2015). In some cases, these tests can predict underlying AD pathology with greater than 85% accuracy, yet AD can only be diagnosed post-mortem with the presence of neuropathological hallmarks.

The defining pathological hallmarks of AD are neuritic plaques and neurofibrillary tangles (NFT). A β was identified as the major component of the extracellular plaques found in AD brains (Masters *et al.*, 1985). A β is formed from the cleavage of the amyloid precursor protein (APP) by β - and γ -secretase, resulting in A β 40 and A β 42. A β 42 is more prone to aggregation and is associated with neurotoxicity (Greenfield *et al.*, 1999; Gouras *et al.*, 2000). The A β aggregates assemble into β -sheets and can be stained with Congo Red or thioflavin dyes (Selkoe, 2002). Multiple aggregated forms of A β (multimer/oligomer, protofilaments, fibrils, and plaques) compose the spectrum of amyloid pathology species.

Neurofibrillary tangles are intracellular inclusions composed of aggregated tau proteins in the form or paired helical or straight filaments (Goedert *et al.*, 2006). Alternative splicing leads to formation of 6 isoforms of the tau protein in the human brain, 3 isoforms with 3 microtubule binding repeats (3R) and 3 isoforms with 4 binding repeats (4R) (Binder *et al.*, 1985; Goedert *et al.*, 1991). Both 3R and 4R tau isoforms comprise tau aggregates in AD (Buee & Delacourte, 1999). The tau protein in tangles and filaments is heavily phosphorylated, up to 4 times higher than endogenous tau, creating a conditions that may facilitate aggregation *in situ* (Grundke-Iqbal *et al.*, 1986a; Grundke-Iqbal *et al.*, 1986b). Again, a range of tau pathologies is observed that

includes abnormally modified monomers, multimers/oligomers and filamentous aggregates. Among these, our attention is shifting towards the pathologically modified monomers and/or small soluble oligomeric forms as the likely toxic tau species. Tau pathologies are found throughout the affected neurons, including the cell bodies (where tangles reside), as well as dendrites and axons (referred to as neuropil threads) (Braak & Braak, 1991).

Despite extracellular plaques being studied as the main pathological hallmark for much of last 30 years, the density of Aβ does not correlate closely to progression of AD (Braak & Braak, 1991; Arriagada *et al.*, 1992). Spatiotemporal development of tau pathology, however, associates very well with the cognitive decline of AD (Morris *et al.*, 1991; Wischik *et al.*, 1992). Characterization of this progression led to the development of Braak staging (Braak & Braak, 1991; 1995). Divided into stages I-VI, Braak staging of neurofibrillary changes describes the initial pathology in the transentorhinal region of the temporal lobe (I-II), progression into the hippocampus (III-IV), and spread to the neocortex where neuronal death is prevalent (V-VI) (Braak & Braak, 1995).

The mechanisms that lead to AD are hotly debated between amyloid, tau or something else altogether being the causative factor is disease pathogenesis (Herrup, 2015; Musiek & Holtzman, 2015). 95% of AD is considered sporadic, but the 5% of familial AD is associated with mutations in APP or APP cleaving enzymes (i.e. presenilin-1 and 2), all of which can affect the amount of A β production (Goate *et al.*, 1991; Rogaev *et al.*, 1995; Wang *et al.*, 2018). This provided the original evidence to support a causative role of A β and led to the amyloid cascade hypothesis. This hypothesis posits that A β pathology the main driving force behind disease pathogenesis and responsible for the formation of tau pathology and subsequent toxicity (Hardy & Higgins, 1992). It was proposed that A β may induce tau dysfunction in some way that would

lead to development of NFTs, and that tau involvement in disease was coincidental (Lewis *et al.*, 2001). The discovery of inherited mutations in the tau gene that cause early-onset frontotemporal dementia (FTD) complicated this hypothesis and established a direct causative role for tau in neurodegenerative toxicity that was independent of Aβ (Hutton *et al.*, 1998). Studies suggesting that the toxic effects of Aβ could be dependent on the presence of tau provided more evidence for a role of tau in neurotoxicity (Rapoport *et al.*, 2002; Roberson *et al.*, 2007; Ittner *et al.*, 2010). The role of Aβ in disease remains unclear, but Aβ may directly or indirectly induce neurodegenerative effects such as synaptic defects through interactions with receptors or axonal transport dysfunction through kinase dysregulation (Shankar *et al.*, 2007; Pigino *et al.*, 2009). Ultimately, the toxic effects of abnormal forms of tau are thought to lead to dysfunction and degeneration of synapses and axons that in turn lead to the loss of memory and cognitive deficits that characterizes AD (Kowall & Kosik, 1987; DeKosky & Scheff, 1990; Kanaan *et al.*, 2013; Di *et al.*, 2016).

NON-ALZHEIMER'S DISEASE TAUOPATHIES

Tau inclusions are present in over 25 neuronal diseases, several of which are termed tauopathies and are characterized by their tau pathology (Spillantini & Goedert, 2013). Specifically, Pick's disease (PiD), progressive supranuclear palsy (PSP), corticobasal degeneration (CBD), chronic traumatic encephalopathy (CTE), and frontotemporal dementia with Parkinsonism linked to chromosome 17 (FTDP-17) are described in brief detail here to emphasize the scope of human tauopathies and the complexity of tau pathogenesis in neurodegenerative disease. Tauopathies are differentiated by differences in the cell types affected, anatomical brains regions involved, and the tau isoforms present in pathologies

(Kovacs, 2015). For a more extensive comparisons of these tauopathies and potential mechanisms of tau toxicity, see (Kneynsberg *et al.*, 2017).

Pick's disease

Pick's disease is characterized by severe atrophy of the frontal, temporal, and parietal lobes and distinct argyrophilic neuronal tau inclusions called Pick bodies. The disease was described in 1891 by Arnold Pick, a colleague of Dr. Alzheimer, while working at the Prague neuropathological school. Clinical symptoms of Pick's disease include behavioral changes and difficulties with language, allowing diagnostic distinction between AD (Kovacs, 2017). Pick bodies represent the major neuropathological hallmark of PiD, and are typically found in the frontal and temporal cortices and dentate gyrus of the hippocampus (Pollock et al., 1986; Probst et al., 1996). Histological analysis of post-mortem brain tissue reveals pathological forms of tau in axons and dendrites surrounding neuronal Pick bodies as well as in glial cells in affected brain regions (Cochran et al., 1994; Probst et al., 1996). These tau aggregations are largely composed of the 3R tau isoform. Neuritic threads and spheroids are observed in mossy fibers projecting to the dentate nucleus along with abnormal tau in cerebellar white matter and other axons in PiD brains (Probst et al., 1996; Braak et al., 1999). Magnetic resonance imaging (MRI) studies of Pick's disease cases document severe atrophy of cortical white matter (Wang et al., 2006; Yamakawa et al., 2006). Loss of myelinated axons is observed in subcortical white matter as well as a loss of synapses at the termination of the perforant pathway (Dickson, 1998; Lippa, 2004).

Progressive supranuclear palsy

PSP is characterized by abundant tau lesions termed coiled bodies within oligodendrocytes, the cells responsible for generating myelin sheaths in the central nervous system. Demyelination is particularly evident in white matter tracts of PSP-affected brains, directly correlating with tau burden in the superior cerebellar peduncle and red nucleus, suggesting that tau-induced oligodendrocyte dysfunction could contribute to the axonal degeneration phenotype observed in PSP (Ishizawa et al., 2000). Symptoms of PSP are first described as loss of balance and further develop into postural instability and frequent falls (Dickson et al., 2010). Clinical presentation also includes difficulty controlling eye movements (e.g. the hallmark vertical gaze palsy) and the muscles required for speech and swallowing, in addition to development of symptoms of dementia. Diffusion tensor imaging (DTI) studies in early PSP cases found evidence of white matter degeneration within the pons, substantia nigra, cerebellar peduncles and corpus callosum and the degree of atrophy in some of these regions correlates to disease severity and onset of symptoms (Padovani et al., 2006; Knake et al., 2010; Whitwell et al., 2011; Zhang et al., 2016). In addition to glial cell pathology (tufted astrocytes and coiled bodies), tau aggregates are also observed in neurons (NFTs and globose tangles) and contain primarily the 4R isoform (Pollock et al., 1986; Hauw et al., 1994). The presence of neuropil threads in PSP indicates the presence pathological tau in axons, particularly in the basal ganglia, internal capsule, and thalamic fasciculus (Hauw et al., 1990; Dickson, 1999).

Corticobasal degeneration

CBD is a devastating progressive disease that presents clinically with symptoms of progressive rigidity, apraxia, aphasia, and behavioral changes (Rebeiz *et al.*, 1968; Litvan *et al.*,

1997). The characteristic tau pathology of CBD includes astrocytic plaques, occasional coiled bodies, and neuronal globose inclusions that are found in the grey and white matter of the frontal and parietal lobes of the cerebral cortex, basal ganglia, and the cerebellum (Feany & Dickson, 1995; Dickson, 1999). The extensive astroglial lesions in CBD and other tauopathies suggest that pathological forms of tau may affect astrocyte-specific functions critical to neuronal health, including sustained trophic support (Kahlson & Colodner, 2015). Additional studies identified pathological changes in specific hand sensorimotor fiber tracts in patients who manifested limb apraxia at early CBD stages, furthering the linkage between axonal degeneration and specific symptomatic outcomes(Borroni *et al.*, 2008). The predominant 4R tau pathology and similar clinical presentation suggest that the distinct disorders of PSP and CBD could represent a spectrum of the same tauopathy affecting neurons and glia (Kouri *et al.*, 2011).

Chronic traumatic encephalopathy

CTE is a neurodegenerative disease associated with repetitive subconcussive and mild traumatic brain injuries (Corsellis *et al.*, 1973; Blennow *et al.*, 2016). Clinical presentation of CTE is classified into 4 stages, with the first stage defined by deterioration of attention and concentration, with depression, explosivity, and short-term memory loss occurring in stage II (McKee *et al.*, 2013). Stage III is characterized by executive dysfunction and cognitive impairment, while the final clinical stage IV includes overt dementia and aggression. 4R tau inclusions in both neurons and astrocytes found in the frontal and temporal cortices, as well as the hippocampus represent the pathological hallmarks of CTE (McKee *et al.*, 2012; Gelpi *et al.*, 2016). Mounting evidence suggests that damage and degeneration of axons contributes to the development and progression of CTE. Neuropil threads are a prominent neuropathological

feature of CTE and cognitive decline correlates with axonal atrophy in subcortical white matter (Tokuda *et al.*, 1991; Kraus *et al.*, 2007; McKee *et al.*, 2009). Pathological forms of tau, identified by conformation-dependent tau antibodies, were recently found to localize within axons of cortical white matter and the cholinergic basal forebrain (Kanaan *et al.*, 2016; Mufson *et al.*, 2016). Diffuse axonal injuries, including axonal swellings, unregulated calcium influx, and cytoskeletal abnormalities are evident within the first 24 hours after concussion and may persist for weeks (Blumbergs *et al.*, 1994; Maxwell *et al.*, 1995; Giza & Hovda, 2001). Additionally, a multitude of DTI studies have identified white matter changes in athletes at risk for concussions or repetitive subconcussive impacts and veterans exposed to blast trauma (Zhang *et al.*, 2003; Koerte *et al.*, 2012a; Koerte *et al.*, 2012b; McAllister *et al.*, 2014; Petrie *et al.*, 2014).

Frontotemporal dementia with Parkinsonism linked to chromosome 17

FTDP-17 represents a subgroup of inherited early-onset tauopathies resulting from mutations in the gene encoding tau. FTDP-17 mutations are autosomal dominant and there is over 60 identified missense mutations in the tau protein, as well as several silent or deletion mutations. The mutations can effect tau in two ways, either by altering the protein sequence, or altering the mRNA to cause splicing variations, many of which favor the production of the 4R isoform over the 3R isoform (Goedert *et al.*, 2012). Exon mutations altering the protein sequence largely occur in the microtubule binding region within exon 10 (e.g. aa N296, aa P301, and aa S305) although multiple mutations do exist outside of this region. The discovery of FTDP-17 tau mutations is a landmark finding because it demonstrated that tau dysfunction alone is sufficient to cause neurodegeneration and axonal pathology (Foster *et al.*, 1997; Hutton *et al.*, 1998). Clinically, FTDP-17 exhibits a heterogeneous symptomatic presentation with shared phenotypic

outcomes of other tauopathies, including CBD, Pick's disease, and PSP (Forrest *et al.*, 2018). Patients with symptoms of FTD can be diagnosed with FTDP-17 following genetic screening for mutation of the tau gene and confirmation of tau pathology post-mortem. Similar to neuropil threads in AD, mutant tau filaments localize within dystrophic axons of FTDP-17 brains, and aggregates are found in neurons and glial (Delisle *et al.*, 1999; Murrell *et al.*, 1999; Lippa *et al.*, 2000; Kouri *et al.*, 2014).

One of the first mutations to be discovered and most prevalent in the initial report is the leucine substitution at aa 301 (P301L), located within the second microtubule binding repeat (Hutton *et al.*, 1998). P301L tau alters the conformation of the protein facilitating increased β-sheets formation, the structure necessary for the formation of tau filaments (von Bergen *et al.*, 2001; von Bergen *et al.*, 2005). Indeed, the P301L mutant tau protein shows an increase filament formation over wild-type tau, suggesting that the aggregation-prone nature of P301L contributes to its toxicity in the brain (Arrasate *et al.*, 1999). In addition to increased aggregation, P301L exhibits impaired microtubule binding (Barghorn *et al.*, 2000; Sun & Gamblin, 2009). Not surprisingly, this mutant tau protein is used extensively in animal models and they display overt synapse loss, axonal degeneration and neurodegeneration, as well as motor and/or cognitive decline (reviewed in (Combs *et al.*, 2016)). Many of the other mutant forms of tau display similar properties related to aggregation *in vitro*, impaired MT binding and inducing neurodegeneration *in vivo*, but they are less well-studied or have yet to be studied.

BIOLOGY OF TAU LOCALIZATION IN DISEASE

Purification of MTs revealed a unique protein factor found to be essential for MT assembly *in vitro* (Weingarten *et al.*, 1975). This protein was named 'tau factor', designating the

Greek letter τ to signifying its interaction with tubulin. Tau was found to be sufficient to promote both nucleation and elongation of tubulin into MTs in vitro (Cleveland et al., 1977b). Purification of tau from porcine brains revealed 4 isoforms of tau, with a high capacity for incorporating phosphate (Cleveland et al., 1977a). Similarly, rodents express 4 isoforms of tau, which exhibit differential expression over the course of development, while humans express 6 isoforms of tau in the brain (Goedert et al., 1989; Bullmann et al., 2009). In addition to the 6 isoforms found in the human CNS, a 7th, larger isoform containing exon 4a is present in the PNS (also known as "big tau") (Boyne et al., 1995). Exons 2, 3, and 10 of the tau DNA can be alternatively spliced to form proteins with 0,1, or 2 N-terminal inserts and 3 or 4 microtubule binding repeats (Goedert et al., 1991). The unique structural domains of tau contribute to its multiple roles in cellular physiology (Mandelkow et al., 1995). Tau's N-terminal domain acts as a microtubule (MT) bundling and spacing regulator, can function as a signaling component for phosphatase activity, can differentially mediate protein-protein interactions in primates, and interacts with the plasma membrane (Kanai et al., 1992; Brandt et al., 1995; Kanaan et al., 2011; Chung et al., 2016; Stefanoska et al., 2018). The microtubule binding region (MTBR) is composed of three or four MT binding motifs, regulating its interaction with MTs and facilitating aggregation in disease, while the C-terminal domain facilitates folding and tertiary structure of the tau protein through interaction with the N-terminal domain (Gustke et al., 1994; von Bergen et al., 2001; Jeganathan et al., 2006).

Identification of tau as a core component of AD pathology, the neurofibrillary tangle, led to intense interest in tau biology and function (Goedert *et al.*, 1988). Though tau was recognized as a phospho-protein early after its initial characterization, the important disease-related implications of tau phosphorylation did not become apparent until it was discovered that

abnormally phosphorylated tau accumulates in neurofibrillary tangles of AD (Cleveland *et al.*, 1977a; Grundke-Iqbal *et al.*, 1986b; Wood *et al.*, 1986). The biological role of tau in neuronal physiology is now being studied to understand the mechanisms of toxicity that contribute to disease (Hoover *et al.*, 2010; Arendt *et al.*, 2016; Kneynsberg *et al.*, 2017).

A number of studies have evaluated the intraneuronal distribution of tau, but the first description of tau localization was as an axonal protein (Binder et al., 1985). Dephosphorylation of tau revealed a very different staining pattern in healthy neurons with the Tau-1 antibody (Papasozomenos & Binder, 1987). Subsequent characterization of tau revealed a presence throughout all compartments of the neuron, including the soma, dendrites and an enrichment in axons (Binder et al., 1986; Mandell & Banker, 1995). Through these studies we learned that the phosphorylation state of tau plays an important role in axonal tau enrichment, as axonal tau exhibits less phosphorylation than tau in the somatodendritic compartment (Papasozomenos & Binder, 1987; Mandell & Banker, 1996b). Further work with Tau1 in healthy human brains tissue with and without phosphatase treatment elucidated an axonal tau staining before phosphatase and a somatic tau distribution after phosphatase treatment, establishing a baseline of tau immunohistochemistry in the human brain for comparison to changes associated with disease pathology (Trojanowski et al., 1989). However, the mechanisms which regulate the localization of phosphorylated tau remained unknown. Axonal enrichment of tau could be shown in cultured neurons, demonstrating that tau was selectively localized with the development of cell polarity, but this did not reveal what could lead to redistribution of tau enrichment in disease (Mandell & Banker, 1996a).

Current thinking in the field hypothesizes that the redistribution of tau from the axonal compartment to the somatodendritic compartment is an important event in tau-mediated toxicity

of disease. Further, pre-tangle, diffuse granular tau accumulations in the somatodendritic compartment were shown to precede the formation of classical neurofibrillary tangles in human disease pathology (Bancher *et al.*, 1989). These accumulations were discovered to be phosphorylated tau and it was suggested that phosphorylation of tau causes its mislocalization (Kopke *et al.*, 1993; Iqbal *et al.*, 2005). Specific domains of MAPs dictate their localization within the neuron (e.g. N-terminal projection of MAP2 prevents localization into the axon), suggesting modifications of tau could do the same and cause its mislocalization (Kanai & Hirokawa, 1995). Tau proteins can be modified in multiple ways (e.g. phosphorylation, truncation, etc.) in tauopathies and many studies evaluated how these modifications affect tau protein behavior (i.e. MT binding and aggregation). Phosphorylation of tau at many epitopes impairs MT association and altering tau's conformation to expose the MTBR increases aggregation of tau into filaments, but there is little direct evidence suggesting what influences axosomatic distribution (Barghorn & Mandelkow, 2002; Jeganathan *et al.*, 2008).

Several key phosphoepitope antibodies recognize tau pathologies and characterize its enrichment within neurons. Further, the somatic localization of phosphorylated tau can be used to stage disease pathology (Braak & Braak, 1995; Kimura *et al.*, 1996). Prevalent modifications of somatic localized tau in disease modify the conformation of tau, specifically PHF1 (S396 and S404), AT8 (S199, S202, and T205), and AT100 (T212 and S214) (Jeganathan *et al.*, 2008). Despite our understanding of post-translational tau modifications and the presence of them in disease, little is known about how these disease-related modifications affect the ability of the neuron to maintain axonal tau enrichment and inhibit axosomatic tau diffusion (Biernat *et al.*, 1992; Sun & Gamblin, 2009). Elucidating the mechanism of tau localization could shed new light on the investigation of pathological tau distributions. A central question that remained

unanswered in the field was what dictates development and maintenance of the natural and pathological differential distribution of tau in neurons.

THE AXON INITIAL SEGMENT AS A RETROGRADE DIFFUSION BARRIER

Several cellular components and processes may play a role in neuronal tau distribution differences; however, recent studies have clearly implicated a region of the proximal axon known as the axon initial segment (AIS). The AIS is defined as the proximal region of the axon containing tightly bundled MTs and a thickened membrane rich with ion channels and membrane bound cytoskeletal proteins (Palay *et al.*, 1968; Peters *et al.*, 1968). Most of what is known about the AIS is regarding developing and maintaining axon polarity and regulating the mechanisms necessary for establishing neuronal excitability. The functional mechanisms underlying the AIS's role as a protein barrier is more elusive by comparison, with most work focusing on size exclusion or lipid membrane protein localization (Winckler *et al.*, 1999; Sun *et al.*, 2014).

Several structural components are key to defining and functionally maintaining the AIS in neurons. This includes the actin cytoskeleton, MTs, cell adhesion molecules, and scaffolding proteins linking these complexes together. One particularly important AIS-specific scaffolding protein is Ankyrin G (AnkG). AnkG plays an essential role in tethering together the ion channels, cell adhesion and extracellular matrix molecules, and cytoskeletal scaffolding proteins of the AIS (Bennett & Lorenzo, 2013). Specifically, AnkG binds neurofascin within its membrane-bound domain, spectrin tetramers within the submembrane domain, and has a long proline rich tail with a C-terminal domain associated with end-binding proteins (Davis *et al.*, 1996; Leterrier *et al.*, 2011; Jenkins *et al.*, 2015) Actin rings form along the AIS, bound to αII-and βIV-spectrin tetramers, creating a periodic submembrane complex (Leterrier *et al.*, 2015).

For further perspective on the AIS and its function outside the scope of this dissertation see the recent comprehensive reviews (Zhang & Rasband, 2016; Nelson & Jenkins, 2017; Leterrier, 2018).

AnkG is required for the formation the AIS, development of axonal polarity, and the localization of other AIS components, while its reduction via genetic knockdown leads to disruption of the AIS and redistribution of numerous AIS tethered proteins (Hedstrom *et al.*, 2008; Sobotzik *et al.*, 2009; Rasband, 2010). The discovery of tripartite motif containing protein 46 (TRIM46) highlighted a new MT-binding protein, and more recently TRIM46 was shown to play an important role within the AIS (Short & Cox, 2006; van Beuningen *et al.*, 2015). TRIM46 localizes to the AIS where it functions to orient the direction of MT elongation, contribute to axonal formation, bundle MT into evenly spaced arrays, and modulate normal axonal transport (van Beuningen *et al.*, 2015). The role of these central structural components of the AIS in maintaining the retrograde diffusion barrier for axonal tau remains poorly defined.

We know that the transition from lower somatic tau levels to an increased level of tau in the axon spatially corresponds to the AIS. Using a photoconvertible fluorophore (dendra2) to track the live diffusion of tau within neurons, Li and colleagues showed that axosomatic diffusion of tau is inhibited at the AIS (Li *et al.*, 2011). This group also showed that MT binding of tau is an important component of localization and that inhibition of axosomatic tau diffusion requires intact/polymerized MTs. Extension of this work reduced protein components of the AIS with shRNA and observed an increase of axosomatic tau diffusion (Zempel *et al.*, 2017). Due to the duration of the shRNA treatment (i.e. viral vector over lipofection) it remains unclear whether these effects were due to deficits in a specific mechanism that localizes axonal tau or a lack of maintaining axonal identity in the treated neurons. Nonetheless, these initial studies have

led to the current thinking in the field that preferential localization of tau in axons is mediated, at least in part, by the AIS, which acts as a retrograde diffusion barrier just beyond the axon hillock. What remains unknown, is through what mechanistic pathway the AIS selectively enriches tau in the axon, while reducing retrograde axosomatic diffusion. Insights into this important biological process would increase the understanding of tau biology in normal and disease conditions.

Several variables may play a role in tau mislocalization during the disease process, including changes to the structure and/or function of the AIS. Very little is known about the changes in the AIS that occur during AD or other tauopathies. Transgenic mouse models of AD or treatment of primary neurons with Aβ show reduced AnkG intensity in the AIS, but a mechanistic change in neuronal excitability or protein trafficking and localization is not described (Sun *et al.*, 2014; Marin *et al.*, 2016). In the P301L transgenic mouse model of FTDP-17 (rTg4510), neuron excitability was reduced in hippocampal neurons corresponding to a relocation of the AIS along the axon seen with AnkG staining (Hatch *et al.*, 2017). Additionally, the interaction between tau and the AIS is more complicated because tau can disrupt the AIS cytoskeleton and subsequently AIS integrity (Sohn *et al.*, 2016). Thus, much work remains to better understand the potential pathological variables involved in the AIS function and tau mislocalization in disease.

TAU MISLOCALIZATION OR AIS DYSFUNCTION IN NORMAL AGING

Aging is the number one risk factor for developing AD, ahead of family history and apolipoprotein E genotype. The percentage of people with AD grows from 3% at 65-74 to 32% of people over 85 (Hebert *et al.*, 2013; Alzheimer's, 2016). The changes of aging that lead to this increased risk of disease are unknown, but the pathological process of disease is thought to

develop for decades before symptomatic onset. If that pathology is defined by the accumulation of pathological forms of tau protein in the somatodendritic compartment, it is logical to posit that aging might contribute to the mislocalization of tau from the axon to the somatodendritic compartment. This positions aging-related AIS dysfunction as a likely player contributing to the progression of tau pathology deposition in disease. However, very little is known about the effects of normal age on AIS structure and function.

Our current understanding of AIS changes during aging and disease is limited to a small selection of related proteins in varying models. Comparison of AIS structural proteins between 3 and 25 month old mice using immunoblotting indicated a reduction in total ankyrin protein, but did not specify AIS specific isoforms (i.e. 270 & 480 kDa isoforms) (Bahr et al., 1994). There is evidence that the AIS maintains plasticity from development into adulthood, seen with shortening of the AnkG positive AIS in the hippocampus of marmosets (Atapour & Rosa, 2017). AIS impairments are noted in a few studies of amyloid-β models of AD, including disruption of neuronal polarity and impaired selective filtering into the axon (Sun et al., 2014; Tsushima et al., 2015). The electrophysiological role of AIS appears to play a role in many other disease, such as epilepsy, schizophrenia, bipolar disorder, autism, and neuronal injury, but whether it is a cause or consequence is yet to be uncovered (Buffington & Rasband, 2011). Last, anti-TRIM46 antibodies were discovered in a paraneoplastic neurological syndrome, showing disruption of TRIM46 could lead to neuronal dysfunction and disease (van Coevorden-Hameete et al., 2017). Based on the links between aging, risk for AD (and other tauopathies), the AIS and tau mislocalization there is a need to better understand the potential role aging may play in AIS malfunction and/or tau mislocalization in neuronal populations vulnerable to degenerative changes in AD and other tauopathies.

DISSERTATION OBJECTIVE

This dissertation aims to increase the knowledge of the factors that mediate tau localization within the neuron and inhibit its axosomatic diffusion, as well as increase the understanding of potentially pathogenic processes involving tau mislocalization in AD and other tauopathies. I investigated the neuronal distribution of tau and the mechanism by which the AIS maintains axonal tau enrichment. The current research in the field of tau localization is somewhat sparse. With little known of the relationship between the AIS and tau localization, new findings could change the current dogma in the field and implicate novel factors involved in tauopathy pathogenesis. Existing research suggests the AIS is responsible for regulation of tau localization to the axonal compartment, but investigation into the mechanistic aspects of this barrier have yet to be done (Li *et al.*, 2011; Zempel *et al.*, 2017).

My research analyzed the mislocalization of tau with quantitative measure of axosomatic diffusion, comparison of AIS protein contributions to axonal enrichment, and investigation into the direct AIS interactions with tau. Applying this quantitative method to wild-type tau established a baseline for comparison, so that domains and disease related tau modifications could be investigated for further understanding of what mechanisms may be responsible for an effective retrograde barrier. I combined techniques of protein detection and visualization to explore tau mislocalization in live cells with manipulations of the AIS components. I also examined the distribution of tau and the AIS through development in neuronal culture and in rats over the course of aging. The results of these experiments further the understanding of the biological factors that contribute to proper localization of tau in healthy neurons. Knowledge of the basic neuronal biology of tau localization could significantly contribute to understanding what biological processes malfunction in the events of disease and cause mislocalization of tau.

If the mechanism leading to disease-related tau mislocalization is elucidated, it could provide a new target for the development of a therapy or treatment for neurodegenerative tauopathies.

This dissertation investigated the localization of tau in three specific aims.

Specific Aim 1: What AIS components normally mediate tau localization in the axon? Specific Aim 1 is addressed in Chapter 2 with an evaluation of the development of axonal tau enrichment in cultured neurons. The development of the AIS was tracked together with tau during its development. The domains of the tau protein were tested individually in live neurons to identify the necessary component for maintaining axonal tau enrichment. Interactions between tau and AIS proteins were investigated with protein-protein interaction assay and mass spectrometry. I hypothesize that the barrier function of the AIS is mediated through selective protein-protein interactions between AIS components and tau.

Specific Aim 2: Does normal aging in the rat hippocampus change AIS structure, AIS protein composition, or the localization of the tau protein?

Specific Aim 2 is addressed with analysis of aging Fisher 344 rats in Chapter 3. The axonal and somatic localization of tau were measured and compared between 4-, 14-, and 24-month-old rats. The AIS was visualized with AnkG at each timepoint and the structure of the AIS was evaluated stereologically for length, diameter, and volume. Total tau, phosphorylated tau, and a range of AIS proteins was evaluated on immunoblot to compare total protein expression in the hippocampus. I hypothesized that the integrity of the AIS as a retrograde diffusion barrier is impaired in aging neurons and this allows tau to accumulate in the somatodendritic compartment.

Specific Aim 3: Do pathological modifications of tau facilitate abnormal axosomatic diffusion of tau in neurons?

Specific Aim 3 is addressed in Chapter 2. Using the same methods as testing the live-cell localization of wild-type tau, I tested tau-AT8, tau-ps262, tau-4KXGE, and tau-P301L for differential axo-somatic diffusion. Quantitative comparison showed if disease-related phosphorylations or mutation that causes familial tauopathy alter the localization of tau in neurons. I hypothesized that pathological forms of tau will show an increase in axosomatic diffusion.

CHAPTER 2

TRIM46 Knockdown and Pathological Tau Modifications Increase the Axosomatic Diffusion of
Tau in Hippocampal Neurons

INTRODUCTION

The microtubule-associated protein tau was first characterized as an axonal protein where it was found to be enriched in the axons of mature cells and to interact with MTs (Weingarten *et al.*, 1975; Binder *et al.*, 1985). Further investigation into the localization of tau within neurons revealed compartmental separation of modified tau with phosphorylated protein localizing to the somatodendritic compartment while unphosphorylated tau was localized to the axon (Papasozomenos & Binder, 1987). Study within cultured neurons similarly described two populations of tau (phosphorylated and unphosphorylated at the Tau-1 antibody epitope, aa S192 - S199), but described an enrichment of tau in the axonal compartment (Dotti *et al.*, 1987; Mandell & Banker, 1995; 1996b). The domains of microtubule associated proteins (MAP) contribute to their compartmental sorting, and interaction of tau with MTs could regulate this mechanism of sorting, suggesting that modification of protein domains or phosphorylation status could dictate axosomatic localization (Kanai & Hirokawa, 1995; Mandelkow *et al.*, 1995).

The pathological hallmark of AD, neurofibrillary tangles, are composed of heavily phosphorylated Tau, and highly phosphorylated tau accumulates in the somatodendritic compartment of neurons (Grundke-Iqbal *et al.*, 1986b; Wood *et al.*, 1986). Identification of tau as a core component of AD pathology led to intense interest in how tau formed pathological structures and what contributed to increased somatic tau in disease (Goedert *et al.*, 1988). Pretangle accumulations of tau contain abnormally phosphorylated tau (detected with monoclonal

antibodies Tau-1 and AT8 as well as polyclonal antibody 92e⁹) proteins in neurons before the development of classical tangle pathology in AD (Bancher *et al.*, 1989; Braak *et al.*, 1994). This led to the hypothesis that phosphorylation contributed to tau accumulation in the neuron, and that the buildup of somatodendritic tau led to reduced concentration of tau in the axon (Kopke *et al.*, 1993). However, the mechanisms regulating tau localization in healthy neurons and with specific disease-related forms of tau remain poorly defined. The division between the somatodendritic and axonal domains of tau concentration was identified as the proximal region of the axon, named the axon initial segment (AIS) (Li *et al.*, 2011). Li *et al* showed that maintenance of a retrograde diffusion barrier requires an intact MT cytoskeleton and that the phosphorylation state of tau influences retrograde diffusion. Further work demonstrates that architecture of the AIS is specifically important to inhibiting retrograde tau diffusion, as knockdown of AnkG led to enhanced axosomatic diffusion of tau (Zempel *et al.*, 2017). To understand the mechanisms of sorting tau and enriching the axonal compartment, the interactions between the AIS and tau must be identified.

The AIS contains tightly bundled MTs, a thickened membrane rich with ion channels, membrane bound cytoskeletal proteins, and lacks ribosomes (Palay *et al.*, 1968; Peters *et al.*, 1968). A key structural component of the AIS is Ankyrin-G (AnkG), a large anchoring protein with isoforms of 270 kDa or 480 kDa (Kordeli *et al.*, 1995). The subdomains of AnkG include membrane binding, spectrin-binding, and an End-binding protein interaction domain in the C-terminus (Leterrier *et al.*, 2011; Bennett & Lorenzo, 2013). Together, AnkG and βIV-spectrin form a periodic structure of actin rings, organizing the AIS domain (D'Este *et al.*, 2015; Leterrier *et al.*, 2015). The recent discovery and description of the tripartite motif containing protein (TRIM46) identified a new protein in the AIS, required for maintaining neuronal polarity (van

Beuningen *et al.*, 2015). TRIM46 is a required component for AIS establishment but is not needed for maintenance of other AIS proteins. Along with TRIM46, AnkG localizes to the AIS via targeting domains required for independent AIS localization during development. AnkG associates with the actin-spectrin scaffold and aids in the recruitment and localization of additional AIS proteins (Hedstrom *et al.*, 2008; Zhong *et al.*, 2014; Jenkins *et al.*, 2015). This complex structure of organized proteins allows many dynamic functions for the AIS within the axon including clustering of ion channels to regulate excitability and action potentials, acting as a membrane diffusion barrier, a cytosolic diffusion barrier for large proteins, and a regulator or intracellular trafficking (Nakada *et al.*, 2003; Song *et al.*, 2009; Grubb & Burrone, 2010; Leterrier & Dargent, 2014). Contrary to the somata, dendrites, and distal axon, the MTs within the AIS are uniquely spaced and bundled in parallel arrays and TRIM46 maintains this MT organization (Conde & Caceres, 2009; Hoogenraad & Bradke, 2009; van Beuningen *et al.*, 2015).

Here, we describe the development of endogenous tau enrichment in the axon concurrently with the establishment of the AIS using cultured primary hippocampal neurons. We found that axosomatic enrichment appears in neurons at the same time as TRIM46 localizes to the AIS, but before AnkG. We identified that the microtubule binding region (MTBR) of tau is required for preventing retrograde diffusion at the AIS, and disease-related modifications of tau lead to more axosomatic diffusion than wild-type tau. We further identified that the AIS protein TRIM46, and not AnkG, is required for maintenance of the axosomatic tau diffusion barrier. By quantifying endogenous protein localization, diffusion in live-cell analysis, shRNA knockdown, and protein interaction assays, we propose that TRIM46 maintains axonal tau localization and

prevents mislocalization through its organization of the AIS cytoskeleton without a direct interaction with tau.

METHODS

Antibodies and reagents

The following antibodies were used in this study: mouse anti-Ankyrin G (1:2000; 106/36, NeuroMab), mouse anti-MAP2 (1:10000; AP14, Kanaan Lab), rabbit anti-TRIM46 (1:1000; 377003, Synaptic Systems), rabbit anti-tau (1:5000; R1, Kanaan Lab) mouse anti-tau (1:10000, Tau7, Kanaan Lab) mouse anti-tau (1:5000; Tau66, Kanaan Lab), mouse anti-neurofascin (1:2000, A12/18 NeuroMab), goat anti-rabbit (Alexa 405, A-31556; Alexa 488, A-11008; Alexa 568, A-11011; Alexa 647, 27040; Life Technologies), goat anti-mouse IgG1 (Alexa 488, A-21121; Alexa 568, A-21124; Alexa 647, A-21240; Life Technologies), goat anti-mouse IgG2a (Alexa 488, A-21131; Alexa 568, A-21144; Alexa 647, A-21241; Life Technologies), goat antimouse IgG2b (Alexa 647, A-21242; Life Technologies), goat anti-mouse IgM (Alexa 568, A-21043; Life Technologies) and rabbit IgG whole molecule, unconjugated (011-000-003, Jackson). Concentrations listed were used for immunocytofluorescence. The Dual-Luciferase Reporter assay system was used to validate shRNA constructs (E1910, Promega). For proximity ligation assay the following Duolink reagents were used: probe anti-mouse PLUS (DUO92001, Sigma Aldrich), probe anti-rabbit MINUS (DUO92005, Sigma Aldrich), FarRed detection reagents (DUO92013, Sigma Aldrich), and fluorescence wash buffers (DUO82049, Sigma Aldrich). For protein interactions, the Nano-BRET Nano-Glo detection system was used (N1662, Promega).

cDNA and shRNA constructs

Mammalian expression plasmids were made using full-length human tau cDNA and the human cytomegalovirus (CMV) promoter. The pDendra2-C vector from Evrogen was used as the source of the dendra2 protein (Addgene, #54694). We attached dendra2 to the C-terminal end of each construct with an amino acid linker of seven Gly to increase structural flexibility and reduce interactions between tau and dendra2. Fusing fluorescent proteins (e.g. green fluorescent protein) to the C-terminus of tau does not negatively affect microtubule binding (both in vitro and in cultured cells) or *in vitro* aggregation assays (i.e. using arachidonic acid induction) (N. Kanaan personal communication). The following tau domain constructs were made with dendra2 fused to the C-terminus: N-terminal aa 1-224, MTBR aa 225-380, and C-terminal aa 381-441. Pseudo-phosphorylated tau at serine 262 (Tau-pS262) was made by substitution Ser-Glu. Tau-4KXGE was made with Ser-Glu in each of the KXGS motifs S262, S305, S324, and S356. AT8 was made with two Ser-Glu substitutions at S199 and S202 and Thr-Glu switch at T205. Tau-P301L was constructed by mutating the Pro to a Leu. Two pSiCheck (C8021, Promega) plasmids were made for shRNA validation. For TRIM46, the plasmid contained the entire human TRIM46 sequence as the target of the shRNA. For AnkG, the plasmid contained only the serine-rich domain (shRNA target domain) due to the size of full-length AnkG protein. shRNA plasmids were constructed with the H1 promoter and the shRNA sequences were as follows for pan rat AnkG: 5'-GCCGTCAGTACCATCTTCT-3', rat TRIM46: 5'-GTTGCTGACAGAGCTTAAC-3', Renilla shRNA 5'-GGCCTTTCACTACTCCTAC-3', and scrambled shRNA: 5'-GTATAATACACCGCGCTAC-3' (Hedstrom et al., 2007; van Beuningen et al., 2015). TRIM46-shRNA and AnkG-shRNA plasmids were also made with a GFP reporter under the CMV promoter. For NanoBRET two plasmids were made with nano-luciferase and halo-tag.

TRIM46 was inserted into a plasmid expressing TRIM46 with a C-terminal halo-tag (pH6HTN, Promega, G8031), while tau was expressed as a fusion with a C-terminal nano-luciferase (pNFL1C, Promega, N1351). TRIM46-halo tag vector was also used for HEK293 immunoprecipitation (IP) assays. Dendra2 was removed from the full-length tau-dendra vector to create a tau only plasmid for HEK293 IPs.

Animals

Timed pregnant female Sprague-Dawley rats (embryonic day 18, E18) were used to obtain hippocampal fetal tissue for primary neuron cultures. 4 adult (14 months) male Fischer 344 rats were used to obtain fresh brain homogenate. Animals were obtained from Harlan Laboratories (Indianapolis, IN). The animals were provided rat chow and water *ad libitum* and housed in a reverse light-dark cycle room (12h:12h, Light:Dark). All animal studies were performed in accordance with standard regulations and were approved by the Michigan State University Institutional Animal Care and Use and Committee.

Primary neurons

Primary neurons were generated from dissected E18 rat hippocampi following a similar procedure as described previously with the following modifications (Kneynsberg *et al.*, 2016). The tissue pieces were incubated in 0.125% trypsin for 15 min at 37°C prior to dissociation. To obtain a single cell suspension, trituration was performed by gently passing the tissue through a 3ml syringe with a 14g needle 30 times, 15g needle 30 times, 17g needle 20 times, 18g needle 20 times and finally a 21g needle 15 times. Cells were plated on poly-D-lysine coated glass bottom chamber slides (Ibidi, 80427) at a density of 26,400 cells/cm² and grown in neurobasal medium

(Gibco, 21103-049) supplemented with L-glutamine (Gibco, 25030-0810 and B27 (Gibco, 17504-044). Half the media was replaced every two days.

For development study, the cells were fixed at desired DIV timepoint with 4% paraformaldehyde in cytoskeletal buffer (10 mM MES, 138 mM KCl, 3 mM MgCl₂, 4 mM EGTA, pH 6.1) for 20 min. Following fixation, the cells were rinsed 3 times in Tris-buffered saline (TBS; Tris 50 mM, NaCl 150 mM, pH 7.4) and then processed for immunocytofluorescence. The entire procedure for harvesting, plating, fixing, and staining developmental neurons was repeated a total of three independent times to confirm the findings.

For live-cell imaging, cells were transfected with DNA construct and Lipofectamine 2000 (Invitrogen, 11668) on DIV6. 1000ng of DNA was incubated with 3µl Lipofectamine in 50µl Opti-MEM (Thermo Fisher, 31985070) for 30 minutes before being added to the chamber slide well with 500µl of media. After 2 hours, half of the media was replaced with NBM plus antineurofascin antibody (1:2000, NeuroMab, A12/18). After 18 hours, all media was replaced with NBM plus AlexFluor647 anti-mouse antibody and incubated for 2 hours. A final full media change was performed before imaging. Each construct was measured in neurons derived from 2-4 independent timed-pregnant females, with all transfected constructs having at least 10 replicate neurons used for measurements.

For shRNA treated neurons, cells were transfected with either shRNA and dendra/taudendra constructs (for live-cell tau diffusion studies) or shRNA-GFP constructs alone (for developmental studies) and Lipofectamine 2000 (Invitrogen, 11668) on DIV4. Our first approach to AnkG knockdown was to reduce expression with shRNA at DIV2 and prevent AnkG from forming an AIS in the axon (similar to the approach employed by (Freal *et al.*, 2016)). We found that neurons treated with this AnkG-shRNA paradigm did not develop predicted neuronal

morphology or form a distinct axonal process (Dotti *et al.*, 1988). Thus, this approach was prohibitive in our hands because we could not examine the axosomatic tau diffusion barrier if an axon did not develop. Our second approach to AnkG knockdown was to treat neurons with AnkG-shRNA at DIV4 after the AIS had just begun to establish and tau enrichment in the axon was already detectable (Figure 2.1I). 1000ng of DNA (or 500ng each of shRNA and dendra/tau-dendra) was incubated with 3µl Lipofectamine in 50µl Opti-MEM for 30 minutes before being added to the chamber slide well with 500µl of media. After 2 hours, half of the media was replaced. For live-cell shRNA with dendra, the neurofascin antibody was used as described above. After 18 hours, all media was replaced with NBM. Cells were then fixed at DIV5-9 for shRNA evaluation or imaged at DIV8 for live-cell analysis. shRNA treatment was replicated and measured the same as described above for development or live-cell analysis.

Immunocytofluorescence

Fixed cells were rinsed 3x in TBS for 5 min each and then blocked and permeabilized with 5% goat serum/1% BSA/0.2% Triton-X for 1 hr at room temperature. Cells were stained with the primary antibodies diluted in 2% goat serum and incubated overnight at 4° C. The cells were washed 6 times for 10 minutes in TBS and then incubated in AlexaFluor goat anti-mouse isotype specific or goat anti-rabbit secondary 1:500 diluted in 2% goat serum in TBS. DAPI counterstain (0.5 μg/ml, D1306, Thermo) was added to the first of four TBS rinses if Alexa Fluor 405 was not used.

Confocal imaging

Neurons were imaged at 60x magnification (oil lens, 1.4 numerical aperture) using a Nikon A1+ laser scanning confocal microscope system equipped with 405, 488, 561, and 640 solid-state lasers. Imaging of live neurons was done using a Tokai Hit stage top incubator system to maintain appropriate humidity and CO₂ levels, and the images/movies were acquired with the same acquisition settings for all transfected neurons (i.e. scan speed, resolution, magnification, optical zoom, gain, offset and laser intensity). Imaging of all fixed cells for developmental timepoints was completed with the same acquisition settings for each timepoint.

Axonal intensity measurements

Nikon Elements AR software was used to for analysis and generation of the intensity profile. An intensity profile of the average within 1 pixel of the drawn line (NIS software setting: neighborhood of: width: 1; in: pixel; mode: mean) was drawn from the nucleus of the cell down the center of the axon for 75µm (DIV2) or 100µm (DIV3-9). The position of the axon hillock was defined at the area of the cell body, at the base of the axonal projection, and all profiles were aligned to the hillock as a distance value of 0µm (Figure 2.1L). The morphological variability of cultured neurons required normalization to account for structural aberrations, focal plane of the image, and crossing of other cell processes in the culture. We used a similar method to that already published in which each X value is transformed to become the average of the 20 values (4µm) before and after that value (Grubb & Burrone, 2010). The intensity values for each smoothed intensity profile were then either normalized to a range of 0-1 based on the maximum and minimum values (Normalized to neuron, Figure 2.2) or to the maximum and minimum values of the average of the DIV9 neurons (Normalized to DIV9 average, Figure 2.3).

Live-cell tracking

For live-cell imaging of dendra2 and tau-dendra constructs, all neurons were imaged at 60x magnification using a confocal microscope (as above) with the same laser intensities and the following parameters. To ensure the protocol would detect the inhibited somatic diffusion due to the retrograde diffusion barrier but also detect a significant increase in diffusion of proteins unaffected by the barrier, we performed initial analysis to validate acquisition criteria. We photoconverted (PC) tau in the distal axon and tracked its retrograde diffusion for 120 minutes to measure the potential distance of diffusion with a duration much longer than the experimental conditions (i.e. 30 min). At 30 minutes, a >200% increase in PC tau from 70-85 µm was seen.

For acquisition, a preliminary image of a neuron was taken in green, red, and far red. We specifically excluded neurons from analysis that had high basal levels of somatic red protein to prevent saturation of the red channel after 30 minutes of conversion, saturation of the 488 channel in the axon (unconverted tau), no clearly identifiable axon, multiple axons (i.e. multiple AISs), or an axon that did not remain in the focal plane (all axons were positively identified using live-cell neurofascin staining (Dumitrescu *et al.*, 2016)). A stimulation box (15µm x 5µm) was drawn and placed lengthwise over the axon beginning 70-85µm from the axon hillock. The box was not placed on top of dendritic projections of the cell; if the box could not be placed on only the axon within 70-85µm, the cell was excluded. An acquisition protocol was run in which the neuron was captured 3x in 488, 561, and 640 with a 1-minute delay between each image. The average values of these 3 images was treated as a baseline (T=0). For conversion of green unconverted (UC) dendra2 to red PC dendra2, the stimulation box was scanned with the 405 laser at 10% power at a scan speed of 0.25. After a 20 second delay the box was scanned again. After 6 repeated scan sessions, the neuron was imaged in the previous channels. This sequence

of stimulations and imaging was repeated 15 times, giving a timepoint for analysis every 2 minutes, and a total imaging time of 30 minutes (T=30).

Retrograde diffusion

The retrograde diffusion of each dendra construct was measured using the image files acquired in the live-cell tracking by drawing an outline of the entire soma in Nikon Elements AR software (Figure 2.1L). The value of PC red intensity of the soma for the first 3 baseline images at T=0 was subtracted from PC red intensity at T=30, giving the change in somatic red protein. This value was then divided by the value of green UC dendra intensity in the stimulation box at T=0. This normalization accounted for the change in somatic red PC dendra from background red signal in the soma, and the second variable normalizes the data for variation in both tau expression levels and axon morphology between individual neurons. These normalization variables are expressed in the following formula for deriving the change in somatic dendra protein:

Change in Somatic dendra =
$$\frac{Final\ PC\ somatic\ dendra\ (red) - Initial\ PC\ somatic\ dendra\ (red)}{Initial\ UC\ axonal\ dendra\ (green)}$$

Dual-luciferase reporter assay

The dual-luciferase reporter assay was conducted to validate knockdown efficiency of AnkG-shRNA and TRIM46-shRNA. The Renilla shRNA and scrambled shRNA were used as positive and negative controls, respectively, along with an empty shRNA plasmid expressing no shRNA. The manufacturer's protocol was followed for these assays. Hek293 cells were plated (200,000 cells/well) in a 24-well plate. After 24 hours, cells were transfected using

Lipofectamine 2000 with pSiCheck plasmid and shRNA plasmid. The cells were incubated for 24 hours until the media was replaced, and the cells were grown for another 24 hours. On day 4, the dual-luciferase assay was performed. Briefly, lysis buffer was added to each well and lysates transferred to a 96-well plate where they were treated with luminescent substrates using the GloMax-Multi Detection System (E7061, Promega). Luminescent intensity was recorded for both the Renilla and Firefly luciferases, and the ratios were compared to determine knockdown efficiency.

Proximity ligation assay

The proximity ligation assay (PLA) was performed on DIV7 primary hippocampal neurons (obtained as described above) to identify a colocalization between tau and TRIM46. Previous work has established the PLA as a method to identify colocalizations of tau and other proteins (Bretteville et al., 2017). The tau7 and TRIM46 antibodies were used with the standard manufacturer's protocol for DuoLink Proximity Ligation Assay from Sigma-Aldrich. Briefly, the neurons are incubated with primary antibodies for tau and TRIM46. PLA probes (anti-mouse-PLUS and anti-rabbit-MINUS) were incubated with the cells to bind the tau and TRIM46 antibodies, respectively. The DNA attached to the PLA probes is then ligated by incubating the cells in ligation enzyme at 37°C. The ligated DNA can then be amplified in the presence of a fluorescent reporter (FarRed) producing fluorescent DNA structures at the site of ligated DNA. Following final washes from the PLA detection, the neurons were incubated with traditional Alexa Fluor secondary antibodies (described above) to visualize TRIM46 and tau7 with the PLA signal.

NanoBRET donor saturation assay

A donor saturation assay was utilized to demonstrate a specific interaction between the tau and TRIM46. The DNA constructs were expressed in low passage Hek293 cells through a lipid transfection using Lipofectamine2000 in a 12 well plate. Each well was transfected with 10 ng of donor DNA (tau-NanoLuciferase) as well as a varying amount of acceptor DNA (TRIM46-Halo or HaloTag-only control). The amount of acceptor DNA ranged from 1000 ng to 1.4 ng for final acceptor:donor DNA ratios of 100:1, 33.3:1, 11.1:1, 3.7:1, 1.2:1, 0.4:1, and 0.1:1. A control well that was transfected with donor DNA but no acceptor DNA was also included. In order to standardize the amount of DNA present in the transfection reaction, an empty pTRE3G plasmid was added to a final DNA concentration of ~1000 ng/transfection in order to act as a carrier DNA. The pTRE3G is a TetOn system plasmid that will not express any gene in the absence of doxycycline.

After an 18 hour expression period, the cells were detached from the plate upon addition of 500 μl of 0.5% trypsin and a brief incubation at 37°C. After dissociation, the trypsin was quenched with 1 ml of cell culture media. The cells were centrifuged at 200xg for 2 minutes and resuspended in 1 ml of OptiMEM (no phenol red, 4% FBS, Thermo Fisher, 11058021). Aliquots of each sample were diluted in trypan blue (Bio-Rad), counted, and diluted to 660 μl at 200 cells/μl in OptiMEM (no phenol red, 4% FBS). The cells were divided evenly and 0.33 μl of 618 ligand (Promega) or 0.33 μl of DMSO control were added to each sample. The 618 ligand attaches to the HaloTag and acts as the acceptor fluorophore while the DMSO control contains no fluorophore. Six wells of each transfection condition were plated onto a 96-well, white-wall, clear-bottom plate (3 with 618 ligand and 3 with DMSO) at 20,000 cells and 100 μl/well. The cells incubated for 18 hours at 37°C and 5% CO2. A 5x stock solution of Nano-Glo substrate

(Promega) was prepared by performing a 1:100 dilution of the provided substrate into OptiMEM (no phenol red, 4% FBS). 25 µl of the Nano-Glo substrate stock was then added to each well and immediately placed in the BioTek Synergy NEO HTS plate reader (BioTek). After shaking the plate for 30 seconds, the filtered luminescence values were read using a 410/80 bandpass filter (donor signal) and 610 nm longpass filter (acceptor signal). The raw milliBRET ratio was calculated by dividing the acceptor luminescence values by the donor luminescence values and then multiplying by 1000. These values were then corrected by subtracting the control milliBRET ratios (with DMSO) from the experimental milliBRET ratios (with 618 ligand). The mean and SEM of these values were then plotted versus the transfection DNA ratios and fit to a hyperbolic curve using GraphPad Prism (v7.0).

Tissue processing

Animals used for collection of fresh brain tissue were transcardially perfused with 200 ml of 0.9% saline containing heparin (10,000 U/L). The brains were extracted and the HP was dissected and frozen on dry ice. The HP was homogenized in 300 μl of 10 mM Tris/1 mM EDTA/0.8 mM NaCl/10% sucrose buffer containing protease and phosphatase inhibitors (10 μg/ml pepstatin, 10 μg/ml leupeptin, 10 μg/ml bestatin, 10 μg/ml aprotinin, 1mM PMSF; 10 mM β-glycerophosphate, 1 mM sodium orthovanadate, 10 mM sodium fluoride, 1 mM tetra-sodium pyrophosphate decahydrate), using a sonicator (XL-2000, Misonix, 10X 1 sec bursts at power level 1). Lysates were cleared of cellular debris by centrifugation at 22,000 x g for 20 min at 4°C. The resulting supernatants were collected for analysis and the total protein content was assessed using the Bradford protein assay (B6916, Sigma).

TRIM46 immunoprecipitation

NHS-Mag Sepharose beads (28-9513-80, GE Healthcare) were used with TRIM46 antibody to immunoprecipitate TRIM46 and its interacting partners our of hippocampal brain lysate. Following manufacturer's protocol, 100µl of bead slurry (20µl bead volume) was added to a 1.5mL Eppendorf tube. Using a MagRack (28-9489-64, GE Healthcare), the storage buffer was removed, and 500µl of ice-cold 1mM HCl was added. 20µg of TRIM46 or 20µg rabbit unconjugated IgG was added to a final volume of 50µl of coupling buffer (0.15 M triethanolamine, 0.5 M NaCl, pH 8.3). The HCl was removed from the beads, the antibody binding solution was added, and the beads were incubated end-over-end for 3 hours at room temperature. The antibody solution was removed and 500µl buffer A (0.5 M ethanolamide, 0.5 M NaCl, pH 8.3) was added and removed. 500µl of buffer B (0.1 M Na-acetate, 0.5 M NaCl, pH 4.0) was added and removed, followed by adding 500µl buffer A. The beads were incubated endover-end for 15 minutes. Buffer A was removed and 500µl buffer B was added and removed followed again my 500µl of buffer A. Buffer A was removed and 500µl buffer B was added. Buffer B was then removed and 50µl BSA (1mg/ml) was added and incubated for 30 minutes at room temperature end-over-end. The BSA was removed, the beads were resuspended in 500µl TBS, and divided into 4 new Eppendorf tubes. The TBS was removed and 250µl of 2 µg/µl hippocampal lysate was added to both the TRIM46 and rabbit conjugated beads. The tissue lysates were incubated for 24 hours at 4°C end-over-end. The lysate was then removed, and the beads were washed in 500µl TBS 5x 10 minutes, and then transferred to a new tube and washed one last time with 500µl TBS.

To increase the amount of TRIM46 and tau protein available for detection after immunoprecipitation, TRIM46 and tau were expressed in Hek293 cells as described below. Six

lysis buffer conditions were used to improve binding conditions. As follows, Tris Standard: 50mM Tris-HCl pH 7.5, 150mM NaCl, 1% TritonX-100, 0.5% NP-40, protease inhibitors; Tris TritonX-100: 50mM Tris-HCl pH 7.5, 150mM NaCl, 1% TritonX-100, protease inhibitors; Tris NP-40: 50mM Tris-HCl pH 7.5, 150mM NaCl, 0.5% NP-40, protease inhibitors; Tris No Detergent: 50mM Tris-HCl pH 7.5, 150mM NaCl, protease inhibitors; HEPES: 50mM NaCl, 20mM HEPES, 1% TritonX-100, 0.5% NP-40, protease inhibitors; X/2:175-mM potassium aspartate, 65-mM taurine, 35-mM betaine, 25-mM glycine, 10-mM HEPES, 6.5-mM MgCl₂, 5mM EGTA, 1.5-mM CaCl₂, 0.5-mM glucose, 10-mM adenosine triphosphate, pH 7.2, protease inhibitors. Protease inhibitors were as follows: 1mM PMSF, 10 µg/ml pepstatin, 10 µg/ml leupeptin, 10 μg/ml bestatin, and 10 μg/ml aprotinin. Wash buffers used were: Tri: 50mM Tris-HCl pH 7.5, 150mM NaCl; HEPES: 50mM NaCl, 20mM HEPES; X/2:175-mM potassium aspartate, 65-mM taurine, 35-mM betaine, 25-mM glycine, 10-mM HEPES, 6.5-mM MgCl₂, 5mM EGTA, 1.5-mM CaCl₂, 0.5-mM glucose, 10-mM adenosine triphosphate, pH 7.2. Low passage Hek293 cells were plated at 300,000 cell/well in a 12 well plate and allowed to grow for 24 hours. Each well was transfected through a lipid transfection using Lipofectamine2000 with 1000 ng of total DNA. Wells were transfected with either 1000ng dendra2 plasmid, 500ng dendra2 and 500ng tau, 500ng dendra2 and 500ng TRIM46-Halo, or 500ng tau and 500ng TRIM46-Halo. After 18 hours, media was carefully removed from the plate and 150µl lysis buffer (Table 2.2) was added. The cells were scrapped off with a pipette tip and sample was collected in an Eppendorf tube. The samples were dounced 20 times with a pestle and spun at 14,000xg for 5 minutes at 4°C. The supernatant was transferred to a new tube. 350μl of wash buffer was added to sample. 450µl of sample was then added to HaloLink Resin (Promega, G1912), leaving 50µl of pre-IP lysate. Resin was prepared by thoroughly mixing HaloLink slurry and aliquoting 50µl for each sample. The resin was washed 3x in 500µl of wash buffer (Table 2.2), centrifuging 2 minutes at 800xg to settle the resin between washes. Immediately before adding the sample, the wash buffer was removed. 450µl of sample was incubated with the resin for 60 minutes at room temperature with an end-over-end agitator. The sample was then centrifuged for 2 minutes at 800xg and the supernatant was removed from the resin and saved as the post-IP lysate. The resin was washed 4x 5 minutes with 800µl of wash buffer using the end-over-end agitator. The proteins were eluted by adding 50µl Laemelli buffer and shaking tube at 1000rpm at 30°C. Sample was centrifuged for 2 minutes at 800xg before loading the supernatant for western blot.

Weak or transient protein interactions would be undetectable using this method, so a pretreatment of formaldehyde was used to crosslink a TRIM46-tau interaction prior to lysis and protein extraction (Vasilescu *et al.*, 2004; Nilsen, 2014). To do this the protocol was followed as above, but after the transfected cells had grown for 18 hours, the media was replaced with 500µl warmed media with 0.5% PFA. The cells were incubated for 10 minutes at room temperature on an orbital shaker (100rpm). The media was then removed and the residual PFA was quenched with 500µl of media with 125mM Glycine for 5 minutes. After glycine media was removed, lysis buffer was added, and the IP was continued as described above.

Mass spectrometry

After IP, TBS buffer was removed and $50\mu L$ of 25mM ammonium bicarbonate/50% acetonitrile was added. The sample was incubated at 37°C for 5hrs and $2\mu L$ of Trypsin Gold ($1\mu g/\mu L$) was added then incubated at 37°C overnight. The magnetic beads were removed, and the supernatant was transferred to a clean 1.5 mL tube. The sample was dried using a speed

vacuum and resuspended in 50μL of 25mM ammonium bicarbonate/5% Acetonitrile. The resuspended sample was transferred to a glass vial and placed in the autosampler. From this, 35μL was automatically injected by a Thermo EASYnLC 1000 onto a Thermo Acclaim 0.1 x 20mm C18 Peptide nanotrap and washed with buffer A (0.1% formic acid in water) for 5 minutes. Bound peptides were then eluted onto a Thermo Acclaim RSLC 0.075mm x 150mm C18 column over 55 minutes with a gradient of 4% buffer B (0.1% formic acid in acetonitrile) to 10% buffer B in 5 minutes, increasing to 35% B by 40 minutes, 50% B by 45 minutes, and ramping to 90% buffer B at 46 minutes where it was held for the 7 minutes. Buffer B was reduced to 4% by 53 minutes and remained for 5 minutes. The sample was run at a constant flow rate of 0.3μL/min.

Tandem mass spectra were extracted by Scaffold (version Scaffold_4.4.1.1, Proteome Software Inc.). Charge state deconvolution and deisotoping were not performed. All MS/MS samples were analyzed using Mascot (Matrix Science; version 2.5.0) and X! Tandem (The GPM, thegpm.org; version CYCLONE (2010.12.01.1)). Mascot was set up to search the uniprot- rattus norvegicus fasta database assuming the digestion enzyme strict trypsin. X! Tandem was set up to search a subset of the uniprot- rattus norvegicus fasta database also assuming strict trypsin.

Mascot and X! Tandem were searched with a fragment ion mass tolerance of 0.02 Da and a parent ion tolerance of 10 PPM. Carbamidomethyl of cysteine was specified in Mascot and X!

Tandem as a fixed modification. Deamidated of asparagine and glutamine and oxidation of methionine were specified in Mascot as variable modifications. Glu->pyro-Glu of the n-terminus, ammonia-loss of the n-terminus, gln->pyro-Glu of the n-terminus, deamidated of asparagine and glutamine and oxidation of methionine were specified in X! Tandem as variable modifications. Scaffold was used to validate MS/MS based peptide and protein identifications.

Peptide identifications were accepted if they could be established at greater than 99.0% probability. Peptide Probabilities from X! Tandem were assigned by the Peptide Prophet algorithm with Scaffold delta-mass correction (Keller *et al.*, 2002). Peptide Probabilities from Mascot were assigned by the Scaffold Local FDR algorithm. Protein identifications were accepted if they could be established at greater than 99.0% probability to achieve an FDR less than 1.0% and were detected in both samples. Protein probabilities were assigned by the Protein Prophet algorithm (Nesvizhskii *et al.*, 2003). Proteins that contained similar peptides and could not be differentiated based on MS/MS analysis alone were grouped to satisfy the principles of parsimony. Proteins sharing significant peptide evidence were grouped into clusters. Proteins were positively identified from a sample if they were pulled down with the TRIM46 antibody (in addition to TRIM46), but not with the rabbit IgG control of the same brain tissue. Only the proteins present is all samples with a TRIM46 positive pull-down would qualify as a positive interacting partner.

Immunoblotting

For blotting of rat tissue IP samples, the pre- and post-IP samples for one representative rat hippocampus were diluted in Laemelli buffer, while the beads of the TRIM46 and rabbit IgG IP of that same animal were incubated in 50µl of Laemelli buffer. For blotting Hek293 IP samples, the pre-and post-IP samples were diluted in Laemelli buffer. The HaloLink resin was already resuspended in Laemelli buffer. The samples were heated to 95°C for 10 minutes, then separated using SDS-PAGE on 4-20% Criterion TGX (Bio-Rad) gradient gels at 250V. The samples were transferred to nitrocellulose membranes for 50 minutes (66458; Pall Life Sciences) to visualize the TRIM46 protein immunoprecipitated from the sample. The membrane was

blocked in 2% nonfat dry milk in Tris-buffered saline (NFDM-TBS) for 1 hour at room temperature and incubated with primary antibody in NFDM-TBS overnight at 4°C. Blots were probed with TRIM46 antibody (1:500) and Tau7 (1:10000). After incubation with primary antibodies, the membranes were washed in TBS/0.1% Tween 20 and incubated in appropriate species-specific IRDye 680RD or 800CW secondary antibodies (1:20,000 in NFDM-TBS; LICOR Biotechnology). The membranes were washed and the reactivity visualized with a LI-COR Odyssey infrared imager.

Statistical analyses

All data were analyzed using Prism software (v7.0) and all data are presented as mean \pm either the standard error of the mean (SEM) or standard deviation (SD), as indicated in figure legends. Variability in live-cell data was controlled by applying the ROUT method for outlier removal, combining robust regression and outlier removal (Motulsky & Brown, 2006). As recommended, we set the coefficient Q to 1.0% and applied to all data sets, ensuring that the discovery of outliers would have a false discovery rate \leq 1.0%. Each neuron for live-cell analysis was treated as a biological replicate because each neuron was treated individually (stimulated with the UV laser in the individually drawn conversion box). The D'Agostino-Pearson omnibus normality test was performed on each set of live-cell diffusion data to determine whether the data sets met the assumption of normality. Only one data set did not pass the normality test (i.e. P301L-tau, p= 0.0279), and in this case the data were compared using the non-parametric Mann-Whitney U test. All other tests were performed using an unpaired student's T-test to determine differences between two groups (i.e. dendra2 vs tau-dendra) or one-way ANOVAs to determine the differences between more than two groups (i.e. tau domains, phosphorylations, or shRNA

treatments). Significance was set at $p \le 0.05$ for all comparisons. If overall significance in the ANOVA was achieved, the Sidak post-hoc test was used for multiple comparisons to the control (i.e. tau-dendra). If overall significance was not achieved, no post-hoc analyses were used.

RESULTS

Axonal tau enrichment occurs coincident with TRIM46 localization to the AIS during development

Tau and MAP2 are commonly used as axonal and somatodendritic markers, respectively, but a daily developmental time course of the distribution of these proteins together with the AIS proteins that regulate distribution was not done (Goedert *et al.*, 1991; Mandell & Banker, 1995). As defined by the traditional AIS markers (e.g. AnkG, βIV-spectrin, etc.), the AIS develops over a fairly well-established time course, but TRIM46 has yet to be studied within that timeline (Dotti *et al.*, 1988; Yoshimura & Rasband, 2014; Freal *et al.*, 2016). Here, we analyzed the intensity of the immunofluorescent staining from the cell body into the axonal projection of hippocampal neurons from DIV 2-9 using confocal microscopy to establish the developmental distribution of tau, TRIM46, AnkG and MAP2 (Figure 2.1L).

At DIV 2, tau is expressed throughout the neuron during axon formation and differential distribution between the somatodendritic and axonal compartments is not apparent (Figure 2.2A). Interestingly, MAP2 at DIV2 is the first of the markers assessed here that shows a distinct distribution peak at the proximal axon region preceding the AIS (Figure 2.2A). Neither TRIM46 nor AnkG display a distinct localization along the somata and axonal regions evaluated (Figure 2.2A). We show that by DIV3 the initial detection of a differential distribution of tau with increased tau expression in the axon over the soma corresponds to an initial peak of TRIM46

forming in the proximal axon (Figure 2.2B). The intensity profile of AnkG at DIV3 does not yet show a clear localization to the axon or AIS (Figure 2.2B). The magnitude of axosomatic tau difference increases at DIV4, while AnkG exhibits an increased segregation to the AIS and MAP2 tightens its distribution peak to only within the hillock region of the axon (Figure 2.2C). TRIM46 expression becomes less variable and forms a distinct peak just proximal to AnkG at DIV4-5 (Figure 2.2C-D). AnkG increases within the AIS at DIV5 (Figure 2.2D). From DIV5-8, the intensity of the axosomatic tau distribution lessens while MAP2 remains stable. TRIM46 and AnkG increase in intensity to form tighter distributions from DIV6-8 (Figure 2.2E-G). The final time point (DIV9) demonstrates a distribution increase of axonal tau distal to defined peaks of TRIM46 and AnkG in the AIS and shows enrichment of MAP2 within the proximal axon (Figure 2.2H). We show the localization of TRIM46 follows a progressive shortening and densification from DIV5-9 where the intensity of TRIM46 from ~25-50µm remains constant or decreases slightly, while TRIM46 continues to accumulate from ~0-25µm from the hillock (Figure 2.2D-H) A similar pattern of shortening and densification was seen with AnkG (shown in Figure 2.2D-H), as was previously described in the AIS (Kuba et al., 2014; Le Bras et al., 2014). This process is believed to represent a refinement process indicative of AIS and axonal maturation (Kuba et al., 2014; Le Bras et al., 2014).

We also normalized the intensity profiles for each marker to the signal intensity measured at DIV9 to better understand the relative magnitude of changes in signal across the soma, AIS, and axon of neurons during the developmental time course *in vitro*. DIV2 sees the highest levels of tau expressed in the soma, while the other proteins are expressed at their lowest levels (Figure 2.3A). MAP2 expression is detectable in the axon hillock at DIV2 at lower levels and increases in peak intensity until DIV6, where is levels off through DIV9 (Figure 2.3). Both TRIM46 and

AnkG are relatively undetectable at DIV2, but TRIM46 has a small expression in the AIS by DIV3 (Figure 2.3A-B). Tau intensity increases in the axon at DIV3, while remaining constant in the soma, but shows the first sign of somatic decrease at DIV4 (Figure 2.3B-C). AnkG doesn't exhibit a notable increase in expression until DIV4, where it rises quickly and approaches a maximum by DIV6 (Figure 2.3C-E). DIV5 and DIV6 maintain robust differential distribution of tau but show slight decreases in somatic and axonal tau intensity (Figure 2.3D-E). TRIM46 gradually increases intensity in the AIS from DIV4 – DIV7, then increases more only in the proximal AIS for its relative maximum at DIV9 (Figure 2.3C-H). AnkG decreases slightly around the axon hillock at DIV7 while increasing in intensity only slightly more at DIV8 and DIV9 (Figure 2.3F-H). Tau dramatically decreases in axonal intensity at DIV7 which continues into DIV8 and DIV9 with reduction of somatic and axonal tau, but a differential distribution is maintained (Figure 2.3F-H). It is of interest to note that the somatic intensity of tau at DIV3 (Figure 2.3B) is higher than the axonal tau intensity at DIV9 (Figure 2.3H), but axosomatic enrichment is maintained in both instances.

Retrograde axonal diffusion of tau is inhibited in the proximal axon

Previous studies identified that the AIS acts a barrier to the diffusion of tau proteins from the axon to the somatodendritic compartment using live-cell imaging of tau fused with dendra2, a fluorescent protein that is permanently photoconverted from green to red upon exposure to UV light (Gurskaya *et al.*, 2006; Li *et al.*, 2011). We found that when using the published methods by Li and colleagues, the concentration of tau-dendra in the axon (Figure 2.4F) directly affected the amount of tau-dendra that diffused into the soma (Figure 2.4I), so we built upon their approach, adding new key features. First, we include live-cell detection of the AIS using

neurofascin antibody labeling (Dumitrescu *et al.*, 2016). In our studies, this allowed for positive identification of axons and exclusion of neurons containing multiple axons. Second, we utilized three important normalization methods, including 1) measuring soma intensities with individual outlines of the entire soma to account for the variability in cell morphology, 2) strict placement of the UV dendra conversion box within 75-90µm from the axon hillock to ensure the conversion was well within the retrograde diffusion potential of tau-dendra (determined empirically as >200µm in 30 minutes, Figure 2.7E), and 3) measurement of the starting UC dendra protein signal in the axon to account for variations in axon morphology and level of axonal dendra or tau-dendra available for conversion in different axons. Using this methodology, we set out to further identify the factors involved in mediating the retrograde barrier for tau diffusion.

In the live-cell tau diffusion studies, we used dendra2 fusion proteins (Figure 2.3A) and dendra2 alone as a freely diffusing protein control. Confirming published work, we observed robust axosomatic diffusion of dendra2 protein, but tau did not freely diffuse from the axon to the soma indicating a retrograde diffusion barrier exists for tau (Figure 2.3B-I) (Li *et al.*, 2011; Zempel *et al.*, 2017). Our quantification of protein diffusion revealed significantly more dendra2 passed from the axon into the soma than tau-dendra (Figure 2.3J). To further elucidate the domain of tau that contributes to this phenomenon, we evaluated the domains of tau independently and found that the N-terminal tau domain (aa 1-220) and C-terminal domain (aa 381-441) show significant axosomatic diffusion when compared to full-length tau (Figure 2.3K). In contrast, the microtubule binding region did not diffuse from the axon into the soma, indicating that this region of tau is necessary and sufficient for the restricted diffusion of axonal tau (Figure 2.3K).

Disease-related tau modifications mislocalize to the somatodendritic compartment

Post-translational modifications of tau, such as phosphorylation, alter its function and can reduce MT binding affinity, possibly leading to somatic mislocalization (Mandelkow et al., 1995; Fischer et al., 2009). Since the MTBR was critical to the retrograde diffusion barrier, we investigated two phosphorylation constructs modified within the MT binding repeats known to impair the tau-MT interaction. The first site was S262, a phosphorylation in the first MT binding repeat of tau found in PHF samples from human AD and shown to inhibits MT binding in in vitro assays (Hasegawa et al., 1992; Biernat et al., 1993). This modification did not affect the axosomatic diffusion of tau (Figure 2.3L). Next, we studied a combination of modifications at S262, S305, S324, and S356 (an artificial construct known as the 4KXGE tau), which reduces binding of tau to the MT by obstructing interactions of the binding repeat motifs (Biernat & Mandelkow, 1999). This more extensive modification within the MTBR led to a significant increase in the extent of retrograde diffusion in live neurons (Figure 2.3L). These results indicate that the ability to maintain axonal enrichment depends on unphosphorylated binding repeat motifs, but the single phosphorylation in first repeat (S262) found in disease pathology is insufficient to cause axosomatic diffusion alone.

Other disease-related modifications lie outside of the MTBR, specifically, AT8 was identified by describing the epitope of an antibody raised against pathological tau (Biernat *et al.*, 1992). AT8 is used to identify early pathological tau in the neurons of human brain (Su *et al.*, 1994). To answer questions of whether phosphorylation in the MTBR is required for mislocalization we examined the live diffusion of tau-AT8 compared to tau-dendra and found an increase in axosomatic diffusion (Figure 2.3L). This indicates that modification of the binding motifs is not required for axosomatic diffusion, instead the possible conformational change

known to occur with the AT8 modification may play a role in tau localization (Jeganathan *et al.*, 2006).

The P301L mutation causes an inherited tauopathy known as FTDP-17. This mutation was previously linked to inducing tau abnormalities that included enhanced aggregation, altered conformation, and reduced MT binding (Hutton *et al.*, 1998; Arrasate *et al.*, 1999; Xia *et al.*, 2016. Here, we identified that the P301L mutation significantly increases the amount of tau that can retrogradely diffuse from the axon to the soma in neurons when compared to wild-type tau (Figure 2.3M). Together, these data suggest both a role for the MTBR and the conformation of the protein, that affects MT interactions, dictate mislocalization.

TRIM46 is required for axonal tau enrichment

After determining which domains of tau are required for axonal localization, we set out to identify components located in the proximal axon that are responsible for inhibiting the diffusion of tau from the axon to the soma. TRIM46 and AnkG were two strong candidates because of their roles in organizing cytoarchitecture and associated proteins. We constructed shRNAs against TRIM46 and AnkG to knockdown expression of proteins and evaluate the effect on retrograde tau diffusion in live-cells. In our fixed cell experiments, the shRNAs were delivered using a plasmid that independently expresses GFP as a marker of shRNA-containing neurons. In our live-cell tau diffusion studies, the shRNA (without GFP) was co-transfected with dendra or tau-dendra constructs which reliably produces 100% co-localization. Validation of our plasmid constructs showed an ~80% knockdown in TRIM46 expression and a ~90% knockdown in AnkG with the Dual-Luciferase Reporter assay *in vitro* assay compared to control (Figure 2.5A). Transfection of neurons with TRIM46-shRNA at DIV4 showed a loss of axonal TRIM46 by

DIV8, while maintaining significant AnkG in the proximal axon at the AIS (Figure 2.5B). Similarly, AnkG-shRNA treated neurons showed a knockdown of AnkG protein without loss of TRIM46 protein or disruption of TRIM46 localization in the AIS region (Figure 2.5C).

Disruption of axonal tau enrichment in response to knockdown of TRIM46 or AnkG was evaluated in fixed neurons for endogenous tau (Figure 2.5B-E) and in live cells for retrograde diffusion of tau (Figure 2.5F-J). TRIM46 knockdown reduced the level of total axonal tau and tau enrichment in the axon relative to the soma was not observed (Figure 2.5B). In contrast, axonal tau remained high with a robust difference over somatic tau with AnkG knockdown (Figure 2.5C). In live-cell experiments, the quantitative analysis of the axosomatic diffusion of tau-dendra following TRIM46 shRNA showed a significant increase in diffusion from the axon to the soma when compared to control and AnkG shRNA (Figure 2.5J). In contrast, AnkG-shRNA treated neurons did not show increased tau diffusion over control.

Tau is not a direct binding partner with TRIM46

After demonstrating that the knockdown of TRIM46 results in retrograde diffusion of tau into the soma, we looked for a direct interaction between TRIM46 and tau. Using immunoprecipitation in rat hippocampal tissue (Figure 2.6F-G) and HEK293 cells expressing exogenous human tau and TRIM46 (Figure 2.6H) we were unable to detect an interaction between the two proteins. Utilization of multiple buffer conditions or cross-linking proteins with PFA did not change this result (Table 2.1). In these experiments, we successfully immunoprecipitated tau or TRIM46 as the target proteins but were unable to detect the other protein on western blot. With negative interaction results from immunoblots to detect co-IP protein, we used bottom-up proteomics with tandem mass spectrometry of IP samples from rat

hippocampi as a sensitive technique for identify whether TRIM46 and tau interact (Table 2.2). Though we successfully detected the TRIM46, we did not detect tau using MS analysis. We did identify several cytoskeletal and signaling proteins with the TRIM46 IP, including tubulin, microtubule-associated proteins (MAP2, MAP6, and MAP1a), actin-associated proteins (αspectrin, cofilin, profilin, and drebrin), and calcium/calmodulin-dependent protein kinase type II, a kinase associated with AIS relocation (Figure 2.6I, Table 2.2) (Evans et al., 2013). To determine whether an in-cell protein-protein interaction assay would reveal an interaction we used the NanoBRET assay. This assay helps minimize the potential disruption of an interaction between tau and TRIM46 during cell lysis and/or the IP procedure. The NanoBRET assay showed no significant interaction between tau and TRIM46 (data not shown). Finally, we used the proximity ligation assay (PLA) to determine if there was a close association (30-40 nm) between tau and TRIM46 in primary neurons within the AIS. We found positive PLA signal clustered in the region of the AIS (Figure 2.6C), showing close proximity between tau and TRIM46 throughout the AIS (Figure 2.6D). A positive signal in the PLA with negative IP, NanoBRET and MS results suggests the two proteins do not directly interact, but more likely share a common binding partner, such as MTs or other AIS localized MAPs (e.g. MAP1a or MAP6).

DISCUSSION

Axonal protein distribution

Axonal enrichment of tau and somatodendritic localization of MAP2 are established characteristics of neurons, and mislocalization of both proteins is an event believed to be related to early disease pathogenesis (Goedert *et al.*, 1991). We studied the developmental localization

of MAPs in respect to AIS to help us understand the required elements driving and maintaining these distributions. We have provided developmental data that puts the axonal enrichment of tau in a spatial and temporal context with the emergence of the proteins in the AIS. The development of the AIS is well characterized in culture (Rasband and colleagues), but this work does not extend to TRIM46, as a newly characterized protein. As the first daily characterization of TRIM46 development in cultured hippocampal neurons we know of, we show that TRIM46 localization to the AIS occurs at DIV3, before AnkG shows axonal localization at DIV4 (Figure 2.1H). Further, we observed tau development of axonal enrichment concurrently with the localization of TRIM46 to the AIS at DIV3, suggesting that TRIM46 and not AnkG contributes to axonal tau localization as previously reported (Zempel *et al.*, 2017). Additionally, we found that the levels of enriched axonal tau are only ~2x higher than somatic tau, indicating a significant level of endogenous somatic tau, consistent with original findings in human brains (Binder *et al.*, 1986).

The microtubule binding domain of tau exhibits impaired axosomatic diffusion

Using proteins of 3 tau domains (N-terminal, MTBR, or C-terminal) we demonstrate that the inability of tau to undergo axosomatic diffusion requires the MTBR. These findings are consistent with previous studies showing that nocodazole, a MT disrupting drug, leads to enhanced axosomatic diffusion of tau protein in cultured neurons (Li *et al.*, 2011). Both the N-terminal and C-terminal domains of tau lack MT binding repeats, confirming that the ability to interact with intact MTs is required for inhibition of axosomatic tau diffusion. This conclusion is important to the study of tau's physiology in disease. As discussed in Chapter 1, two factors believed to play an important role in tauopathies are mislocalization of tau to the somatodendritic

compartment and modifications of tau that inhibit MT binding. We can then suggest that tau mislocalization may occur by impaired MT binding leading to and mislocalization of tau specifically by uninhibited axosomatic diffusion.

Disease-related tau modifications disrupt tau diffusion barrier

To further investigate this connection between tau mislocalization and the pathological forms of tau found in disease we created tau-dendra constructs with modifications or mutations implicated in tauopathies. We showed that certain phosphorylation modifications of the MTBR (pS262) do not affect axosomatic diffusion of tau while others (4KXGE) increase somatic diffusion from the axon. These data are consistent with previous studies showing that the 4KXGE protein shows enhanced axosomatic diffusion but are discordant from results showing that pS262 was sufficient to facilitate mislocalization of tau (Li et al., 2011). While the underlying reasons for these differences are unknown, there are several distinctions between our approaches that may be responsible. For example, we used neurofascin labeling in live-cells to positively identify axonal processes, but this was not done in prior studies. Also, we used a normalization process that included expressing the change in photoconverted tau as a function of the starting unconverted tau intensity within the axonal segment used for conversion. This allows normalization for the variations observed in protein expression levels and axonal morphology, but this normalization was not performed in prior studies. Instead, the primary normalization was to an artificial tau construct consisting of 8 MT binding repeats (Zempel et al., 2017). While both pS262 and 4KXGE show impaired microtubule binding, they do not diffuse the same in vitro (Biernat et al., 1993; Biernat & Mandelkow, 1999). This suggest a complexity to the interaction

that facilitates inhibition of axosomatic diffusion, in which pS262 does not significantly disrupt this interaction, but the 4KXGE modifications are sufficient to increase diffusion.

Investigation into additional disease-related tau modifications revealed that direct phosphorylation of the MTBR is not required for axosomatic mislocalization. The AT8-tau diffused to the somata, showing that phosphorylation modifying protein conformation and MT binding is sufficient to cause its mislocalization, potentially adding context to the somatic accumulations of AT8 that is prevalent in the earliest stages of tau deposition in disease.

Independent of phosphorylation, the tau-P301L mutation mislocalized to the soma. Additionally, AT8 and P301L tau exhibit the same steady state binding capacity as wild-type tau *in vitro*, but both have a significantly higher dissociation constant (K_d) than wild-type tau (Sun & Gamblin, 2009). We can conclude then that the mechanism of axonal enrichment of tau relies on the MT affinity of tau and not the protein stoichiometry.

TRIM46 maintains axosomatic tau diffusion barrier in neurons

Our data demonstrate that the knockdown of TRIM46 disrupts the retrograde diffusion barrier and allows diffusion of axonal tau into the somata. Moreover, knockdown of AnkG did not disrupt the axosomatic distribution of tau, and distributions of AnkG (TRIM46-shRNA treated) and TRIM46 (AnkG-shRNA treated) remain largely intact (Figure 2.5B-C), allowing us to further differentiate the effects of TRIM46 and AnkG on retrograde diffusion. Our AnkG-shRNA treated cells help not only exclude AnkG from having an effect on the barrier to axosomatic tau diffusion, but also several other AIS components that were previously shown to become disrupted with AnkG knockdown (Hedstrom *et al.*, 2007; Hedstrom *et al.*, 2008; Freal *et al.*, 2016). This includes βIV-spectrin, Nav1, neurofascin-186, end-binding protein 1, end-

binding protein 3, and glial-related cell adhesion molecule (NrCAM) which no longer localize to the AIS after AnkG shRNA treatment. Thus, we can conclude that the interactions of TRIM46 in the AIS that maintain the retrograde diffusion barrier do not rely on traditional AIS components, at least to block tau diffusion. A prominent role for TRIM46 in maintaining a differential distribution of tau aligns with the developmental appearance of axonal tau enrichment being coincident with TRIM46 AIS localization prior to AnkG. The shRNA findings appear to contradict a previous finding, showing that knockdown of AnkG and several other AIS proteins increase axosomatic tau diffusion (Zempel et al., 2017). In addition to the difference in our normalization criteria, mentioned above, this difference could be accounted for by the timecourse of shRNA treatment. First, our shRNA treatment is not administered until after the AIS and axonal tau enrichment is detectable, ensuring that we have an established retrograde diffusion barrier at the onset of shRNA treatment. Second, we analyzed the diffusion of tau as soon as the AIS protein expression is reduced, as extended disruption of the AIS leads to loss of axon identity compromising the ability to assign the observed effects specifically to the reduction of the protein.

TRIM46 interactions and mass spectrometry

Our attempts to identify a protein-protein interaction between tau and TRIM46 to explain TRIM46's role in the retrograde diffusion barrier were not successful. We tried IPs from cultured rat primary neurons, rat hippocampal lysates, and cell lines over expressing proteins, as well as various IP buffer conditions, formaldehyde fixation to preserve transient interaction, and Nano-BRET interaction assay for in-cell analysis. Finally, we performed mass spectrometry on TRIM46 IPs to confirm the lack of an interaction with tau and to detect novel interacting proteins

in hippocampal neurons. Of the proteins identified as TRIM46 interaction partners, we found 11 potentially relevant to TRIM46 function as a retrograde diffusion barrier in the AIS (Figure 2.6I). TRIM46 is known to interact with MTs, so while finding tubulin is not unexpected it also serves a positive control (Short & Cox, 2006). The interactions between TRIM46 and MAPs other than tau likely represent the interaction partners related to TRIM46's function in organizing parallel MT arrays with appropriate polar orientation (van Beuningen *et al.*, 2015). Particularly, MAP1a regulates microtubule dynamics by promoting growth and stability while maintaining a rigidity in their structure (Faller & Brown, 2009). Also, mutation of the MAP1a protein can cause cellular degeneration, exhibiting disruption of AIS morphology (Liu *et al.*, 2015). Further, MAP6 is an axonally localized protein recently described to control MT stabilization during development of neuronal polarity and promote organelle trafficking in the axons of hippocampal neurons (Tortosa *et al.*, 2017).

Conclusions

We show here that the development of the axonal tau enrichment corresponds to the development of TRIM46 in the AIS (Figure 2.8A-B). Knockdown of TRIM46 then caused the axosomatic diffusion of tau (Figure 2.8C). Finally, we did not identify a direct interaction between TRIM46 and tau. Our data show that the tau-MTBR is necessary and sufficient for axonal localization and suggests that TRIM46 forms a retrograde diffusion barrier for tau through MT interaction but without directly interacting with the tau protein. Based on the interactions of TRIM46 with MTs and MAPs revealed by mass spectrometry, we hypothesize that TRIM46 creates a retrograde diffusion barrier by maintaining parallel MT arrays in the AIS.

This organization then promotes axonal enrichment and prevents retrograde tau diffusion (Figure 2.8).

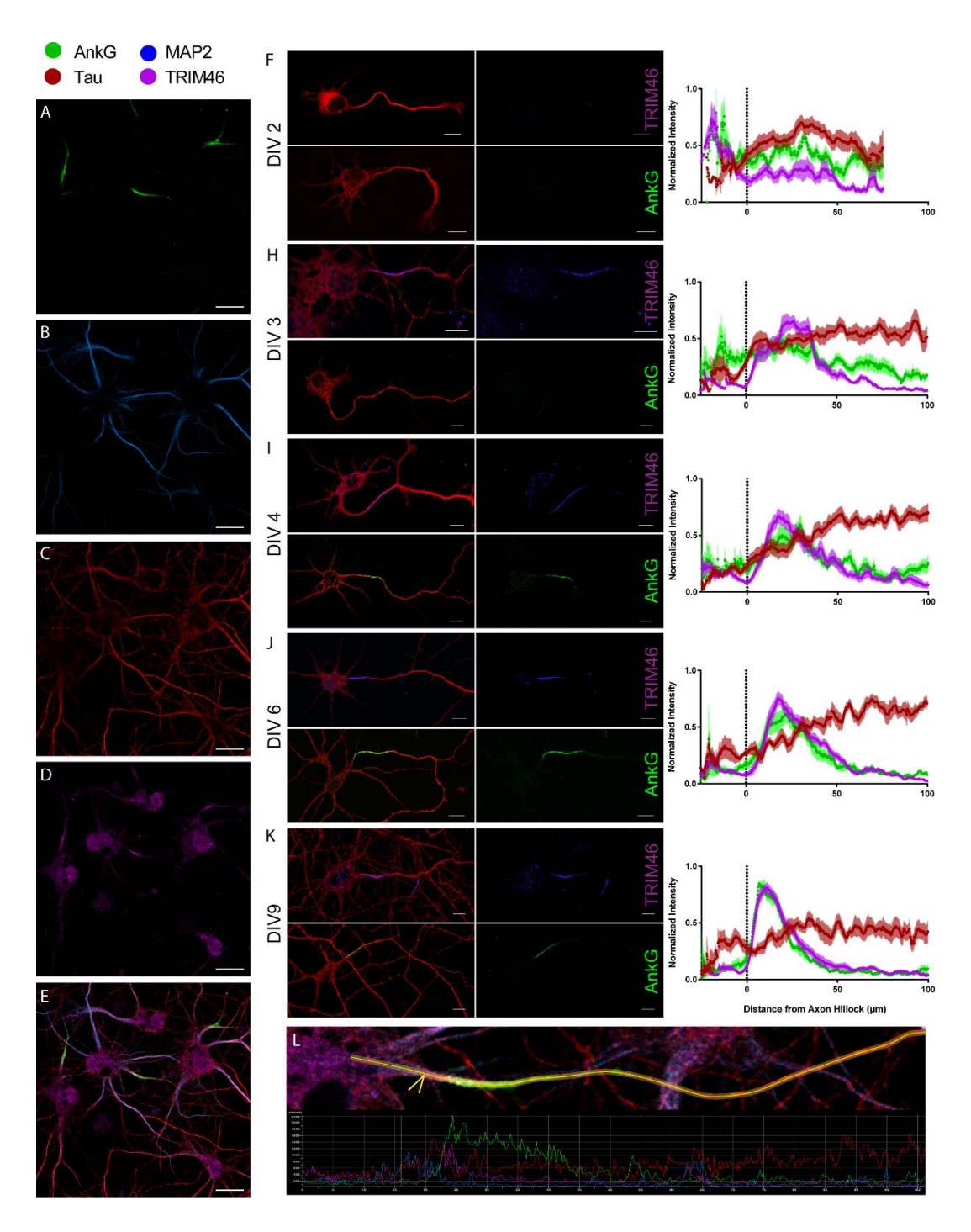


Figure 2.1: Axonal tau enrichment is coincident with TRIM46 localization to the axon initial segment in developing cultured hippocampal neurons.

(A-E) Cultured hippocampal neurons plated at (26,400 cells/cm²), immunolabeled for Ankyrin-G (AnkG, A), MAP2 (B), Tau, (C), and TRIM46 (D), and the merged image (E). (F-K)

Figure 2.1 (cont'd)

Representative images of neurons stained for tau (red) and TRIM46 or tau AnkG during development in culture and the corresponding intensity profiles of all neurons analyzed (graphs to the right are smoothed average intensity profiles expressed as mean \pm SEM, n = 15-20 individual neurons per stain). (F) At DIV2, there is no evidence of clear axonal tau enrichment or axon initial segment (AIS) localization of TRIM46 or AnkG. (H) Neurons at DIV3 show AIS enrichment of TRIM46 and axonal enrichment of tau, without AnkG presence. (I) AnkG develops in the AIS at DIV4 while the magnitude of axosomatic tau distribution increases and TRIM46 expression increases. (J-K) Axonal tau enrichment is maintained as expression of TRIM46 and AnkG increases and distribution refines to the proximal axon. (L) Representative intensity profile drawn from the soma into the axon, centered at the axon hillock (arrow head) and corresponding intensity graph below. Scale bar is $20\mu m$ in (A-E) and $10\mu m$ in (F-K). Data represent mean \pm SEM (n=15-20 individual neurons analyzed per stain).

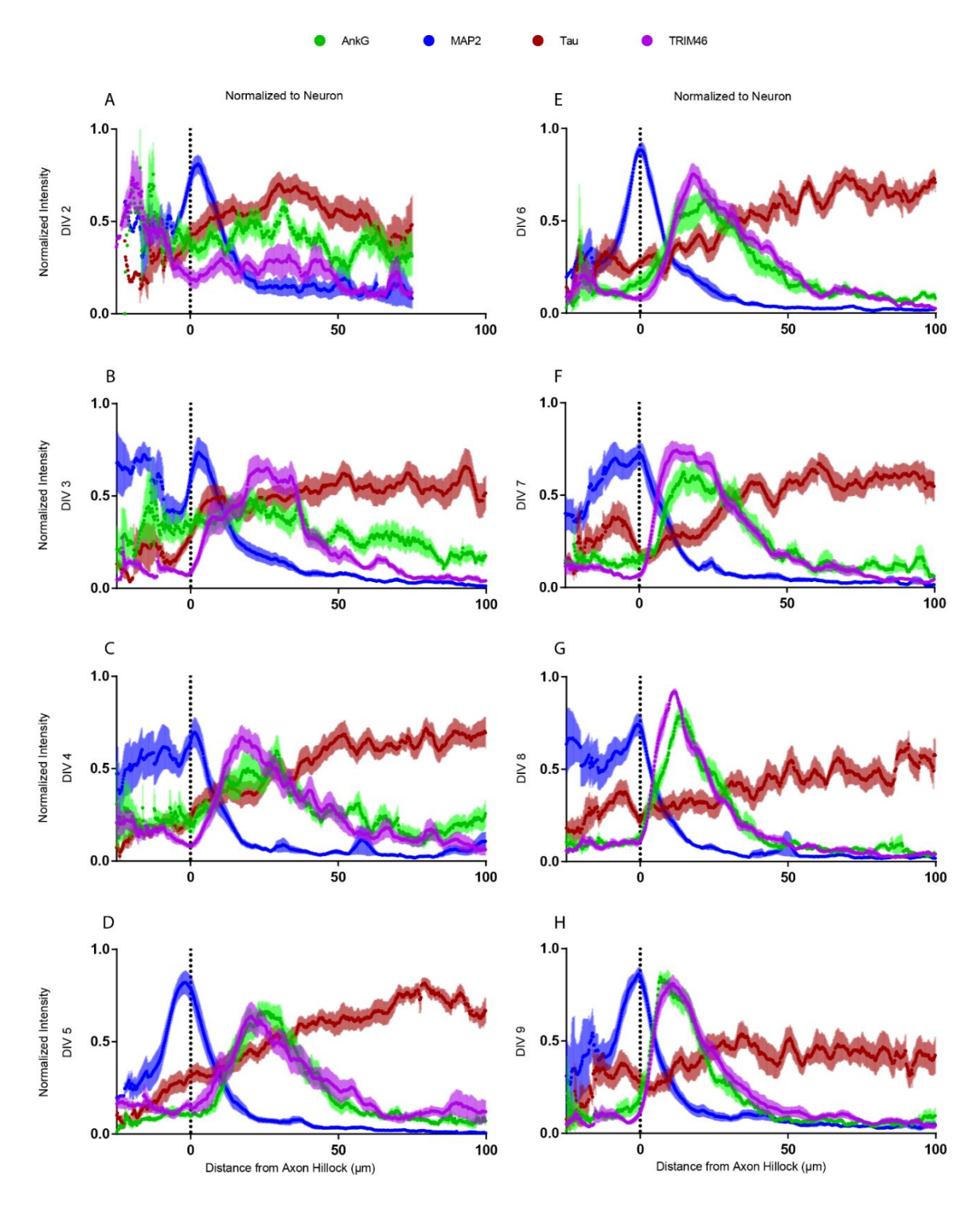


Figure 2.2: Normalized axonal intensity profiles from DIV 2-9 show axonal tau distribution corresponds to development of TRIM46 in the AIS.

(A-H) Smoothed intensity profiles for Ankyrin-G (green), MAP2 (blue), Tau (red), and TRIM46 (purple) normalized individually to a 0 – 1 maximum intensity at DIV2-DIV9. (A) Tau is

Figure 2.2 (cont'd)

expressed throughout the neuron during axon formation. MAP2 shows a distinct distribution peak at the proximal axon region preceding the axon initial segment (AIS). (B) Differential distribution of tau is detected with increased tau expression in the axon. An initial peak of TRIM46 forms in the proximal axon at DIV3. (C) The magnitude of axosomatic tau difference increases at DIV4. AnkG exhibits increased expression within the AIS and MAP2 tightens its distribution peak to only within the hillock region of the axon. (D) TRIM46 expression becomes less variable and forms a distinct peak just proximal to the increased AnkG peak. (E-G) The magnitude of axosomatic tau distribution lessens while MAP2 remains stable. TRIM46 and AnkG increase in intensity to form tighter distributions. (H) Axonal tau demonstrates an increased distribution, distal to defined peaks of TRIM46 and AnkG in the AIS. MAP2 is enriched within the axon hillock. TRIM46 and AnkG exhibit shortened and densified distribution. Data represent mean ± SEM (n=15-20 individual neurons analyzed per stain).

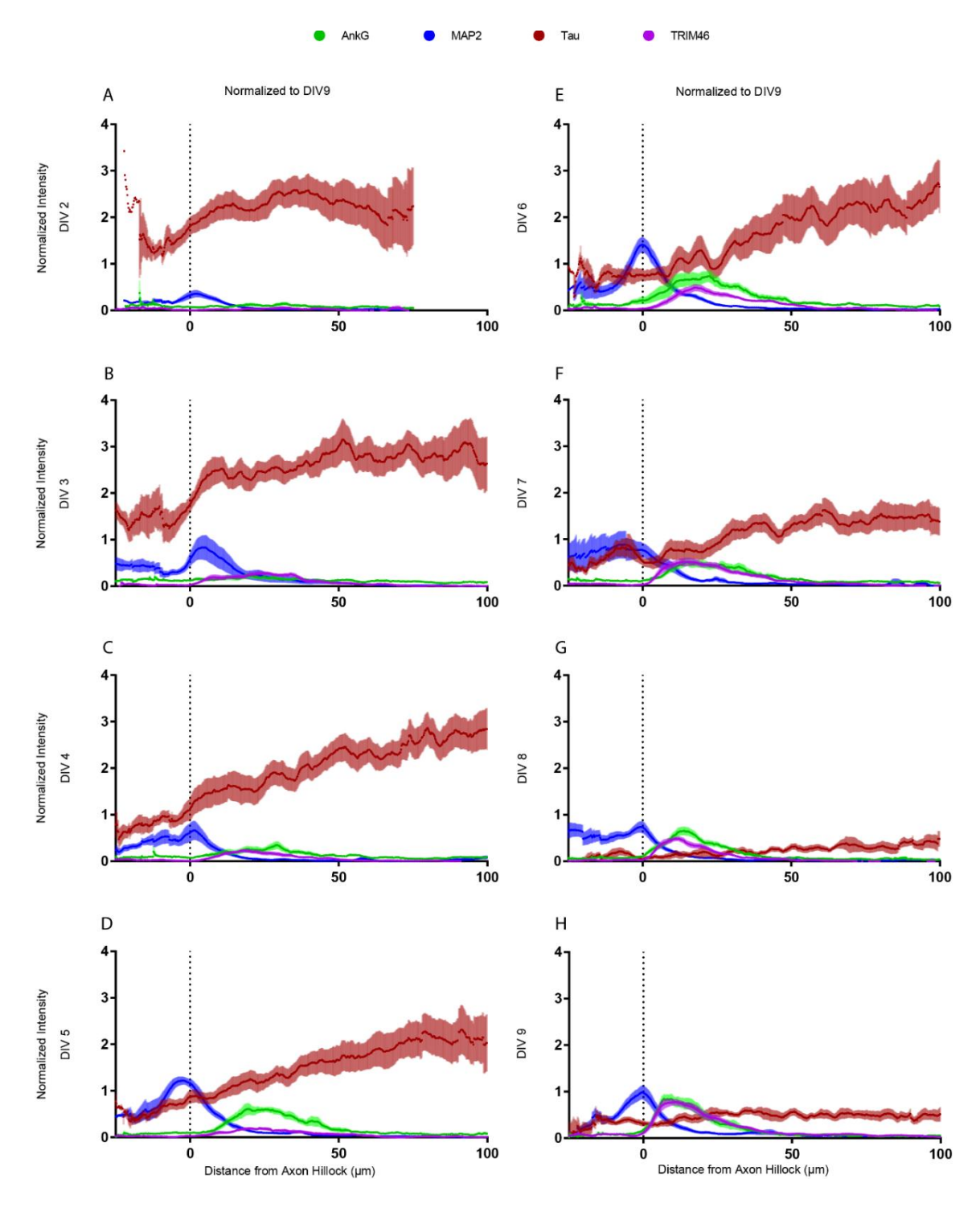


Figure 2.3: Intensity profiles from DIV 2-9 normalized to DIV9 levels show decrease in total tau expression and increase of TRIM46, AnkG, and MAP2.

(A-H) Smoothed intensity profiles for Ankyrin-G (green), MAP2 (blue), Tau (red), and TRIM46 (purple) normalized to a 0-1 maximum intensity of the DIV9 average demonstrate relative

Figure 2.3 (cont'd)

changes in magnitude of protein expression during the developmental time course *in vitro*. Relative to DIV 9, overall tau expression is highest during DIV2-6 and decreases from DIV7-9. Tau distribution starts in both the soma and the axon and as the neurons mature the differential distribution between the soma and axon is exacerbated, which is maintained up to DIV9. MAP2 expression is lower at DIV2 than DIV9 but quickly reaches levels at or near DIV9 levels by DIV3. Both TRIM46 and AnkG start much lower at DIV2 than at DIV9 and during the developmental time course they do not start approaching DIV9 levels until DIV6-8. The emergence of TRIM46 AIS localization and differential axosomatic distribution of tau is apparent at DIV3, while AnkG AIS localization does not occur until DIV4. Data represent mean \pm SEM (n=15-20 individual neurons analyzed per stain).

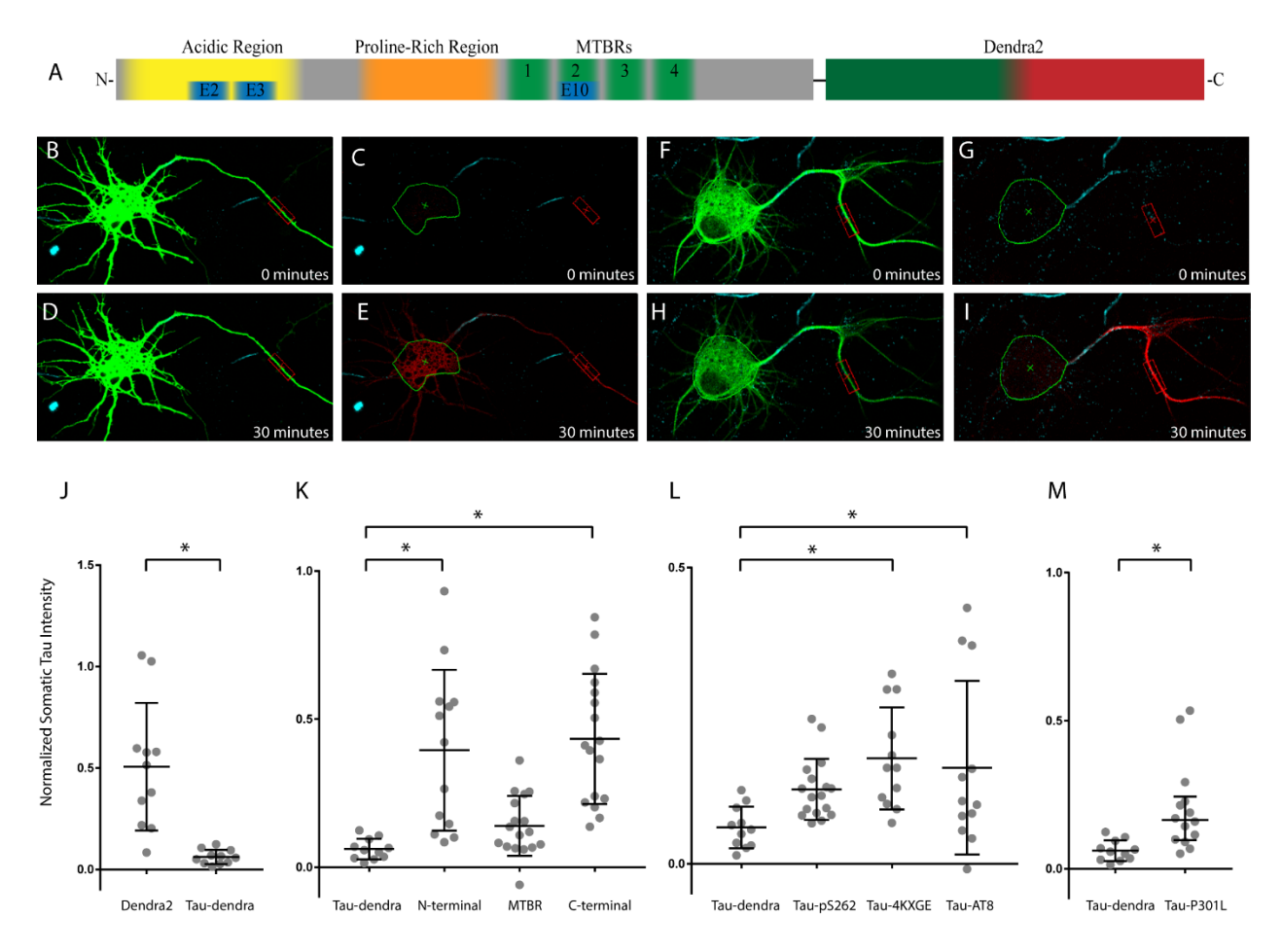


Figure 2.4: Retrograde diffusion of tau is dependent on the microtubule binding region and increases with disease-related modifications.

(A) Representation of the tau protein with C-terminal dendra2 photoconvertible fluorophore. (B-E) The unconverted dendra2 protein (green) is stimulated within the red box where it is photoconverted to red fluorescent protein starting at T=0 (C) and proceeds to freely diffuse into the soma (E, green outline). The change of somatic photoconverted dendra2 represents the amount of diffusion from the axon, across the axon initial segment (AIS, cyan), and into the soma. It is normalized by dividing the change in converted tau intensity (red) by the starting axonal unconverted dendra2 intensity (green). (F-I) Tau-dendra is photoconverted in the axon, but its diffusion is obstructed by the AIS, resulting in less accumulation in the soma (I) after 30 minutes. (J) There is significantly more axosomatic diffusion of dendra2 alone when compared

Figure 2.4 (cont'd)

to tau-dendra (t = 4.671, p = 0.0001). (K) Comparison of the diffusion of tau domains shows that the N-terminal domain ($F_{3,54}$ = 14, p = 0.0001) and C-terminal domain ($F_{3,54}$ = 14, p < 0.0001) diffuse past the AIS significantly more than tau-dendra, but the MTBR does not ($F_{3,54}$ = 14, p = 0.625). (L) Pseudophosphorylation of the tau protein significantly increases somatic diffusion of tau-4KXGE ($F_{3,48}$ = 3.941, p = 0.0079) and tau-AT8 ($F_{3,48}$ = 3.941, p = 0.0257), but not tau-ps262 ($F_{3,48}$ = 3.941, p = 0.1839). Data represent mean \pm SD. (M) The tau-P301L protein diffuses (median = 0.1651) into the soma significantly more than tau-dendra (median = 0.0673) (data represent median \pm interquartile range; U = 51, p = 0.031). For all comparisons * p < 0.05.

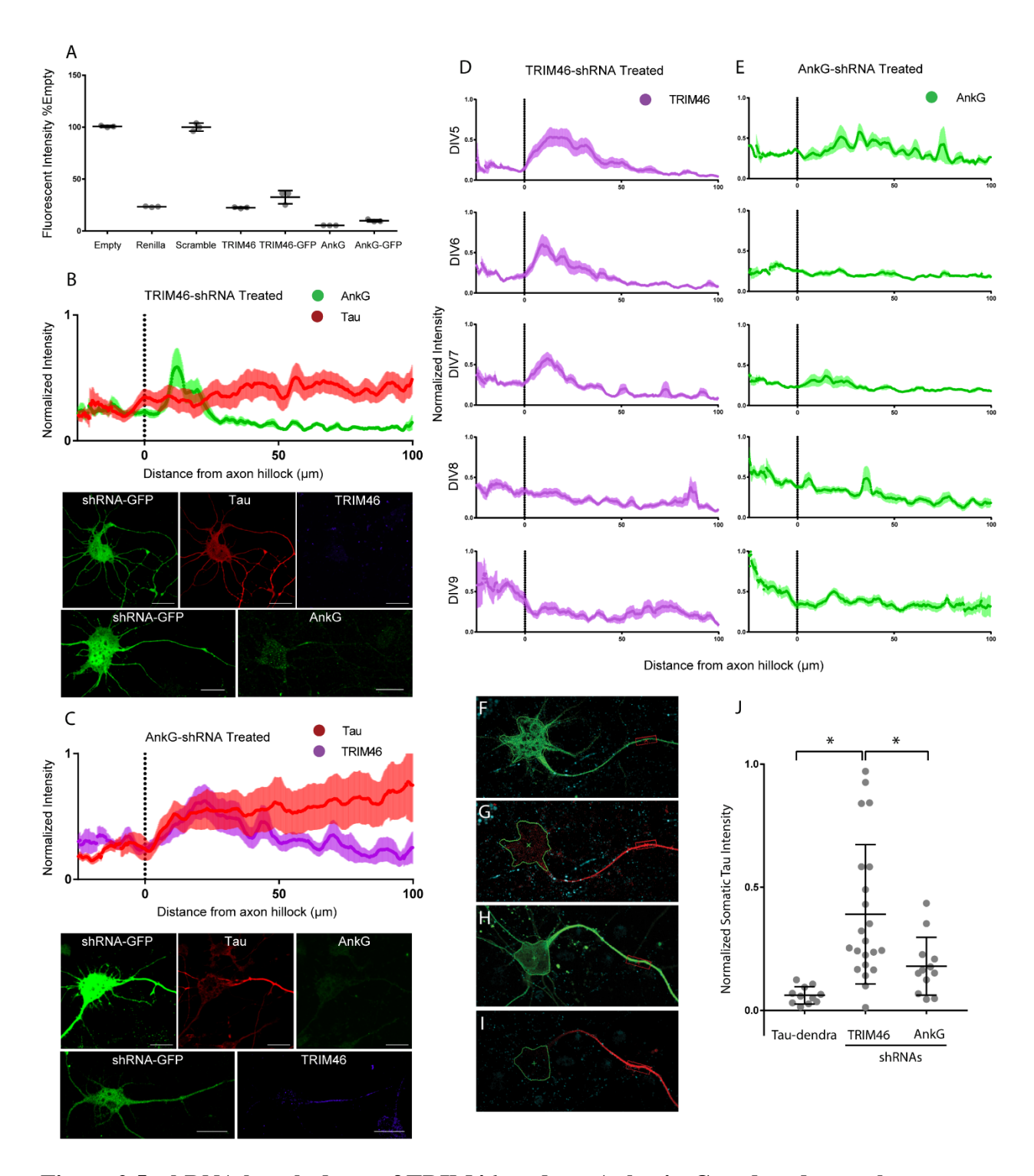


Figure 2.5: shRNA knock-down of TRIM46, and not Ankyrin-G, reduced axonal tau enrichment and increase axosomatic tau diffusion.

(A) The Dual-Luciferase Reporter assay was used to validate shRNA constructs, showing ~80% knockdown of TRIM46 and ~90% knockdown of Ankyrin-G (AnkG) expression in HEK293

Figure 2.5 (cont'd)

cells compared to no shRNA or scrambled shRNA control. The shRNAs were similarly effective whether they were in plasmids with or without the GFP reporter construct. (B) Intensity profiles of neurons treated with TRIM46-shRNA for 4 days (treatment at DIV4) and stained for tau and AnkG shows reduced axonal enrichment of tau at DIV8 without disruption of AnkG localization to the axon initial segment (AIS). Representative images of neurons positive for shRNA-GFP, tau (red), TRIM46 (purple), and AnkG (green). (C) Intensity profiles of AnkG-shRNA treated neurons at DIV8 stained for tau and TRIM46 indicate that there was no disruption of tau distribution or TRIM46 enrichment at the AIS. Representative images of neurons positive for shRNA-GFP, tau (red), TRIM46 (purple), and AnkG (green). (D-E) Time-course of neurons treated at DIV4 with shRNA for TRIM46 (D) or AnkG (E) show reduction of both AIS proteins in the AIS at DIV8. (F-G) TRIM46-shRNA treated neurons show tau-dendra diffusion into the soma at DIV8. (H-I) AnkG-shRNA treated neurons do not exhibit axosomatic tau diffusion in live-cell analysis. (J) Quantification of the levels of tau that diffused from the axon to the soma shows significantly more tau-dendra in the soma after TRIM46-shRNA treatment compared to no shRNA ($F_{2,42} = 10.08$, p = 0.0003) or AnkG-shRNA ($F_{2,42} = 10.08$, p = 0.0223). AnkGshRNA treatment did not increase the axosomatic diffusion of tau ($F_{2,42} = 10.08$, p = 0.4589). Scale bar is $10\mu m$ in (B-C). Cell intensity profile data represent mean \pm SEM (n=12-24 individual neurons analyzed per stain). Live-cell data represent mean \pm SD. * P < 0.05.

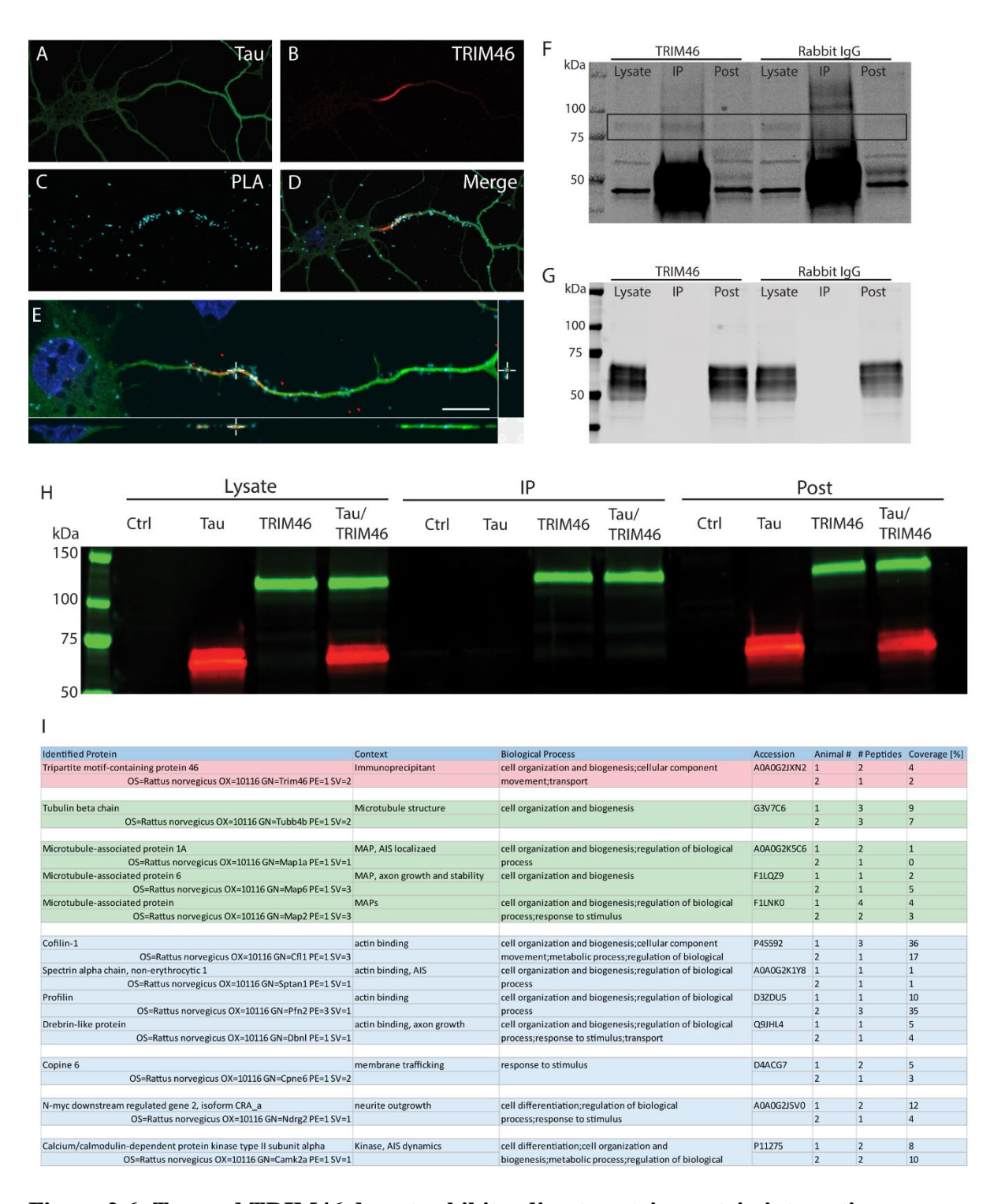


Figure 2.6: Tau and TRIM46 do not exhibit a direct protein-protein interaction

(A-D) Proximity ligation assay for tau and TRIM46 shows colocalization in PLA signal at the site if the AIS. (E) Confocal z-stack shows colocalization of tau and TRIM46 within the AIS. (F) Immunoblot of TRIM46 in samples of rat hippocampal lysate immunoprecipitated (IP) for

Figure 2.6 (cont'd)

TRIM46 or rabbit IgG control. TRIM46 band is present in the lysate and IP sample of TRIM46 IP but not the rabbit IgG control. Post IP flow through shows depletion in TRIM46 in the TRIM46 IP, but not in the rabbit IgG control IP. (G) Immunoblot of tau in samples of rat hippocampal lysate IP for TRIM46 or rabbit IgG control shows no pull-down of tau with TRIM46 or Rb IgG. (H) Immunoblot of Hek293 IP with TRIM46-halo (green) and tau (red) shows successful pull-down of TRIM46-halo, but no tau was detected. (I) Identified proteins from mass spectrometry of TRIM46 IP from two rat hippocampal lysates show identification of TRIM46 (red) interactions with tubulin and microtubule-associated proteins (green), and axon cytoskeleton related proteins (blue).

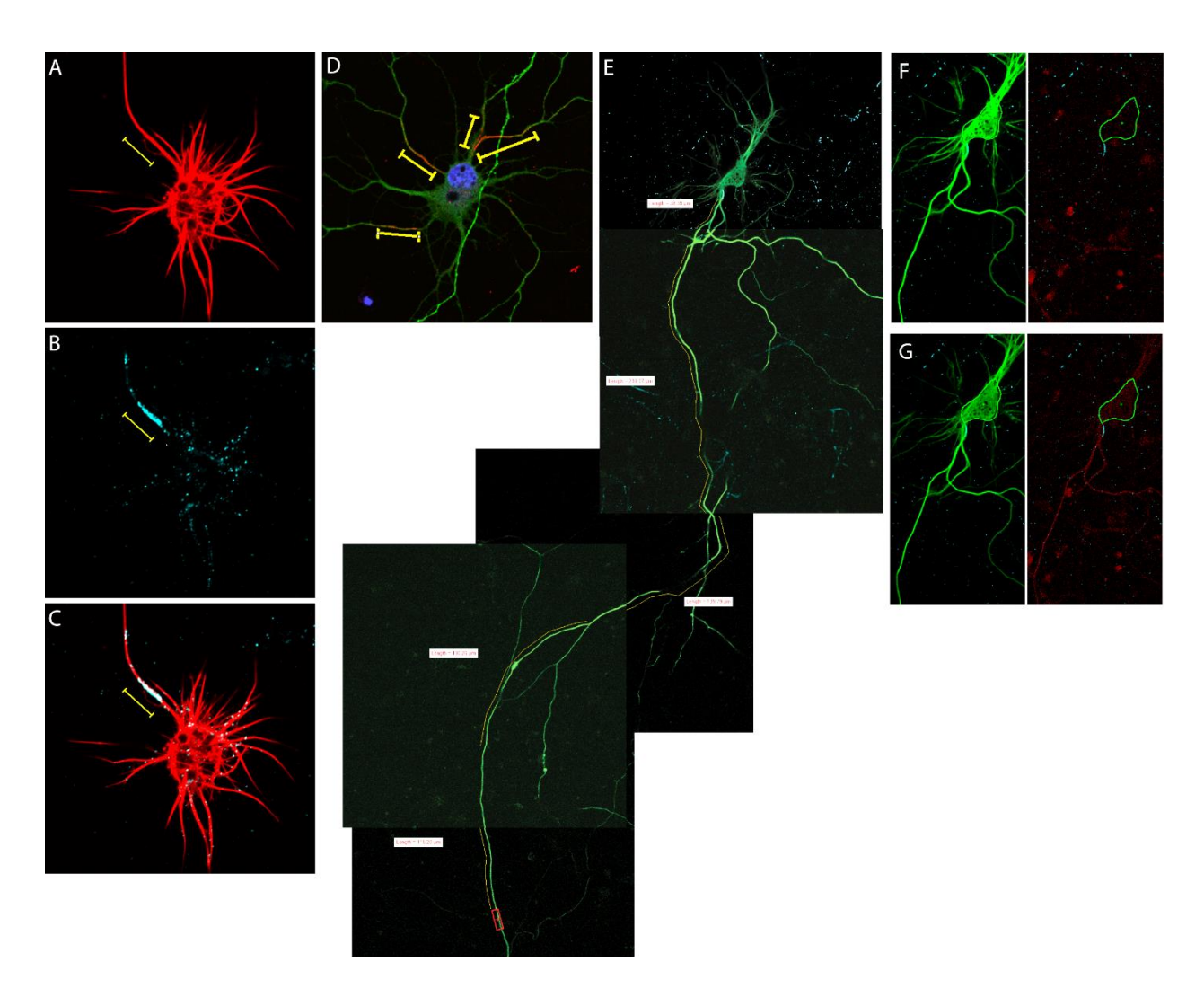


Figure 2.7: Positive identification of axonal processes and validation of retrograde diffusion potential.

(A-C) Tau-dendra (red, A) expressing neuron stained with the live-cell neurofascin labeling technique (cyan, B) indicates that the AISs are readily labeled, and as described previously (Dumitrescu *et al.*, 2016); the neurons remain intact and appear healthy (merged image, C). (D) Neuron stained for TRIM46 (red) and Tau (green) showing a neuron with 4 developed axons, which would be excluded from analysis. (E) Neuron transfected with Tau-dendra demonstrating retrograde diffusion potential (i.e. the distance converted axonal tau can diffuse without a barrier) from photoconversion in distal axon. (F-G) Enlargement of soma and proximal axon of

Figure 2.7 (cont'd)

(E) before photoconversion (F) showing no converted tau in the axon (red) and after photoconversion (G) demonstrating diffusion of tau into the proximal axon that was $636.71\mu m$ from the point of conversion in the distal axon.

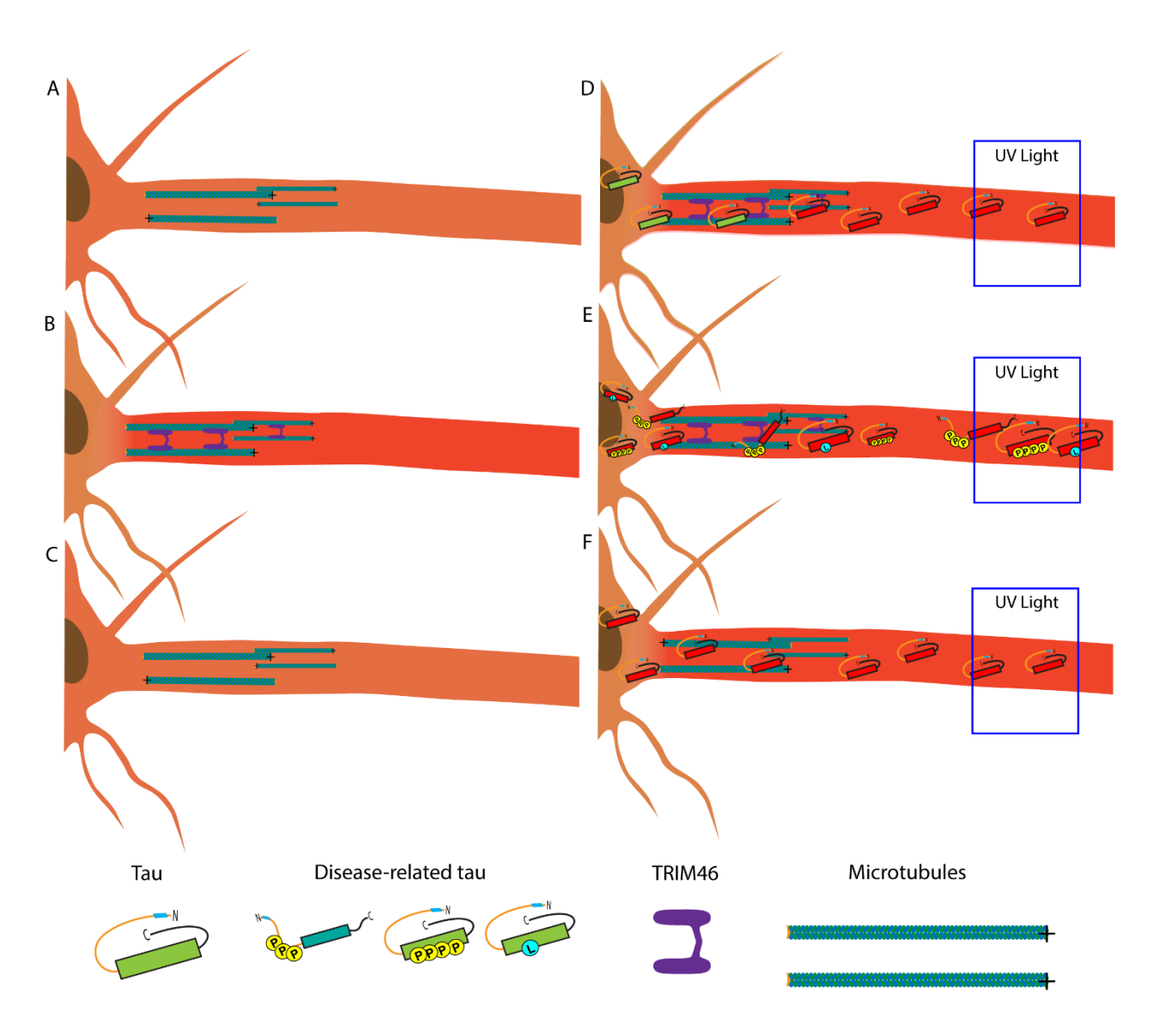


Figure 2.8: TRIM46 mediates axonal tau enrichment and inhibits axosomatic diffusion.

(A) A DIV2 neuron does not exhibit axonal tau (orange-red shading) enrichment and AIS proteins (i.e. TRIM46 or AnkG are not present). (B) Localization of TRIM46 to the axon initial segment (AIS) at DIV3 corresponds to axonal tau enrichment. (C) Knockdown of TRIM46 with shRNA causes reduction in differential tau distribution, at least in part, due to the disorganization of MTs (e.g. reversed orientation) loss of TRIM46 causes (van Beuningen *et al.*, 2015). (D) Wild-type tau (represented by Tau-dendra) exhibits impaired axosomatic diffusion at the AIS, which is dependent on MT binding. (E) Disease-related tau modifications (e.g. 4KXGE, AT8,

Figure 2.8 (cont'd)

and P301L) increase axosomatic diffusion of tau, likely due to reduced MT binding affinity (Sun & Gamblin, 2009). (F) TRIM46-shRNA reduces TRIM46 at the AIS leading to disruption of MT organization (e.g. reversal of orientation) and increased diffusion of tau into the soma.

Table 2.1: An interaction between tau and TRIM46 was not detected with multiple methods of co-immunoprecipitations using HEK293 cells, primary hippocampal culture, and hippocampal brain lysates.

Source	Pull-down target	TRIM46 Expression	Tau Expression	Method	Crosslinking	Lysis Buffer *	Wash Buffer *	Result
HEK 293 Cells	TRIM46	TRIM46-Halo	Tau	HaloLink Resin	No	Tris Standard	Tris	No tau
						Tris TritonX-100	Tris	No tau
						Tris NP-40	Tris	No tau
						Tris No Detergent	Tris	No tau
						HEPES	HEPES	No tau
						X/2	X/2	No tau
					0.5%	Tris Standard	Tris	No tau
					1.0%	Tris Standard	Tris	No tau
				Magne HaloTag Beads	No	Tris Standard	Tris	No tau
		TRIM46	Tau	TRIM46 Antibody NHS Mag Sepharose	No	Tris Standard	Tris	No tau
		TRIM46-Flag	Tau	Anti-FLAG M2 Magnetic Beads	No	Tris Standard	Tris	No tau
	Tau	TRIM46	Tau-Halo	HaloLink Resin	No	Tris Standard	Tris	No tau
Primary Hippocampal Culture	TRIM46	Endogenous	Endogenous	TRIM46 Antibody NHS Mag Sepharose	No	Tris Standard	Tris	No tau
					0.5%	Tris Standard	Tris	No tau
Hippocampal Lysates	Tau	Endogenous	Endogenous	Tau-1 Antibody NHS Mag Sepharose	No	Tris Standard	Tris	No TRIM46
				Tau 5 Antibody NHS Mag Sepharose	No	Tris Standard	Tris	No TRIM46
				Tau7 Antibody NHS Mag Sepharose	No	Tris Standard	Tris	No TRIM46
	TRIM46	Endogenous	Endogenous	TRIM46 Antibody	No	Tris Standard	Tris	No tau
				NHS Mag Sepharose		Tris No Detergent	Tris	No tau

^{*} Buffer recipes can be found in the methods section above.

 Table 2.2: TRIM46 immunoprecipitation mass spectrometry

B 1.0			Coverage	#	#	# Unique	,, , ,	MW G D 1
Description		Accession	[%]	Peptides		_		MW [kDa]
Tripartite motif-containing protein 46		A0A0G2JXN2	4		2	2	759	83.4
	Rat 2	A0A0G2JXN2	2		1	1	759	83.4
Tubulin beta chain	Rat 1	G3V7C6	9		3	2	548	61.1
	Rat 2	G3V7C6	7		9	1	548	61.1
Microtubule-associated protein 1A	Rat 1	A0A0G2K5C6	1	2	2	2	3014	325.4
	Rat 2	A0A0G2K5C6	0		1	1	3014	325.4
Microtubule-associated protein 6	Rat 1	F1LQZ9	2	1	1	1	952	100.4
	Rat 2	F1LQZ9	5		1	1	952	100.4
Microtubule-associated protein	Rat 1	F1LNK0	4	4	4	4	1942	210.6
	Rat 2	F1LNK0	3	2	2	2	1942	210.6
Cofilin-1	Rat 1	P45592	36	3	5	3	166	18.5
	Rat 2	P45592	17	1	3	1	166	18.5
Spectrin alpha chain, non-	Rat 1	A0A0G2K1Y8	1	1	1	1	2498	287.5
erythrocytic 1	Rat 2	A0A0G2K1Y8	1	1	1	1	2498	287.5
Profilin	Rat 1	D3ZDU5	10	1	1	1	148	16
	Rat 2	D3ZDU5	35	3	4	3	148	16
Drebrin-like protein	Rat 1	Q9JHL4	5	1	1	1	436	48.6
	Rat 2	Q9JHL4	4	1	1	1	436	48.6
Copine 6	Rat 1	D4ACG7	5	2	2	1	557	61.7
	Rat 2	D4ACG7	3	1	3	1	557	61.7
N-myc downstream regulated gene	Rat 1	A0A0G2JSV0	12	2	3	2	371	40.7
2, is of orm CRA_a	Rat 2	A0A0G2JSV0	4	1	1	1	371	40.7
Calcium/calmodulin-dependent	Rat 1	P11275	8	2	4	1	478	54.1
protein kinase type II subunit alpha	Rat 2	P11275	10	2	2	2	478	54.1
Protein kinase C gamma type	Rat 1	P63319	4	1	1	1	697	78.3
	Rat 2	P63319	2	1	1	1	697	78.3
Phosphatidylethanolamine-binding	Rat 1	P31044	11	1	1	1	187	20.8
protein 1	Rat 2	P31044	18	2	2	2	187	20.8
Synapsin-1	Rat 1	P09951	2	1	1	1	704	73.9
	Rat 2	P09951	2	1	1	1	704	73.9
Endophilin-A1	Rat 1	O35179	9	1	1	1	352	39.9
	Rat 2	O35179	3	1	1	1	352	39.9
Transformer-2 protein homolog beta	Rat 1	P62997	6	1	1	1	288	33.6
	Rat 2	P62997	6	1	1	1	288	33.6
LUC7-like 3 pre-mRNA-splicing	Rat 1	D3ZFB2	3	1	1	1	491	58.4
factor	Rat 2	D3ZFB2	3		1	1	491	58.4
2',3'-cyclic-nucleotide 3'-	Rat 1	P13233	3		1	1	420	47.2
phosphodiesterase	Rat 2	P13233	3		1	1	420	47.2

CHAPTER 3

Aging Does Not Affect Axon Initial Segment Structure and Somatic Localization of Tau Protein in Hippocampal Neurons of Fischer 344 Rats

INTRODUCTION

Alzheimer's disease (AD) is the most prevalent neurodegenerative disease of individuals over the age of 65, and affects over 6.4 million adults in the United States (James et al., 2014). The leading risk factor for developing the disease is aging, and while the cause of AD is still unclear, the accumulation of inclusions comprised of tau protein is a hallmark of the disease (Santuccione et al., 2013). It remains unclear whether changes in the distribution of tau that are reminiscent of AD-related changes, such as accumulation in the somatodendritic compartment, occur during normal aging. Aged Fischer 344 rats are commonly used for aging research and exhibit age-related behavioral deficits of learning and memory as well as motor impairment (Spangler et al., 1994; van der Staay & Blokland, 1996; Cochran et al., 2014). Additionally, aging causes altered neuronal protein expression, axonal atrophy, and some gliosis in the F344 rat model (Parhad et al., 1995). For example, glial fibrillary acidic protein (GFAP) is shown to increase significantly in the hippocampus of aged rats both with and without cognitive impairment (VanGuilder et al., 2011). Thus, Fischer 344 rats are a good model to recapitulate factors of human aging (van der Staay & Blokland, 1996) and determining whether aging effects the AIS and tau distribution. The underlying hypothesis is that aging causes alterations in AIS integrity and tau mislocalization, which may represent events that contribute to aging as a strong risk factor for AD.

Tau, a microtubule-associated protein, is thought to contribute to the development and progression of AD pathology, but the mechanisms behind tau toxicity remain largely unknown. Age-related accumulations of tau were reported in some non-human primate brains (Oikawa *et al.*, 2010; Perez *et al.*, 2013), yet systematic analysis of the cellular localization of tau accumulation across aging is not well studied. Unfortunately, human tissue studies are often limited in scope across age groups making it hard to appreciate changes from young to old age. In healthy neurons, tau is enriched in the axonal compartment, where it may stabilize microtubules and play a role in regulating axonal functions such as transport (Tytell *et al.*, 1984; Binder *et al.*, 1986; Kanaan *et al.*, 2013). The redistribution of tau from the axonal compartment to the somatodendritic compartment is thought of as an important event in tau-mediated neurotoxicity (Buee *et al.*, 2000). The preferential localization of tau in axons is mediated, at least in part, by the axon initial segment (AIS), which acts as a retrograde barrier for freely diffusing tau (Li *et al.*, 2011; Sun *et al.*, 2014; Zempel & Mandelkow, 2014; Sohn *et al.*, 2016).

Importantly, very little is known about the connections between aging, the AIS, and tau distribution. The AIS is a selective diffusion barrier separating the axonal compartment from the somatodendritic compartment (Winckler *et al.*, 1999). The establishment of the AIS creates a filter that regulates intracellular traffic based on protein size or the type of motor proteins carrying cargo along microtubules (Song *et al.*, 2009; Leterrier & Dargent, 2013). Ankyrin G (AnkG) is well established as a necessary protein for the development and maintenance of the AIS as a selective filter, as well as a necessary protein for developing and maintaining axonal polarity (Zhou *et al.*, 1998; Hedstrom *et al.*, 2008). AnkG also has an integral role in recruiting and binding structural proteins to the AIS, such as βIV-spectrin and neurofascin (Hedstrom *et al.*, 2007; Freal *et al.*, 2016). Interestingly, a single previous report showed that some structural

proteins in the AIS (specifically ankyrin) are reduced with age in wild-type mice (Bahr *et al.*, 1994). Thus, we set out to determine whether the structure of the AIS and/or tau localization is altered during normal aging. Our data show that AIS structure, levels of multiple AIS proteins, and the distribution of tau in hippocampal (HP) neurons are not altered with advancing age in Fischer 344 rats.

METHODS

Animals

Young adult (4 months), middle-aged (14 months) and aged (24 months) male Fischer 344 rats were used for all experiments. Six animals per age group (n=6) were used to obtain fixed tissue for histological analysis while five or six animals (n=5-6) per age group were used for fresh brain homogenate. The animals were provided rat chow and water *ad libitum* and housed in a reverse light-dark cycle room. All animal studies were performed in accordance with standard regulations and were approved by the Michigan State University Institutional Animal Care and Use and Committee.

Tissue processing

Animals used for collection of fresh brain tissue were transcardially perfused with 200 ml of 0.9% saline containing heparin (10,000 U/L). The brains were extracted and the HP was dissected and frozen on dry ice. For collection of fresh tissue for AnkG immunoblotting, animals were perfused for 5 minutes with saline containing heparin. The extracted HPs were then immediately frozen in liquid nitrogen and stored in liquid nitrogen until processing for AnkG immunoblotting. To collect fixed tissue, the saline perfusion was followed by 200 ml phosphate

buffered 4% paraformaldehyde. The brains were post-fixed in 4% paraformaldehyde for 24 hours. After post-fixation, the brains were embedded into gelatin blocks for sectioning (Smiley & Bleiwas, 2012). The gelatin block was equilibrated in 20% glycerol. The gelatin block was cut into 40 µm thick coronal sections on a freezing, sliding stage microtome. Sections were stored in cyroprotectant until processed for immunohistochemistry or immunofluorescence.

Immunoblotting

Tissue from the HP was homogenized in 300 μl of 10 mM Tris/1 mM EDTA/0.8 mM NaCl/10% sucrose buffer containing protease and phosphatase inhibitors (10 μg/ml pepstatin, 10 μg/ml leupeptin, 10 μg/ml bestatin, 10 μg/ml aprotinin, 1mM PMSF; 10 mM β-glycerophosphate, 1 mM sodium orthovanadate, 10 mM sodium fluoride, 1 mM tetra-sodium pyrophosphate decahydrate), using a sonicator (XL-2000, Misonix, Farmingdale, NY, 10X 1 sec bursts at power level 1). Lysates were cleared of cellular debris by centrifugation at 22,000 x g for 20 min at 4°C. The resulting supernatants were collected for analysis and the total protein content was assessed using the Bradford protein assay (B6916, Sigma, St. Louis, MO). The samples were diluted in Laemelli buffer and heated to 95°C for 10 minutes. Lysate samples separated using SDS-PAGE (50 μg total protein/lane for AIS proteins; 20 μg/lane for tau protein) on 4-20% Criterion TGX (Bio-Rad, Hercules, CA) gradient gels at 250V and transferred to nitrocellulose membranes for 50 minutes (66458; Pall Life Sciences, Port Washington, NY) to quantify the amount of AIS proteins and tau between age groups (n = 5/group).

Due to the large size of the AnkG protein, a blotting protocol optimized for large molecular weight proteins was used (Fairbanks *et al.*, 1971; Davis & Bennett, 1982; Bolt & Mahoney, 1997). The flash frozen hippocampi were dropped into 9 volumes of urea buffer (8 M

urea, 5% SDS, 5 mM N-ethyl maleimide, 10 mM HEPES, 10 ug/ml leupeptin, 10 ug/ml pepstatin) at 65°C and immediately pulverized with an Eppendorf tube pestle (#12-141-363, Thermo Fisher) for 10 seconds and then sonicated, as described above. The samples were then diluted in Laemelli buffer and heated to 95°C for 10 minutes. The protein concentrations of the resulting lysate samples were measured using the SDS Lowry protein assay as described (Cox *et al.*, 2016). Lysate samples (100 μg/lane; n = 6/group) were separated using SDS-PAGE on 3-8% Criterion XT Tris-Acetate in XT buffer (Bio-Rad, Hercules, CA) gradient gels at 150V and transferred to nitrocellulose membranes in transfer buffer (40mM Tris, 20 mM sodium acetate, 2 mM EDTA, pH 7.4, 20% (v/v) methanol, 0.05% (w/v) SDS) for 120 minutes at 10V. After transferring, the blots were stained with Ponceau S (0.04% (w/v) Ponceau S (#P3504, Sigma), 0.1% (v/v) acetic acid) for 5 minutes followed by 2 x 5 minute washes in 5% acetic acid (v/v) and then 2 washes in water. The blots were imaged before proceeding to blocking and Ponceau bands were used to normalize the quantified AnkG signals.

All membranes were blocked in 2% nonfat dry milk in Tris-buffered saline (NFDM-TBS; Tris 50 mM, NaCl 150 mM, pH 7.4) for 1 h at room temperature and incubated with primary antibody in NFDM-TBS overnight at 4°C. Blots were probed with Ankyrin G antibody (H-215, Santa Cruz sc-28561, 1:2,000), βIV-spectrin (NeuroMab #75-377, 1:1,000), Neurofascin (NeuroMab #75-172 1:1,000), SMI312 (abcam, ab24574, 1:20,000), R1 (1:100,000, (Berry *et al.*, 2004)), Tau7 (1:500,000, (Horowitz *et al.*, 2006)), AT8 (phospho-Ser199/Ser202/Thr205, 1:10,000), PHF-1 (phospho-Ser396/Ser404, 1:50,000), phospho-Ser422 (1:2,000), βIII-tubulin antibody (Tuj1, 1:10,000; (Caccamo *et al.*, 1989)), GFAP (G3893 Sigma, 1:2000), and loading control glyceraldehyde 3- phosphate dehydrogenase (GAPDH, Cell Signaling, 5174, 1:2,000). After incubation with primary antibodies, the membranes were washed in TBS/0.1% Tween 20

and incubated in appropriate species-specific IRDye 680RD or 800CW secondary antibodies (1:20,000 in NFDM-TBS; LI-COR Biotechnology, Lincoln, NE). The membranes were washed and the reactivity visualized with a LI-COR Odyssey infrared imager. The signal intensity for each band was quantified using the Licor Image Studio software (v5.2) and signal intensities for AIS proteins or tau are expressed as a ratio to GAPDH signal intensities. AnkG 270kDa and 480kDa are expressed as a ratio of the Ponceau S intensity of a protein band at ~200kDa. The intensities of GAPDH and Ponceau that were used as loading controls for normalization of immunoblotting signals were not changed across age (GAPDH: Figure 3.1L, F_{2, 12} = 0.001261, p = 0.9987; Figure 3.1C Ponceau S: F_{2, 15} = 1.322, p = 0.2959).

Immunohistochemistry and immunofluorescence

A one in six series of tissue sections were processed for each age group (n = 6) for immunohistochemical detection of Ankyrin G. The tissue was rinsed in 0.1M Tris-buffered saline (TBS; pH 7.4) containing 0.5% Triton X-100 (TBS-Tx) 6 times for 10 minutes each. The tissue was then incubated in 3% H₂O₂ in TBS-Tx for 1 h at room temperature to quench endogenous peroxidase activity, and then rinsed again. An avidin/biotin blocking kit (Vector Labs SP-2001) was used to block endogenous avidin in the gelatin matrix. Non-specific antibody binding was inhibited by incubating the tissue in blocking buffer (10% goat serum (GS)/2% bovine serum albumin/0.5% TBS-Tx) for 1 h at room temperature. The tissue was then incubated over night at 4°C with rabbit anti-ankyrin G primary antibody (H-215, Santa Cruz sc-28561, Dallas, TX) 1:1,000 in dilution buffer (2%GS/0.5% TBS-Tx). The tissue was rinsed (6 X 10 minutes in 0.5% TBS-Tx) and incubated for 2 hours in biotinylated goat anti-rabbit secondary antibody (BA-1000, Vector, Burlingame, CA) at a concentration of 1:500 in dilution buffer. The

tissue was then rinsed again and incubated in avidin-biotin complex (ABC) solution (PK-6100, Vector) for 1hour. The ABC solution contained 50 μl of solution A and 50 μl of solution B in 10 ml TBS made according to the manufacturer's instructions. After rinsing the tissue, the staining was developed using 3,3'-Diaminobenzidine (DAB, D5637, Sigma) solution (50 mg/mL /0.5%TBS-Tx/0.003% H₂O₂) for 12 minutes. The tissue was then rinsed, mounted on microscope slides, and coverslipped with CYTOSEAL 60 (#8310-16, Thermo Scientific, Waltham, MA).

A one in six series of tissue sections (n = 6/group) was used for the immunofluorescent labeling of tau. All tissue was stained simultaneously in staining dishes using the same reagents. Non-specific antibody binding was inhibited by incubating the tissue in blocking buffer (10% goat serum (GS)/2% bovine serum albumin/0.5% TBS-Tx) for 1 h at room temperature. The tissue was then incubated over night at 4°C with mouse anti-tau primary antibody (Tau7; 1:3,500) in dilution buffer (2% GS/0.5% TBS-Tx). The tissue was rinsed (6 X 10 minutes in 0.5% TBS-Tx) and incubated for 2 hours in Alexa Fluor 488-conjugated goat anti-mouse IgG (H+L) (#A-11001, Thermo Fisher) at a concentration of 1:500 in dilution buffer. The tissue was then incubated in DAPI (0.5 µg/mL in 0.5% TBS-Tx for 10 minutes), rinsed (5 X 10 minutes in 0.5% TBS-Tx), and the sections were mounted on microscope slides. To block endogenous autofluorescence, the tissue was treated with Sudan black. The slides were incubated in 70% ethanol for 2 minutes, then in a saturated solution of Sudan Black B (Fisher, #AC419830100) for 5 minutes. The slides were then differentiated in 70% ethanol until background (grey matter) was pale grey and rinsed in dH₂O (2 x 3 minutes). The slides were then coverslipped using vectashield hardset mountant (H-1400, Vector) (Kanaan et al., 2008).

Stereology

The spaceballs stereological probe is an unbiased and systematic stereological sampling method to estimate the total length of a population of fibers in 3D space, and this probe was used to quantify AIS length in the HP of rats. This stereological method was performed using serial sections (1 in 6 series). Sampling grids (i.e. CA: $500\mu m \times 500\mu m$; DG: $200\mu m \times 500\mu m$) were chosen for each region to allow for ~200 fiber intersections to be counted in the HP for each hemisphere and to yield a Gunderson coefficient of error < 0.1 for all samples. The mean coefficient of error was 0.058 ± 0.001 (SEM). A hemisphere probe with a radius of 11 μm was used to sample sites throughout the HP. The mean measured tissue thickness was ~13-14 μm . A 4x objective was used to outline each region and a 60x oil objective lens (1.35 numerical aperture) was used for all stereological counts.

The AutoNeuron probe in Neurolucida (MBF Bioscience) was used to acquire measurements of individual AIS length, volume and diameter in the regions of the HP (CA1, CA2, CA3 and dentate gyrus) in young, middle and old aged animals. In each region, an image stack was acquired with a 60x oil objective lens through the complete depth of each section at a step-size of 0.5 μm. A 3D representation of each individual AIS in the HP was created in the software using the following settings for AutoNeuron: Image Type: Brightfield; Max Process Diameter: 2.00 μm; XY Region: All; Z Range: All; Trace Somas: No; Soma Sensitivity: 50; Min Soma Diameter: 2.00 μm; Seed Detection Sensitivity: 70; Seed Response Filter: 4; Tracing Sensitivity: 60; Tolerance to Gaps: Low; Connect Branches: No. These settings were chosen to best detect the AIS of each neuron, while not falsely detecting background tissue stain or failing to differentiate individual AISs.

Cellular protein quantification

The tau immunofluorescence stained tissue was imaged on a Nikon AI confocal system and a Nikon Eclipse Ti microscope with a 40x oil objective (1.30 numerical aperture). Image stacks (0.5 µm step size) were acquired of neurons in each HP region (CA1, CA2, CA3, and the dentate gyrus) using acquisition settings in the linear range of fluorescent intensity without saturation of tau signal and the same acquisition settings were used for all animals. Four image stacks were acquired per animal. The neurons were analyzed with NIS Elements (v4.30, Advanced Research, Nikon, Melville, NY). The average intensity of Tau7 immunofluorescent signal was measured in the soma of individual pyramidal neurons in all CA regions (CA1, CA2, and CA3). Cells were chosen as randomly as possible, but only cells with an entire cross-section through the middle of the cell (i.e., the z-slice with the largest nuclear width) within the acquired z-stack and without overlapping cell bodies were used for analysis. To increase the rigor of this analysis, the experimenter was blinded to the condition of the samples. A box (~8-12 µm²) was drawn as large as possible inside the somatic compartment of each neuron, excluding the DAPI positive nuclei (Figure 3.3C-E). The mean value of fluorescence intensity was measured for each box within a total of 180 cells/animal/group. The density and small cytoplasm of dentate granule cells precludes the ability to reliably measure signal intensity within individual cells. Instead, the average fluorescence intensity within a rectangular box (~5000 µm²; 6 boxes/animal/group) was used to perform a regional analysis of immunofluorescence signal intensity within the dentate gyrus (Figure 3.3F-I).

For axonal tau intensity measurements, a 4x objective (0.13 numerical aperture) was used to capture 2-3 images of the dorsal hippocampus in 3 serial tissue sections per animal. The entire visible regions of the fimbria, alveus, stratum lacunosum, and stratum moleculare were outlined

in NIS Elements software. The average fluorescent intensity per area was measured for each axonal region.

Statistical analyses

All data were analyzed using Prism software (v6.0) and all data are presented as mean ±standard error of the mean (SEM). Statistical significance between **age** groups was determined using one-way ANOVA. Significance was set at p<0.05. Tukey's post-hoc test was used for post-hoc comparisons when significance of p<0.05 was reached. If no overall significance was achieved, no post-hoc analyses were used.

RESULTS

Immunoblotting of AIS proteins and tau

Immunoblots of young, middle, and old age tissue were probed for AIS protein markers, including AnkG, β IV-spectrin, and neurofascin. When normalized to GAPDH loading controls, no changes were detected between aged groups (Figure 3.1D, E; β IV-spectrin $F_{2,12} = 0.1095$, p = 0.8972; Neurofascin $F_{2,12} = 0.3654$, p = 0.7014). AnkG protein bands were analyzed at 480kDa and 270kDa for the AIS-localized AnkG isoforms (Figure 3.1A; $F_{2,15} = 0.03397$, p = 0.9667), Figure 3.1B; $F_{2,15} = 0.08969$, p = 0.9147) (Kordeli *et al.*, 1995; Zhang & Bennett, 1998). Additional ankyrin G protein bands were detected at ~190kDa that did not change with age (data not shown), but these represent other canonical isoforms that are not specific to the AIS (Bennett & Baines, 2001). Blots were probed with SMI-312, an axon-specific neurofilament antibody, to confirm that aging-related axonal loss was not present in the HP. No change in the amount of SMI-312 was detected across age groups (Figure 3.1F; $F_{2,12} = 0.4304$, p = 0.6599).

There was no change across age groups in the levels of total tau protein as indicated by Tau7, a C-terminal pan-tau antibody (Figure 3.1G; $F_{2, 12} = 0.7686$, p = 0.4852). As a secondary method to confirm there were no changes in total tau levels we also probed blots with the R1 tau antibody, a pan-tau rabbit polyclonal antibody (Figure 3.1H; $F_{2, 12} = 0.6824$, p = 0.5240) and found no aging-related changes (Berry *et al.*, 2004; Horowitz *et al.*, 2006)). To determine whether specific tau phosphoepitopes were changed with aging in the hippocampus we probed blots with PHF1 antibody and found no differences (Figure 3.1I; $F_{2, 12} = 2.361$, p = 0.1366). We also probed with the AT8 antibody and the phospho-Ser422 antibody, both of which are disease-related modifications of tau (Guillozet-Bongaarts *et al.*, 2006; Jeganathan *et al.*, 2008) and found no signal for either epitope in young, middle or old age animals (data not shown). Tubulin was analyzed to measure the amount of microtubules as a control since tau is a microtubule-associated protein. There was no change in β III-tubulin across age groups (Figure 3.1J; $F_{2, 12} = 0.8679$, p = 0.4446).

As a positive control for detection of age-related changes of protein, blots were probed for GFAP, a protein previously shown to change in hippocampal lysates of aging rats (VanGuilder *et al.*, 2011). A significant increase in GFAP was found in the old rats compared to the young rats (Figure 3.1K; $F_{2, 16} = 4.529$, p = 0.0276).

Stereological assessment of AIS length and morphology

Stereological analysis of the AIS length (using the spaceballs probe in AnkG stained tissue) showed no differences in the total length of all AISs in the HP across age groups (Figure 3.2A; $F_{2, 15} = 0.07323$, p = 0.9297). We used the AutoNeuron module as a second method to analyze individual AISs in the CA1, CA2, CA3, and dentate gyrus regions of the hippocampus

and found that length did not change across age groups in any of these regions (Figure 3.2B; length: CA1: $F_{2,15} = 0.3940$, p = 0.6811; CA2: $F_{2,15} = 1.488$, p = 0.2573; CA3: $F_{2,15} = 1.770$, p = 0.2041; DG: $F_{2,15} = 1.413$, p = 0.2739). No aging-related change occurred in the volume or diameter of individual AISs in CA1, CA3 or DG (Figure 3.2C-D; volume: CA1: $F_{2,15} = 0.3936$, p = 0.6814; CA3: $F_{2,15} = 2.077$, p = 0.1599; DG: $F_{2,15} = 1.216$, p = 0.3241 and diameter: CA1: $F_{2,15} = 0.1559$, p = 0.8545; CA3: $F_{2,15} = 1.061$, p = 0.3706; DG: $F_{2,15} = 0.6705$, p = 0.5261). However, a small but significant change was detected in the volume and diameter of CA2 neurons when comparing young and old animals (Figure 3.2C-D; volume: CA2: $F_{2,15} = 4.460$, p = 0.0302; and diameter: CA2: $F_{2,15} = 4.062$, p = 0.0389). The measured length of the AIS in HP neurons was 32.86 μ m ± 1.99 in young, 32.33 μ m ± 1.379 in middle, and 31.53 μ m ± 1.361 in old aged animals (Figure 3.2B), consistent with previous findings in cultured hippocampal neurons (Grubb & Burrone, 2010; Leterrier *et al.*, 2015).

Optical density measurements of tau levels in somata and axonal layers of the hippocampus

Optical density measurements of Tau7 immunofluorescence in the somatic compartment of individual HP neurons in tissue sections showed no change across age groups (Figure 3.3A). Individual analysis of pyramidal neurons in the CA regions did not show an age-related difference (Figure 3.3A; CA1: $F_{2,15} = 1.775$, p = 0.2033; CA2: $F_{2,15} = 0.7810$, p = 0.4757; CA3: $F_{2,15} = 3.513$, p = 0.0561), nor did the dentate gyrus show a change in regional intensity with advancing age in rats (Figure 3.3A; $F_{2,15} = 1.924$, p = 0.1804). Analysis of tau intensity in hippocampal strata enriched in axonal projections did not detect any change with age (Figure 3.3B; fimbria: $F_{2,15} = 0.3902$, p = 0.6836; alveus: $F_{2,15} = 0.6694$, p = 0.5267; stratum lacunosum: $F_{2,15} = 0.08560$, p = 0.9184; stratum moleculare: $F_{2,15} = 0.1433$, p = 0.8676).

DISCUSSION

With the etiology of Alzheimer's disease still unknown, it is important to investigate known risk factors and pathological changes associated with the disease. The axonal enrichment of tau may deteriorate during the pathogenesis of AD as tau appears to accumulate in the somatodendritic compartment. Considering that aging is the leading risk factor for AD, investigation into the normal aging process may lead to the discovery of previously unappreciated anomalous features that contribute to disease vulnerability. Thus, we investigated the integrity of the AIS, the barrier involved in maintaining axonal localization of tau, over the span of aging in rats to establish whether normal aging might affect the AIS structure and/or tau distribution.

We evaluated age-related changes in tau and the AIS using multiple markers and complementary approaches. However, we found no evidence that the levels of AIS proteins or tau proteins change with age in the HP, nor levels of somatic or axonal tau change in HP neurons with advancing age in rats. The length of the AIS was not found to change in any region of the hippocampus, but a discrete and specific effect was detected in the CA2 region (~8% decrease from young to old). The reduction of AIS volume and diameter without a change in length indicates possible atrophy the axonal projections specifically in CA2 neurons, but biological significance of these changes in the context of tau distribution and AIS functionality remain unclear. Overall, the findings presented here provide a strong case against aging-related changes in the total tau levels, somatic tau levels, some phosphorylated forms of tau (i.e., PHF1, AT8, pS422), levels of AIS structural proteins (i.e., AnkG, neurofascin, βIV-spectrin), or AIS morphology within the hippocampus are unlikely to contribute to the risk of developing AD. Importantly, these findings do not rule out that other variables related to tau and/or the AIS (e.g.,

other forms of tau, other characteristics/functions of the AIS, etc.) are changed during normal aging and might contribute to susceptibility for AD.

Prior to this work, a single study assessed the aging changes in the AIS and showed changes in Ankyrin and Spectrin proteins using western blots of telencephalic tissue from aged mice (Bahr *et al.*, 1994). The discordant findings reported here could be due to the use of rats instead of mice or the increased specificity of antibodies currently available to the isoforms of proteins localized to the AIS (i.e. ankyrin vs ankyrin G 480 kDa/270 kDa or spectrin vs βIV-spectrin).

Multiple complimentary experimental approaches were used in the evaluation of the effects of aging on both tau and the AIS. Examination of aging-related changes in total tau protein levels was conducted through western blotting using multiple tau markers, however, these methods do not allow cell-specific measurements. To assess aging-related changes specifically within levels of somatic tau we used fluorescence intensity measurements within the soma of individual hippocampal neurons. Since tau is a microtubule-associated protein, we wanted to establish whether changes in tubulin content was altered with advancing age, but there were no age-related changes in total tubulin levels and the amount of tau per tubulin remained constant within the hippocampus, which aligns well with previous studies showing hippocampal neurons are not lost in normal aging (both in humans and in rats) (West *et al.*, 2004; Stanley *et al.*, 2012). These findings demonstrate that the total amount of tau and the amount of tau in the soma remain unchanged in the hippocampus of aging rats.

The same level of rigor was applied to the investigation of the AIS by using a multifaceted approach to evaluate changes in aging rats. Multiple key AIS proteins (ankyrin G, βIV-spectrin and neurofascin) were examined in western blots and we measured SMI312 levels

to determine whether total axonal content was changed. The lack of aging changes in all AIS proteins assessed and SMI312 suggest that axonal content and key structural components of the AIS are not altered with age. This conclusion is further supported by the lack of changes in tubulin described above. Stereological analysis of the AIS was conducted using two complementary approaches. The space balls probe is an established methodology for detecting aging-related changes in fiber structures within the brain (Ypsilanti et al., 2008), and here we used it to measure AIS length. The AutoNeuron method in Neurolucida was used to perform 3dimensional measurements of individual AISs and showed a lack of age-related changes in AIS length and only a mild, region-specific decrease in width and volume. This probe was used previously to measure the diameter of dendrites in pyramidal neurons and compare them across brain regions (Amatrudo et al., 2012). The unbiased stereological measurement of AIS length in the entire hippocampus is a significant advantage of this approach to analyze AIS morphology. The length of the AIS was previously measured with βIV-spectrin using a non-stereological method in selected z-stacks of the hippocampus (Baalman et al., 2013). Interestingly, they report that a shortening of AISs correlates to cognitive impairment following explosion-induced brain trauma in Sprague Dawley rats. This work suggests that a shortening of the AIS may correlate to cognitive impairment, but we did not detect a shortening of AISs with age in the current work. Collectively, these data strongly demonstrate that the gross structure of the AIS (i.e. length, diameter, volume) do not change during the normal aging process in most cells of the hippocampus.

Although we are reporting mostly negative data, it is unlikely that the Fischer 344 rat was not an appropriate model of aging to use for this study. We included age groups that span the spectrum from young (4 months), middle (14 months) and old age (24 months), which is near the

end of the normal lifespan and a time at which aging-related impairments in memory and cognition occur. For example, an age-related decline in learning ability at 24 months of age was observed using a 14 unit T-maze and shock-motivated one-way active avoidance test in Fischer 344 rats (Spangler *et al.*, 1994). Additionally, 24 month-old Fischer 344 rats exhibit pathologies in multiple organ systems associated with advanced aging, further supporting their utility as a model of aging. We confirmed that our techniques and methods are capable of detecting other changes in normal aging that were previously reported (i.e. GFAP increase) (VanGuilder *et al.*, 2011).

Several studies showed that there is heterogeneity among aged animals on a number of learning and memory functions (e.g. water maze), as well as other behavioral tasks, indicating that individual animals respond to the aging process differently (Gage *et al.*, 1984; Collier & Coleman, 1991; Freeman *et al.*, 2009). These studies, made it clear that aged animals can be separated into unimpaired or impaired groups based on performance and that these changes correspond to some neurochemical and neuroanatomical changes. However, the data reported here demonstrate that two distinct populations of aged animals do not exist in regard to the specific AIS and tau parameters studied, suggesting these variables do not underlie the behavioral and cognitive decline seen in aging Fischer 344 rats. Analysis of these parameters in young, middle and old humans may be necessary to definitively establish whether the same holds true for humans.

The negative findings presented here provide important insight into the aging-related changes in tau and AIS in the hippocampus. This information is important considering the contention in the field that tau mislocalization is important in AD and the recent focus on the role of the AIS in tau distribution (Zempel *et al.*, 2010; Li *et al.*, 2011; Sohn *et al.*, 2016). Thus,

future investigations should focus on alternative aspects of tau and the AIS to further identify whether aging-related changes may contribute to the risk of AD.

ACKNOWLEDGEMENTS

We thank Dr. Vann Bennett at Duke University for his assistance and technical expertise with the AnkG immunoblots.

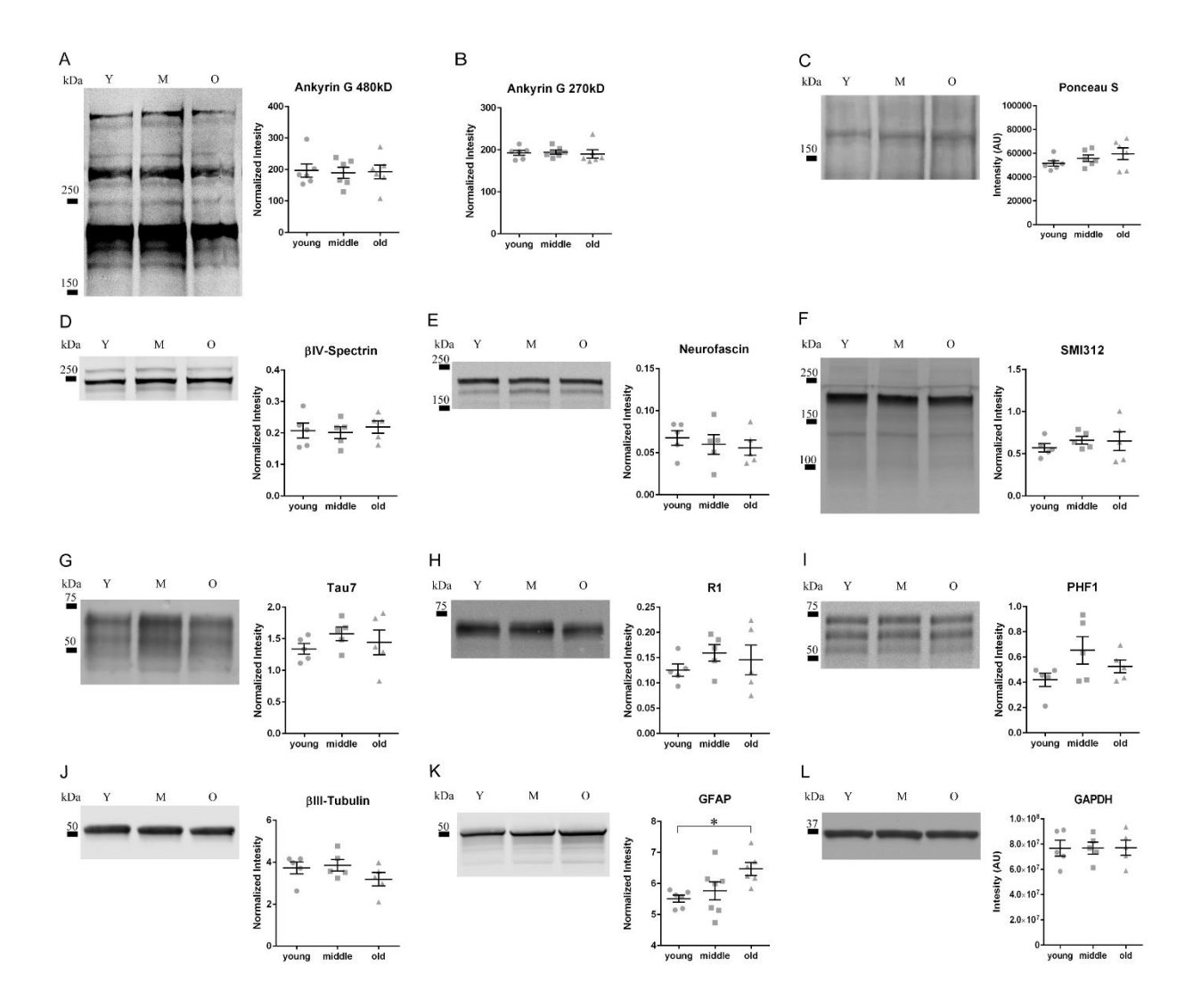


Figure 3.1: Aging does not alter levels of axon initial segment proteins, total tau, and phosphorylated tau proteins. (A, B) Amount of 480kDa (A) and 270kDa (B) isoforms of ankyrin G do not change between young, middle, and old rats. Note that the other isoforms of ankyrin G not analyzed are isoforms that are not AIS-specific. (C) Ankyrin-G western blots were normalized to Ponceau S (C) staining for loading control. (D, E) The amount of βIV-spectrin (D) and neurofascin (E) also remain unchanged during aging in rats. (F) The level of axonal neurofilaments, as indicated by the SMI-312 antibody, The SMI-312 antibody is an axonal marker that labels phospho-neurofilaments in axons. SMI-312 levels are not changed with age, confirming that total axon content is similar across age groups (G, H) The total level of tau

Figure 3.1 (cont'd)

detected with Tau7 (G) and polyclonal R1 (H) do not change with age in the rat HP. (I) The levels of PHF1, a phospho-epitope of tau, are not changed with age. (J) The total levels of microtubules, labeled with β III-tubulin, remained unchanged with advancing age. (K) Glial fibrillary acidic protein (GFAP), an astrocytic marker known to increase with age, is significantly increased in the HP of old age rats compared to young and middle aged rats. (Oneway ANOVA, Tukey's post-hoc, *p < 0.05). (L) Western blot band intensities are normalized to GAPDH (L) which did not change with age. All data are displayed as mean \pm standard error.

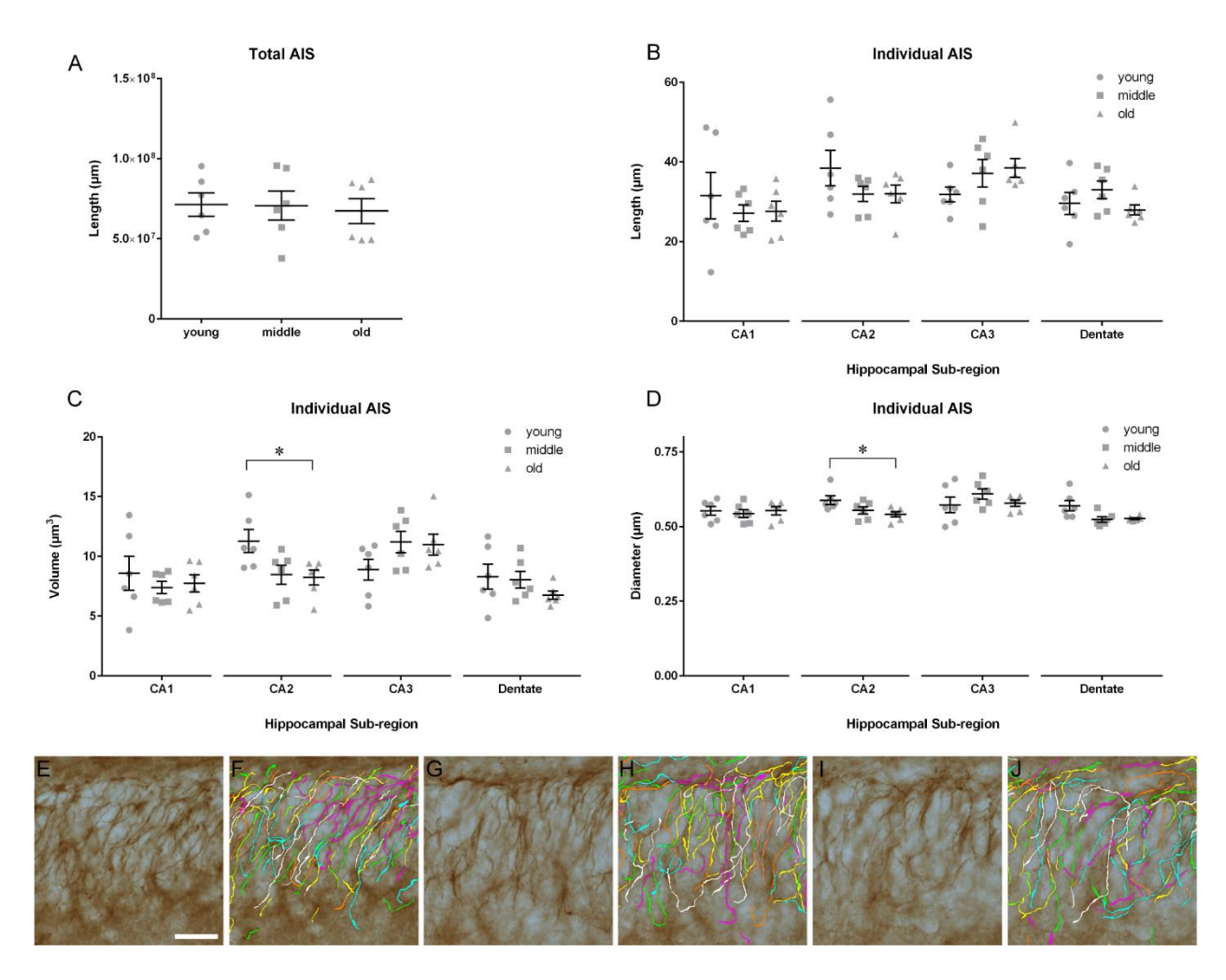


Figure 3.2: Structural analysis of the AIS with Ankyrin G (AnkG) reveals regional changes in the hippocampus during aging. (A) The total length of AISs in the hippocampus estimated with the space balls stereology probe is unchanged across age groups. (B-D) The Neurolucida AutoNeuron analysis reveals that the length (B), volume (C), and diameter (D) of the AISs across young, middle, and old aged rats is not changed in CA1, CA3, or the dentate gyrus of the hippocampus. The volume and diameter of the AISs in the CA2 region were significantly reduced in the old age compared to the young rats (one-way ANOVA, Tukey's post-hoc, *p < 0.05). All data are displayed as mean ±standard error. (E-G) Representative images of the AISs (AnkG positive immunostain, brown) in the dentate gyrus of the hippocampus at ages 4 (E), 14

Figure 3.2 (cont'd)

(G), and 24 (I) months of age, and the corresponding Neurolucida AutoNeuron tracings (F, H, and J; multi-color overlay to visually differentiate individual AISs). Scale bar 20µm for E-I.

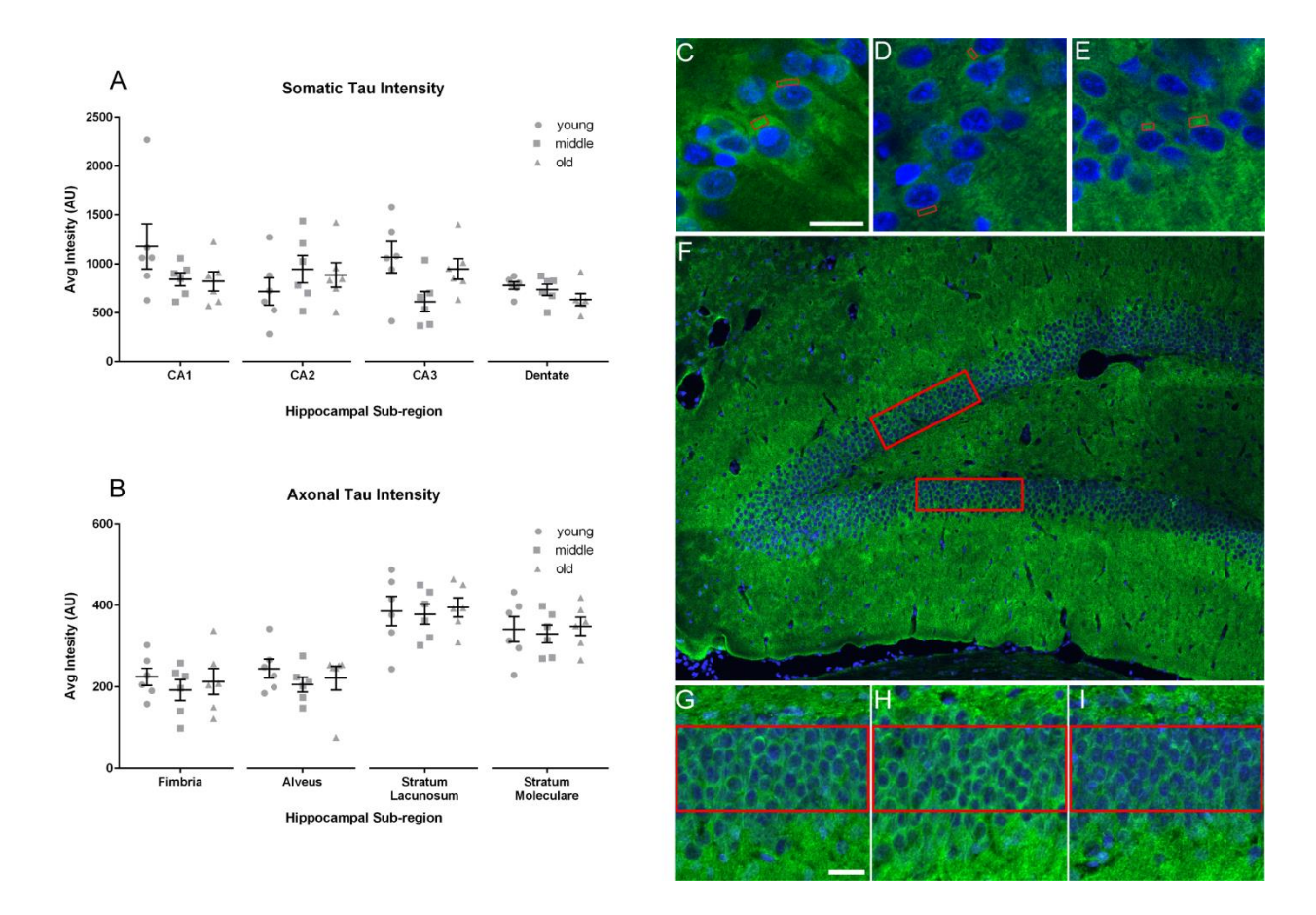


Figure 3.3: Optical density measurement of tau immunofluorescence in the somata and axons of hippocampal neurons shows no changes across age. (A) The intensity of somatic tau (using Tau7, a total tau antibody) in neurons in the CA1, CA2, CA3, and dentate regions of the hippocampus shows no change with advancing age. (B) No change in the regional intensity of tau is detected in the axon-enriched strata of the hippocampus (i.e. the fimbria, alveus, stratum lacunosum, and stratum moleculare). All data are displayed as mean ±standard error. (C-E) Representative images of CA1 hippocampal neurons positive for Tau 7 at 4 (C), 14 (D), and 24 (E) months. The red rectangles are examples of the areas that fluorescence intensities were measured within individual neurons. (F) Image illustrating the regions (in red) used for analysis of somatic tau intensity in the dentate gyrus. (G-I) Enlargements represent the analyzed regions of 4 (G), 14 (H), and 24 (I) month-old rats. Scale bar 20μm.

CHAPTER 4

Overall Discussion

DISCUSSION

Identifying mechanisms of healthy biology in neurons is paramount to understanding disease pathology because often disease processes are aberrations of normal biology. In this dissertation, I set out to elucidate aspects of neuronal tau localization and identify a mechanism by which neurons maintain an enriched localization of tau in the axon. I focused this search around the AIS (the location of a retrograde diffusion barrier) and known risks/causes of tauopathy (i.e. aging, tau modifications and mutant tau associated with inherited tauopathies). I identified novel factors of the AIS and tau biology that contribute axonal localization of tau and found that healthy aging does not lead to alterations in the AIS or tau distribution. I will discuss these findings in the context of a working model that explains and predicts tau distribution in neurons and propose potential future directions for studies into axosomatic localization and mislocalization of tau.

Causes of tau mislocalization

The axosomatic distribution of tau was described in developing neurons in culture as well as aging hippocampal pyramidal and granule neurons *in vivo* (Figure 2.1 and 3.3). Our evaluation of tau distribution supports the hypothesis that tau is mildly enriched in the axon of cultured neurons. In developing cultured neurons, we found ~2x as much total tau in the axon as the soma. This also means that there is still a substantial population of tau protein in the soma of healthy neurons. As our study only analyzed tau concentrations with pan-tau antibodies, further

study should be done to look at distribution of endogenous tau isoforms or post-translational modifications, however, isoform analysis would be limited in rodent neurons because they do not express all six isoforms of tau expressed by primates (Bullmann *et al.*, 2009). Acknowledging that tau is present in the somata of healthy neurons is important for an accurate and comprehensive understanding of normal tau distribution, function and potential role in disease. Several early studies clearly indicate that the phosphorylation status of proteins in the axon are different from tau proteins in the somatodendritic compartment, however, the implications of these normal differences remains elusive. Some of our results suggest that the phosphorylation status of tau may dictate whether it can diffuse from the axon into the soma. Thus, phosphoregulation may help in maintaining the normal distribution of tau in neurons.

It is well-established that the tau phosphorylation also is strongly associated with disease pathogenesis. We hypothesized that post-translational modifications (e.g. phosphorylation) that occur in human disease and tau mutations associated with inherited tauopathies would significantly affect the axosomatic diffusion of tau in neurons. We looked at pseudophosphorylated tau constructs to establish whether they are inhibited from axosomatic diffusion the same as wild-type tau. Further, we narrowed down the tau domain that was necessary and sufficient for maintaining the blockage of retrograde diffusion of tau. The MTBR alone was inhibited from axosomatic redistribution, suggesting modification within aa 221-380 or those causing obstruction of MTBR function (e.g. conformational changes) might have the largest impact on axosomatic tau diffusion.

We found that with four pseudophosphorylations in the MTBR (4KXGE) tau exhibited a significant increase in retrograde diffusion into the soma. This is ~40% more than the average level of endogenous phosphorylation of tau in healthy neurons (~2-3 mol Phos/mol Tau), but not

quite as high as the level of phosphorylation found in disease (~8 mol Phos/mol Tau) (Kopke *et al.*, 1993). Comparatively, a single pseudophosphorylation modification at S262 was insufficient to disrupt the inhibition of axosomatic tau diffusion past the AIS suggesting that more extreme disruption of the MT binding motifs is required to significantly increase axosomatic tau diffusion. Also, the increased axosomatic diffusion of the tau-AT8 construct suggests that somatic mislocalization, along with conformational changes and reduced MT binding, of tau may contribute to disease pathogenesis through inducing misregulation of signaling pathways (Jeganathan *et al.*, 2006; Kanaan *et al.*, 2011).

Lastly, tau with the P301L mutation (causes an inherited tauopathy) displayed significantly enhanced axosomatic diffusion. P301L does not show impaired MT association but does exhibit an increased dissociation constant (K_d) in *in vitro* microtubule binding assays (Sun & Gamblin, 2009). We know that P301L exhibits higher phosphorylation in disease models, but it is unclear whether the structure/dynamics of P301L cause its mislocalization which leads to phosphorylation or whether the altered structure increases its phosphorylation leading to mislocalization (Sahara *et al.*, 2013). Together, these data confirm our hypothesis that some disease-related forms of tau show abnormal levels of axosomatic diffusion in neurons, but also highlight the complexity of this characteristic of tau because not all modifications affected diffusion. These data further demonstrate the importance and dependence of interactions with MTs for the localization and axonal enrichment of tau.

Components of the axon initial segment modify tau enrichment

The AIS is a tightly regulated cytoarchitecture with multiple functions necessary for neuron development, polarization, and activity. The AIS structure is maintained by a few

scaffolding proteins that tether the actin cytoskeleton and MTs together with extracellular matrix and cell adhesion proteins. Due to its ability to regulate the diffusion of larger neurofilaments and properly direct axonal cargos, the AIS has established roles in providing a function barrier between the axonal and somatic compartments. Aligned with this functional characteristic of the AIS, the AIS was shown to act as a barrier against axosomatic diffusion of tau (Li *et al.*, 2011; Zempel *et al.*, 2017). The overarching goal of this work was to further evaluate the function and mechanism of the AIS as a retrograde diffusion barrier for tau.

We hypothesized that knocking down AnkG in cultured neurons would cause total disruption of the AIS and impairment in AIS functions, including the maintenance of the tau diffusion barrier (Hedstrom & Rasband, 2006; Sobotzik *et al.*, 2009; Freal *et al.*, 2016). Our studies revealed that eliminating AnkG did not influence axosomatic diffusion of tau. This result was surprising because AnkG knockdown eliminates several of the commonly studied AIS components (e.g. βIV-spectrin, neurofascin, end-binding proteins, and ion channels), and a single previous report suggested this eliminated the retrograde diffusion barrier for tau (Hedstrom *et al.*, 2008; Zempel *et al.*, 2017). This study used a much longer time course of AIS protein knock-down (9 days vs 4 days in our studies), which could have disrupted cell polarity entirely as is commonly reported in AIS studies. Also, the method of normalization used to detect axosomatic diffusion did not account for individual axon morphology, transfection efficiency or protein expression, which we included to reduce variability between neurons and use larger sample sizes. Thus, our results led us to investigate whether other non-traditional or novel AIS-related factors could play a role in the axosomatic diffusion barrier for tau.

TRIM46 is a recently discovered AIS protein, and importantly its primary function appears to be regulating MT organization within the AIS. After van Beuningen et al.

demonstrated the effect of TRIM46 knockdown on neuronal culture, it became clear that this protein had the potential to affect tau diffusion. They showed that TRIM46 was required for development of an axonal process and localization of AnkG and accomplished this by increasing MT stability. By knockdown of TRIM46, they demonstrated that TRIM46 maintains parallel arrays of MTs in the proximal axon with proper orientation of the +end directed towards the distal axon. We worked from these findings to determine the effect of TRIM46 knockdown on the retrograde diffusion barrier for tau protein. As described above (Chapter 2), we discovered that knocking down TRIM46 led to reduced axonal enrichment of tau and increased axosomatic diffusion. With this discovery, we have identified an AIS localized protein exhibiting a direct effect on tau enrichment and maintenance of the differential distribution of tau in neurons.

The mechanism by which TRIM46 influences axonal tau enrichment and inhibits axosomatic diffusion is still unknown. We used several methods to elucidate a protein-protein interaction between tau and TRIM46 (e.g. several variations of pull-down experiments), but the only positive result was colocalization of tau and TRIM46 in the AIS with the PLA (Chapter 2). These findings suggested the two proteins are closely associated but may not directly interact. Using mass spectrometry as an unbiased approach of identifying TRIM46 interacting partners, we confirmed that tau was not a binding partner. The negative findings of a direct interaction mounted to become positive evidence that tau and TRIM46 are unlikely to interact directly. The results of the mass spectrometry revealed interactions of TRIM46 with several microtubule-associated factors including tubulin, MAPs (MAP1a, MAP6 and MAP2), and actin-associated proteins, supporting TRIM46's function as a cytoskeletal organizer in the AIS. We postulate that the organization of MTs into parallel arrays with proper orientation in the AIS by TRIM46 is integral to its function of maintaining axonal tau enrichment and inhibiting retrograde diffusion.

These data force us to reject our initial hypothesis that the AIS formed a retrograde diffusion barrier for tau through direct protein interactions with the AIS-specific components examined. However, they clearly implicate TRIM46 as a critical component to maintaining axonal localization of tau. Combined with the data revealed about tau modifications, it appears that this indirect inhibition of axosomatic diffusion by TRIM46's organization of MTs, uses MT-tau interactions to form a more dynamic sorting system than was previously appreciated.

Axosomatic tau and AnkG do not change in aged neurons

The process of synaptic loss, axonal degeneration, and cell loss of AD is a quantitatively different process than the neuronal loss of normal aging and does not appear to simply be an accelerated aging process (West et al., 1994; Nelson et al., 2011). However, aging remains the strongest risk factor for developing AD. Thus, we examined the AIS and tau localization through the course of normal aging to reveal potential links between aging and an increased susceptibility for developing AD. We hypothesized that aging-related decline in AIS function may lead to an altered tau distribution with decreased axonal and increased somatodendritic tau levels in regions of the brain susceptible in AD (i.e. the hippocampus). However, our studies revealed that normal aging did not contribute to changes in AnkG structure or tau localization within hippocampal neuronal populations (Chapter 3), leading us to reject our hypothesis. Based on what we revealed above regarding the involvement of TRIM46 in tau distribution and diffusion, it would be beneficial to understand the maintenance of TRIM46 in the AIS during aging. Also, the distribution of tau phosphoepitopes or other post-translational modifications within healthy aging neurons could produce important insights towards understanding tau localization under normal and pathological conditions.

Proposed mechanism of tau localization

A central question from the work described above and from others is how does tau phosphorylation, disease-related modification, and the TRIM46-organized MT cytoskeleton in the AIS work together to maintain tau distribution in neurons? To explain the behavior of tau reported above, I adapt a published mathematical model that predicts tau mislocalization in neurons (Kuznetsov & Kuznetsov, 2017). The Kuznetsov and Kuznetsov model helps to account for factors required to facilitate tau movement within a neuron, resulting in the axonal enrichment seen in healthy neurons and the somatic mislocalization in disease. I will synthesize our findings on tau distribution and diffusion with their mathematical modeling paradigm to propose a working model of the mechanisms underlying normal and abnormal tau distributions.

The movements of tau in the neuron can be divided into two types: passive and active (Konzack *et al.*, 2007). Passive is the movement of MT bound and unbound cytosolic tau that distributes throughout the cell only by means of diffusion. Active movement is the transport of tau along MTs by axonal motors, either anterogradely or retrogradely. The balance of these factors on tau movement result in a mathematical model where tau can dynamically move about the cell via diffusion but remains enriched in the axon because of active movement that favors the anterograde direction within the axon. This drives the distribution of tau we observe in healthy neurons. Next, this localization model discusses the effect of decreased MT-tau interactions on the axosomatic distribution. Our data show that both tau-4KXGE, AT8-tau and tau-P301L have a higher axosomatic diffusion than wild-type tau. This is explained by the altered MT interaction that allows increased axosomatic diffusion. While the decreased interaction with microtubules will not lead to a complete redistribution of modified tau, it will result in a distribution in which the somatic concentration and the axosomatic diffusion rate are

higher compared to that of wild-type tau. This suggests that highly phosphorylated or mutant tau exhibits less axonal tau enrichment.

Finally, the model states increased reversals is the best mechanism for describing somatic tau accumulation and loss of axonal enrichment (Li et al., 2014). Reversals are events where active transport reverses direction and continues the opposite direction of original travel (Uchida & Brown, 2004). In this context, the reversal that would contribute to mislocalization is interruption of anterograde transport by switching to the retrograde direction. Normally, this would only occur in the axon if the tau movement was driven by a different motor protein (i.e. switch from kinesin to dynein) because MTs in the axon are organized in a parallel and polar orientation. Axonal MTs are organized with the labile plus-end in the anterograde direction and transport in this direction is mediated primarily by the kinesin-1 motor complexes (Penazzi et al., 2016). TRIM46 maintains this parallel, polar organization, and its knockdown allows ~30% of MTs in the axon to develop antiparallel orientation (labile plus-end oriented in the retrograde direction) (van Beuningen et al., 2015). I propose that knockdown of TRIM46 increases reversals of active tau transport, leading to the loss of axonal enrichment and mislocalization of tau to the somata. Future studies are required to fully support this newly proposed working model, but the model provides several testable hypotheses that will lead to novel insights into the mechanisms of tau distribution under normal physiological conditions and potential avenues that may go awry during the pathogenesis of tauopathies.

Future directions

Further studies to support the hypothesis that tau distribution is mediated by the function of TRIM46 maintaining parallel MT arrays in the AIS would need to investigate the relationship

between MT orientation and tau diffusion. The model described above assumes that by knocking down TRIM46, MTs become oriented in an anti-parallel fashion within the AIS. Recent work suggests that treatment with Taxol, a MT stabilizing drug, maintains parallel orientation within the AIS when neurons are treated with shRNA for TRIM46 (van Beuningen *et al.*, 2015). Treating neurons with TRIM46-shRNA and Taxol before examining axosomatic tau diffusion would an important next experiment in this study. The results would help elucidate the mechanism by which TRIM46 inhibits axosomatic diffusion of tau, either by maintaining parallel arrays of MTs in the AIS or not. A second study to further investigate the orientation of MTs on the diffusion of tau, would be to measure the speed of retrograde diffusion of tau from the distal dendrites compared to the axon. MTs in the dendrites exhibit anti-parallel orientation, suggesting that if the orientation of MTs affects the transport and free diffusion of tau, tau would diffuse toward the soma at a higher rate in the dendrite over the axon.

Another approach to investigate the mechanism of inhibiting axosomatic tau diffusion would be to disrupt axon directed transport. I proposed that the active transport of tau into the axon at the site of the AIS plays a critical role in maintain axonal tau localization. By inhibiting kinesin motor proteins, it could be possible to see a disruption in tau transportation, resulting in increased axosomatic tau diffusion. Consideration of the additional effects of disrupting axonal transport within the neuron would be important when analyzing the results of this experiment. Disrupting axonal transport can lead to a number of physiological problems within the cell, including impaired vesical transport, synaptic dysfunction, and axonal swellings. It may be difficult to parse out the direct effects of axonal transport inhibition from the additional degenerative features of the treated neuron. Nonetheless, these and other similarly focused

studies in the future may significantly deepen our understanding of the forces directing tau distribution in neurons under physiological and pathological conditions.

REFERENCES

REFERENCES

- Alzheimer's, A. (2016) 2016 Alzheimer's disease facts and figures. *Alzheimer's & dementia : the journal of the Alzheimer's Association*, **12**, 459-509.
- Amatrudo, J.M., Weaver, C.M., Crimins, J.L., Hof, P.R., Rosene, D.L. & Luebke, J.I. (2012) Influence of highly distinctive structural properties on the excitability of pyramidal neurons in monkey visual and prefrontal cortices. *The Journal of neuroscience : the official journal of the Society for Neuroscience*, **32**, 13644-13660.
- Arendt, T., Stieler, J.T. & Holzer, M. (2016) Tau and tauopathies. *Brain research bulletin*, **126**, 238-292.
- Arrasate, M., Perez, M., Armas-Portela, R. & Avila, J. (1999) Polymerization of tau peptides into fibrillar structures. The effect of FTDP-17 mutations. *FEBS letters*, **446**, 199-202.
- Arriagada, P.V., Growdon, J.H., Hedley-Whyte, E.T. & Hyman, B.T. (1992) Neurofibrillary tangles but not senile plaques parallel duration and severity of Alzheimer's disease. *Neurology*, **42**, 631-639.
- Atapour, N. & Rosa, M.G.P. (2017) Age-related plasticity of the axon initial segment of cortical pyramidal cells in marmoset monkeys. *Neurobiology of aging*, **57**, 95-103.
- Baalman, K.L., Cotton, R.J., Rasband, S.N. & Rasband, M.N. (2013) Blast wave exposure impairs memory and decreases axon initial segment length. *Journal of neurotrauma*, **30**, 741-751.
- Bahr, B.A., Lam, N. & Lynch, G. (1994) Changes in the concentrations of tau and other structural proteins in the brains of aged mice. *Neuroscience letters*, **175**, 49-52.
- Bancher, C., Brunner, C., Lassmann, H., Budka, H., Jellinger, K., Wiche, G., Seitelberger, F., Grundke-Iqbal, I., Iqbal, K. & Wisniewski, H.M. (1989) Accumulation of abnormally phosphorylated tau precedes the formation of neurofibrillary tangles in Alzheimer's disease. *Brain research*, **477**, 90-99.
- Barghorn, S. & Mandelkow, E. (2002) Toward a unified scheme for the aggregation of tau into Alzheimer paired helical filaments. *Biochemistry*, **41**, 14885-14896.
- Barghorn, S., Zheng-Fischhofer, Q., Ackmann, M., Biernat, J., von Bergen, M., Mandelkow, E.M. & Mandelkow, E. (2000) Structure, microtubule interactions, and paired helical filament aggregation by tau mutants of frontotemporal dementias. *Biochemistry*, **39**, 11714-11721.

- Bennett, V. & Baines, A.J. (2001) Spectrin and ankyrin-based pathways: metazoan inventions for integrating cells into tissues. *Physiological reviews*, **81**, 1353-1392.
- Bennett, V. & Lorenzo, D.N. (2013) Spectrin- and ankyrin-based membrane domains and the evolution of vertebrates. *Current topics in membranes*, **72**, 1-37.
- Berchtold, N.C. & Cotman, C.W. (1998) Evolution in the conceptualization of dementia and Alzheimer's disease: Greco-Roman period to the 1960s. *Neurobiology of aging*, **19**, 173-189.
- Berry, J.D., Jones, S., Drebot, M.A., Andonov, A., Sabara, M., Yuan, X.Y., Weingartl, H., Fernando, L., Marszal, P., Gren, J., Nicolas, B., Andonova, M., Ranada, F., Gubbins, M.J., Ball, T.B., Kitching, P., Li, Y., Kabani, A. & Plummer, F. (2004) Development and characterisation of neutralising monoclonal antibody to the SARS-coronavirus. *Journal of virological methods*, **120**, 87-96.
- Biernat, J., Gustke, N., Drewes, G., Mandelkow, E.M. & Mandelkow, E. (1993) Phosphorylation of Ser262 strongly reduces binding of tau to microtubules: distinction between PHF-like immunoreactivity and microtubule binding. *Neuron*, **11**, 153-163.
- Biernat, J. & Mandelkow, E.M. (1999) The development of cell processes induced by tau protein requires phosphorylation of serine 262 and 356 in the repeat domain and is inhibited by phosphorylation in the proline-rich domains. *Molecular biology of the cell*, **10**, 727-740.
- Biernat, J., Mandelkow, E.M., Schroter, C., Lichtenberg-Kraag, B., Steiner, B., Berling, B., Meyer, H., Mercken, M., Vandermeeren, A., Goedert, M. & et al. (1992) The switch of tau protein to an Alzheimer-like state includes the phosphorylation of two serine-proline motifs upstream of the microtubule binding region. *The EMBO journal*, **11**, 1593-1597.
- Binder, L.I., Frankfurter, A. & Rebhun, L.I. (1985) The distribution of tau in the mammalian central nervous system. *The Journal of cell biology*, **101**, 1371-1378.
- Binder, L.I., Frankfurter, A. & Rebhun, L.I. (1986) Differential localization of MAP-2 and tau in mammalian neurons in situ. *Annals of the New York Academy of Sciences*, **466**, 145-166.
- Blennow, K., Brody, D.L., Kochanek, P.M., Levin, H., McKee, A., Ribbers, G.M., Yaffe, K. & Zetterberg, H. (2016) Traumatic brain injuries. *Nature reviews. Disease primers*, **2**, 16084.
- Blumbergs, P.C., Scott, G., Manavis, J., Wainwright, H., Simpson, D.A. & McLean, A.J. (1994) Staining of amyloid precursor protein to study axonal damage in mild head injury. *Lancet*, **344**, 1055-1056.
- Bolt, M.W. & Mahoney, P.A. (1997) High-efficiency blotting of proteins of diverse sizes following sodium dodecyl sulfate-polyacrylamide gel electrophoresis. *Analytical biochemistry*, **247**, 185-192.

- Borroni, B., Garibotto, V., Agosti, C., Brambati, S.M., Bellelli, G., Gasparotti, R., Padovani, A. & Perani, D. (2008) White matter changes in corticobasal degeneration syndrome and correlation with limb apraxia. *Archives of neurology*, **65**, 796-801.
- Boyne, L.J., Tessler, A., Murray, M. & Fischer, I. (1995) Distribution of Big tau in the central nervous system of the adult and developing rat. *The Journal of comparative neurology*, **358**, 279-293.
- Braak, E., Arai, K. & Braak, H. (1999) Cerebellar involvement in Pick's disease: affliction of mossy fibers, monodendritic brush cells, and dentate projection neurons. *Experimental neurology*, **159**, 153-163.
- Braak, E., Braak, H. & Mandelkow, E.M. (1994) A sequence of cytoskeleton changes related to the formation of neurofibrillary tangles and neuropil threads. *Acta neuropathologica*, **87**, 554-567.
- Braak, H. & Braak, E. (1991) Neuropathological stageing of Alzheimer-related changes. *Acta neuropathologica*, **82**, 239-259.
- Braak, H. & Braak, E. (1995) Staging of Alzheimer's disease-related neurofibrillary changes. *Neurobiology of aging*, **16**, 271-278; discussion 278-284.
- Brandt, R., Leger, J. & Lee, G. (1995) Interaction of tau with the neural plasma membrane mediated by tau's amino-terminal projection domain. *The Journal of cell biology*, **131**, 1327-1340.
- Bretteville, A., Demiautte, F. & Chapuis, J. (2017) Proximity Ligation Assay: A Tool to Study Endogenous Interactions Between Tau and Its Neuronal Partners. *Methods in molecular biology*, **1523**, 297-305.
- Buee, L., Bussiere, T., Buee-Scherrer, V., Delacourte, A. & Hof, P.R. (2000) Tau protein isoforms, phosphorylation and role in neurodegenerative disorders. *Brain research reviews*, **33**, 95-130.
- Buee, L. & Delacourte, A. (1999) Comparative biochemistry of tau in progressive supranuclear palsy, corticobasal degeneration, FTDP-17 and Pick's disease. *Brain pathology*, **9**, 681-693.
- Buffington, S.A. & Rasband, M.N. (2011) The axon initial segment in nervous system disease and injury. *The European journal of neuroscience*, **34**, 1609-1619.
- Bullmann, T., Holzer, M., Mori, H. & Arendt, T. (2009) Pattern of tau isoforms expression during development in vivo. *International journal of developmental neuroscience: the official journal of the International Society for Developmental Neuroscience*, **27**, 591-597.

- Burrell, J.R. & Piguet, O. (2015) Lifting the veil: how to use clinical neuropsychology to assess dementia. *Journal of neurology, neurosurgery, and psychiatry*, **86**, 1216-1224.
- Caccamo, D., Katsetos, C.D., Herman, M.M., Frankfurter, A., Collins, V.P. & Rubinstein, L.J. (1989) Immunohistochemistry of a spontaneous murine ovarian teratoma with neuroepithelial differentiation. Neuron-associated beta-tubulin as a marker for primitive neuroepithelium. *Laboratory investigation; a journal of technical methods and pathology*, **60**, 390-398.
- Chung, P.J., Song, C., Deek, J., Miller, H.P., Li, Y., Choi, M.C., Wilson, L., Feinstein, S.C. & Safinya, C.R. (2016) Tau mediates microtubule bundle architectures mimicking fascicles of microtubules found in the axon initial segment. *Nature communications*, **7**, 12278.
- Cleveland, D.W., Hwo, S.Y. & Kirschner, M.W. (1977a) Physical and chemical properties of purified tau factor and the role of tau in microtubule assembly. *Journal of molecular biology*, **116**, 227-247.
- Cleveland, D.W., Hwo, S.Y. & Kirschner, M.W. (1977b) Purification of tau, a microtubule-associated protein that induces assembly of microtubules from purified tubulin. *Journal of molecular biology*, **116**, 207-225.
- Cochran, E.J., Fox, J.H. & Mufson, E.J. (1994) Severe panencephalic Pick's disease with Alzheimer's disease-like neuropil threads and synaptophysin immunoreactivity. *Acta neuropathologica*, **88**, 479-484.
- Cochran, J.N., Hall, A.M. & Roberson, E.D. (2014) The dendritic hypothesis for Alzheimer's disease pathophysiology. *Brain research bulletin*, **103**, 18-28.
- Collier, T.J. & Coleman, P.D. (1991) Divergence of biological and chronological aging: evidence from rodent studies. *Neurobiology of aging*, **12**, 685-693.
- Combs, B., Kneynsberg, A. & Kanaan, N.M. (2016) Gene Therapy Models of Alzheimer's Disease and Other Dementias. *Methods in molecular biology*, **1382**, 339-366.
- Conde, C. & Caceres, A. (2009) Microtubule assembly, organization and dynamics in axons and dendrites. *Nature reviews. Neuroscience*, **10**, 319-332.
- Corsellis, J.A., Bruton, C.J. & Freeman-Browne, D. (1973) The aftermath of boxing. *Psychological medicine*, **3**, 270-303.
- Cox, K., Combs, B., Abdelmesih, B., Morfini, G., Brady, S.T. & Kanaan, N.M. (2016) Analysis of isoform-specific tau aggregates suggests a common toxic mechanism involving similar pathological conformations and axonal transport inhibition. *Neurobiology of aging*, **47**, 113-126.

- D'Este, E., Kamin, D., Gottfert, F., El-Hady, A. & Hell, S.W. (2015) STED nanoscopy reveals the ubiquity of subcortical cytoskeleton periodicity in living neurons. *Cell reports*, **10**, 1246-1251.
- Davis, J. & Bennett, V. (1982) Microtubule-associated protein 2, a microtubule-associated protein from brain, is immunologically related to the alpha subunit of erythrocyte spectrin. *The Journal of biological chemistry*, **257**, 5816-5820.
- Davis, J.Q., Lambert, S. & Bennett, V. (1996) Molecular composition of the node of Ranvier: identification of ankyrin-binding cell adhesion molecules neurofascin (mucin+/third FNIII domain-) and NrCAM at nodal axon segments. *The Journal of cell biology*, **135**, 1355-1367.
- DeKosky, S.T. & Scheff, S.W. (1990) Synapse loss in frontal cortex biopsies in Alzheimer's disease: correlation with cognitive severity. *Annals of neurology*, **27**, 457-464.
- Delisle, M.B., Murrell, J.R., Richardson, R., Trofatter, J.A., Rascol, O., Soulages, X., Mohr, M., Calvas, P. & Ghetti, B. (1999) A mutation at codon 279 (N279K) in exon 10 of the Tau gene causes a tauopathy with dementia and supranuclear palsy. *Acta neuropathologica*, **98**, 62-77.
- Di, J., Cohen, L.S., Corbo, C.P., Phillips, G.R., El Idrissi, A. & Alonso, A.D. (2016) Abnormal tau induces cognitive impairment through two different mechanisms: synaptic dysfunction and neuronal loss. *Scientific reports*, **6**, 20833.
- Dickson, D.W. (1998) Pick's disease: a modern approach. *Brain pathology*, **8**, 339-354.
- Dickson, D.W. (1999) Neuropathologic differentiation of progressive supranuclear palsy and corticobasal degeneration. *Journal of neurology*, **246 Suppl 2**, II6-15.
- Dickson, D.W., Ahmed, Z., Algom, A.A., Tsuboi, Y. & Josephs, K.A. (2010) Neuropathology of variants of progressive supranuclear palsy. *Current opinion in neurology*, **23**, 394-400.
- Dotti, C.G., Banker, G.A. & Binder, L.I. (1987) The expression and distribution of the microtubule-associated proteins tau and microtubule-associated protein 2 in hippocampal neurons in the rat in situ and in cell culture. *Neuroscience*, **23**, 121-130.
- Dotti, C.G., Sullivan, C.A. & Banker, G.A. (1988) The establishment of polarity by hippocampal neurons in culture. *The Journal of neuroscience : the official journal of the Society for Neuroscience*, **8**, 1454-1468.
- Dumitrescu, A.S., Evans, M.D. & Grubb, M.S. (2016) Evaluating Tools for Live Imaging of Structural Plasticity at the Axon Initial Segment. *Frontiers in cellular neuroscience*, **10**, 268.

- Evans, M.D., Sammons, R.P., Lebron, S., Dumitrescu, A.S., Watkins, T.B., Uebele, V.N., Renger, J.J. & Grubb, M.S. (2013) Calcineurin signaling mediates activity-dependent relocation of the axon initial segment. *The Journal of neuroscience : the official journal of the Society for Neuroscience*, **33**, 6950-6963.
- Fairbanks, G., Steck, T.L. & Wallach, D.F. (1971) Electrophoretic analysis of the major polypeptides of the human erythrocyte membrane. *Biochemistry*, **10**, 2606-2617.
- Faller, E.M. & Brown, D.L. (2009) Modulation of microtubule dynamics by the microtubule-associated protein 1a. *Journal of neuroscience research*, **87**, 1080-1089.
- Feany, M.B. & Dickson, D.W. (1995) Widespread cytoskeletal pathology characterizes corticobasal degeneration. *The American journal of pathology*, **146**, 1388-1396.
- Fischer, D., Mukrasch, M.D., Biernat, J., Bibow, S., Blackledge, M., Griesinger, C., Mandelkow, E. & Zweckstetter, M. (2009) Conformational changes specific for pseudophosphorylation at serine 262 selectively impair binding of tau to microtubules. *Biochemistry*, **48**, 10047-10055.
- Forrest, S.L., Kril, J.J., Stevens, C.H., Kwok, J.B., Hallupp, M., Kim, W.S., Huang, Y., McGinley, C.V., Werka, H., Kiernan, M.C., Gotz, J., Spillantini, M.G., Hodges, J.R., Ittner, L.M. & Halliday, G.M. (2018) Retiring the term FTDP-17 as MAPT mutations are genetic forms of sporadic frontotemporal tauopathies. *Brain : a journal of neurology*, **141**, 521-534.
- Foster, N.L., Wilhelmsen, K., Sima, A.A., Jones, M.Z., D'Amato, C.J. & Gilman, S. (1997) Frontotemporal dementia and parkinsonism linked to chromosome 17: a consensus conference. Conference Participants. *Annals of neurology*, **41**, 706-715.
- Freal, A., Fassier, C., Le Bras, B., Bullier, E., De Gois, S., Hazan, J., Hoogenraad, C.C. & Couraud, F. (2016) Cooperative Interactions between 480 kDa Ankyrin-G and EB Proteins Assemble the Axon Initial Segment. *The Journal of neuroscience : the official journal of the Society for Neuroscience*, **36**, 4421-4433.
- Freeman, W.M., VanGuilder, H.D., Bennett, C. & Sonntag, W.E. (2009) Cognitive performance and age-related changes in the hippocampal proteome. *Neuroscience*, **159**, 183-195.
- Gage, F.H., Dunnett, S.B. & Bjorklund, A. (1984) Spatial learning and motor deficits in aged rats. *Neurobiology of aging*, **5**, 43-48.
- Gelpi, E., Hoftberger, R., Graus, F., Ling, H., Holton, J.L., Dawson, T., Popovic, M., Pretnar-Oblak, J., Hogl, B., Schmutzhard, E., Poewe, W., Ricken, G., Santamaria, J., Dalmau, J., Budka, H., Revesz, T. & Kovacs, G.G. (2016) Neuropathological criteria of anti-IgLON5-related tauopathy. *Acta neuropathologica*, **132**, 531-543.

- Giza, C.C. & Hovda, D.A. (2001) The Neurometabolic Cascade of Concussion. *Journal of athletic training*, **36**, 228-235.
- Goate, A., Chartier-Harlin, M.C., Mullan, M., Brown, J., Crawford, F., Fidani, L., Giuffra, L., Haynes, A., Irving, N., James, L. & et al. (1991) Segregation of a missense mutation in the amyloid precursor protein gene with familial Alzheimer's disease [see comments]. *Nature*, **349**, 704-706.
- Goedert, M., Crowther, R.A. & Garner, C.C. (1991) Molecular characterization of microtubule-associated proteins tau and MAP2. *Trends in neurosciences*, **14**, 193-199.
- Goedert, M. & Ghetti, B. (2007) Alois Alzheimer: his life and times. *Brain pathology*, **17**, 57-62.
- Goedert, M., Ghetti, B. & Spillantini, M.G. (2012) Frontotemporal dementia: implications for understanding Alzheimer disease. *Cold Spring Harbor perspectives in medicine*, **2**, a006254.
- Goedert, M., Klug, A. & Crowther, R.A. (2006) Tau protein, the paired helical filament and Alzheimer's disease. *Journal of Alzheimer's disease: JAD*, **9**, 195-207.
- Goedert, M., Spillantini, M.G., Jakes, R., Rutherford, D. & Crowther, R.A. (1989) Multiple isoforms of human microtubule-associated protein tau: sequences and localization in neurofibrillary tangles of Alzheimer's disease. *Neuron*, **3**, 519-526.
- Goedert, M., Wischik, C.M., Crowther, R.A., Walker, J.E. & Klug, A. (1988) Cloning and sequencing of the cDNA encoding a core protein of the paired helical filament of Alzheimer disease: identification as the microtubule-associated protein tau. *Proceedings of the National Academy of Sciences of the United States of America*, **85**, 4051-4055.
- Gouras, G.K., Tsai, J., Naslund, J., Vincent, B., Edgar, M., Checler, F., Greenfield, J.P., Haroutunian, V., Buxbaum, J.D., Xu, H., Greengard, P. & Relkin, N.R. (2000) Intraneuronal Abeta42 accumulation in human brain. *Am J Pathol*, **156**, 15-20.
- Greenfield, J.P., Tsai, J., Gouras, G.K., Hai, B., Thinakaran, G., Checler, F., Sisodia, S.S., Greengard, P. & Xu, H. (1999) Endoplasmic reticulum and trans-Golgi network generate distinct populations of Alzheimer beta-amyloid peptides. *Proc Natl Acad Sci U S A*, **96**, 742-747.
- Grubb, M.S. & Burrone, J. (2010) Activity-dependent relocation of the axon initial segment fine-tunes neuronal excitability. *Nature*, **465**, 1070-1074.
- Grundke-Iqbal, I., Iqbal, K., Quinlan, M., Tung, Y.C., Zaidi, M.S. & Wisniewski, H.M. (1986a) Microtubule-associated protein tau. A component of Alzheimer paired helical filaments. *J Biol Chem*, **261**, 6084-6089.

- Grundke-Iqbal, I., Iqbal, K., Tung, Y.C., Quinlan, M., Wisniewski, H.M. & Binder, L.I. (1986b) Abnormal phosphorylation of the microtubule-associated protein tau (tau) in Alzheimer cytoskeletal pathology. *Proceedings of the National Academy of Sciences of the United States of America*, **83**, 4913-4917.
- Guillozet-Bongaarts, A.L., Cahill, M.E., Cryns, V.L., Reynolds, M.R., Berry, R.W. & Binder, L.I. (2006) Pseudophosphorylation of tau at serine 422 inhibits caspase cleavage: in vitro evidence and implications for tangle formation in vivo. *Journal of neurochemistry*, **97**, 1005-1014.
- Gurskaya, N.G., Verkhusha, V.V., Shcheglov, A.S., Staroverov, D.B., Chepurnykh, T.V., Fradkov, A.F., Lukyanov, S. & Lukyanov, K.A. (2006) Engineering of a monomeric green-to-red photoactivatable fluorescent protein induced by blue light. *Nature biotechnology*, **24**, 461-465.
- Gustke, N., Trinczek, B., Biernat, J., Mandelkow, E.M. & Mandelkow, E. (1994) Domains of tau protein and interactions with microtubules. *Biochemistry*, **33**, 9511-9522.
- Halpert, B.P. (1983) Development of the term "senility" as a medical diagnosis. *Minnesota medicine*, **66**, 421-424.
- Hardy, J.A. & Higgins, G.A. (1992) Alzheimer's disease: the amyloid cascade hypothesis. *Science*, **256**, 184-185.
- Hasegawa, M., Morishima-Kawashima, M., Takio, K., Suzuki, M., Titani, K. & Ihara, Y. (1992) Protein sequence and mass spectrometric analyses of tau in the Alzheimer's disease brain. *The Journal of biological chemistry*, **267**, 17047-17054.
- Hatch, R.J., Wei, Y., Xia, D. & Gotz, J. (2017) Hyperphosphorylated tau causes reduced hippocampal CA1 excitability by relocating the axon initial segment. *Acta neuropathologica*.
- Hauw, J.J., Daniel, S.E., Dickson, D., Horoupian, D.S., Jellinger, K., Lantos, P.L., McKee, A., Tabaton, M. & Litvan, I. (1994) Preliminary NINDS neuropathologic criteria for Steele-Richardson-Olszewski syndrome (progressive supranuclear palsy). *Neurology*, **44**, 2015-2019.
- Hauw, J.J., Verny, M., Delaere, P., Cervera, P., He, Y. & Duyckaerts, C. (1990) Constant neurofibrillary changes in the neocortex in progressive supranuclear palsy. Basic differences with Alzheimer's disease and aging. *Neuroscience letters*, **119**, 182-186.
- Hebert, L.E., Bienias, J.L., Aggarwal, N.T., Wilson, R.S., Bennett, D.A., Shah, R.C. & Evans, D.A. (2010) Change in risk of Alzheimer disease over time. *Neurology*, **75**, 786-791.
- Hebert, L.E., Weuve, J., Scherr, P.A. & Evans, D.A. (2013) Alzheimer disease in the United States (2010-2050) estimated using the 2010 census. *Neurology*, **80**, 1778-1783.

- Hedstrom, K.L., Ogawa, Y. & Rasband, M.N. (2008) AnkyrinG is required for maintenance of the axon initial segment and neuronal polarity. *The Journal of cell biology*, **183**, 635-640.
- Hedstrom, K.L. & Rasband, M.N. (2006) Intrinsic and extrinsic determinants of ion channel localization in neurons. *Journal of neurochemistry*, **98**, 1345-1352.
- Hedstrom, K.L., Xu, X., Ogawa, Y., Frischknecht, R., Seidenbecher, C.I., Shrager, P. & Rasband, M.N. (2007) Neurofascin assembles a specialized extracellular matrix at the axon initial segment. *The Journal of cell biology*, **178**, 875-886.
- Herrup, K. (2015) The case for rejecting the amyloid cascade hypothesis. *Nature neuroscience*, **18**, 794-799.
- Hoogenraad, C.C. & Bradke, F. (2009) Control of neuronal polarity and plasticity--a renaissance for microtubules? *Trends in cell biology*, **19**, 669-676.
- Hoover, B.R., Reed, M.N., Su, J., Penrod, R.D., Kotilinek, L.A., Grant, M.K., Pitstick, R., Carlson, G.A., Lanier, L.M., Yuan, L.L., Ashe, K.H. & Liao, D. (2010) Tau mislocalization to dendritic spines mediates synaptic dysfunction independently of neurodegeneration. *Neuron*, **68**, 1067-1081.
- Horowitz, P.M., LaPointe, N., Guillozet-Bongaarts, A.L., Berry, R.W. & Binder, L.I. (2006) N-terminal fragments of tau inhibit full-length tau polymerization in vitro. *Biochemistry*, **45**, 12859-12866.
- Hutton, M., Lendon, C.L., Rizzu, P., Baker, M., Froelich, S., Houlden, H., Pickering-Brown, S., Chakraverty, S., Isaacs, A., Grover, A., Hackett, J., Adamson, J., Lincoln, S., Dickson, D., Davies, P., Petersen, R.C., Stevens, M., de Graaff, E., Wauters, E., van Baren, J., Hillebrand, M., Joosse, M., Kwon, J.M., Nowotny, P., Heutink, P. & et al. (1998)
 Association of missense and 5'-splice-site mutations in tau with the inherited dementia FTDP-17. *Nature*, 393, 702-705.
- Iqbal, K., Alonso Adel, C., Chen, S., Chohan, M.O., El-Akkad, E., Gong, C.X., Khatoon, S., Li, B., Liu, F., Rahman, A., Tanimukai, H. & Grundke-Iqbal, I. (2005) Tau pathology in Alzheimer disease and other tauopathies. *Biochimica et biophysica acta*, **1739**, 198-210.
- Ishizawa, K., Lin, W.L., Tiseo, P., Honer, W.G., Davies, P. & Dickson, D.W. (2000) A qualitative and quantitative study of grumose degeneration in progressive supranuclear palsy. *Journal of neuropathology and experimental neurology*, **59**, 513-524.
- Ittner, L.M., Ke, Y.D., Delerue, F., Bi, M., Gladbach, A., van Eersel, J., Wolfing, H., Chieng, B.C., Christie, M.J., Napier, I.A., Eckert, A., Staufenbiel, M., Hardeman, E. & Gotz, J. (2010) Dendritic function of tau mediates amyloid-beta toxicity in Alzheimer's disease mouse models. *Cell*, **142**, 387-397.

- James, B.D., Leurgans, S.E., Hebert, L.E., Scherr, P.A., Yaffe, K. & Bennett, D.A. (2014) Contribution of Alzheimer disease to mortality in the United States. *Neurology*, **82**, 1045-1050.
- Jeganathan, S., Hascher, A., Chinnathambi, S., Biernat, J., Mandelkow, E.M. & Mandelkow, E. (2008) Proline-directed pseudo-phosphorylation at AT8 and PHF1 epitopes induces a compaction of the paperclip folding of Tau and generates a pathological (MC-1) conformation. *The Journal of biological chemistry*, **283**, 32066-32076.
- Jeganathan, S., von Bergen, M., Brutlach, H., Steinhoff, H.J. & Mandelkow, E. (2006) Global hairpin folding of tau in solution. *Biochemistry*, **45**, 2283-2293.
- Jenkins, P.M., Kim, N., Jones, S.L., Tseng, W.C., Svitkina, T.M., Yin, H.H. & Bennett, V. (2015) Giant ankyrin-G: a critical innovation in vertebrate evolution of fast and integrated neuronal signaling. *Proceedings of the National Academy of Sciences of the United States of America*, **112**, 957-964.
- Kahlson, M.A. & Colodner, K.J. (2015) Glial Tau Pathology in Tauopathies: Functional Consequences. *Journal of experimental neuroscience*, **9**, 43-50.
- Kanaan, N.M., Cox, K., Alvarez, V.E., Stein, T.D., Poncil, S. & McKee, A.C. (2016) Characterization of Early Pathological Tau Conformations and Phosphorylation in Chronic Traumatic Encephalopathy. *Journal of neuropathology and experimental neurology*, **75**, 19-34.
- Kanaan, N.M., Kordower, J.H. & Collier, T.J. (2008) Age-related changes in dopamine transporters and accumulation of 3-nitrotyrosine in rhesus monkey midbrain dopamine neurons: relevance in selective neuronal vulnerability to degeneration. *The European journal of neuroscience*, **27**, 3205-3215.
- Kanaan, N.M., Morfini, G.A., LaPointe, N.E., Pigino, G.F., Patterson, K.R., Song, Y., Andreadis, A., Fu, Y., Brady, S.T. & Binder, L.I. (2011) Pathogenic forms of tau inhibit kinesin-dependent axonal transport through a mechanism involving activation of axonal phosphotransferases. *The Journal of neuroscience : the official journal of the Society for Neuroscience*, **31**, 9858-9868.
- Kanaan, N.M., Pigino, G.F., Brady, S.T., Lazarov, O., Binder, L.I. & Morfini, G.A. (2013) Axonal degeneration in Alzheimer's disease: when signaling abnormalities meet the axonal transport system. *Experimental neurology*, **246**, 44-53.
- Kanai, Y., Chen, J. & Hirokawa, N. (1992) Microtubule bundling by tau proteins in vivo: analysis of functional domains. *The EMBO journal*, **11**, 3953-3961.
- Kanai, Y. & Hirokawa, N. (1995) Sorting mechanisms of tau and MAP2 in neurons: suppressed axonal transit of MAP2 and locally regulated microtubule binding. *Neuron*, **14**, 421-432.

- Keller, A., Nesvizhskii, A.I., Kolker, E. & Aebersold, R. (2002) Empirical statistical model to estimate the accuracy of peptide identifications made by MS/MS and database search. *Analytical chemistry*, **74**, 5383-5392.
- Kimura, T., Ono, T., Takamatsu, J., Yamamoto, H., Ikegami, K., Kondo, A., Hasegawa, M., Ihara, Y., Miyamoto, E. & Miyakawa, T. (1996) Sequential changes of tau-site-specific phosphorylation during development of paired helical filaments. *Dementia*, **7**, 177-181.
- Knake, S., Belke, M., Menzler, K., Pilatus, U., Eggert, K.M., Oertel, W.H., Stamelou, M. & Hoglinger, G.U. (2010) In vivo demonstration of microstructural brain pathology in progressive supranuclear palsy: a DTI study using TBSS. *Movement disorders : official journal of the Movement Disorder Society*, **25**, 1232-1238.
- Kneynsberg, A., Collier, T.J., Manfredsson, F.P. & Kanaan, N.M. (2016) Quantitative and semi-quantitative measurements of axonal degeneration in tissue and primary neuron cultures. *Journal of neuroscience methods*, **266**, 32-41.
- Kneynsberg, A., Combs, B., Christensen, K., Morfini, G. & Kanaan, N.M. (2017) Axonal Degeneration in Tauopathies: Disease Relevance and Underlying Mechanisms. *Frontiers in neuroscience*, **11**, 572.
- Koerte, I.K., Ertl-Wagner, B., Reiser, M., Zafonte, R. & Shenton, M.E. (2012a) White matter integrity in the brains of professional soccer players without a symptomatic concussion. *JAMA*, **308**, 1859-1861.
- Koerte, I.K., Kaufmann, D., Hartl, E., Bouix, S., Pasternak, O., Kubicki, M., Rauscher, A., Li, D.K., Dadachanji, S.B., Taunton, J.A., Forwell, L.A., Johnson, A.M., Echlin, P.S. & Shenton, M.E. (2012b) A prospective study of physician-observed concussion during a varsity university hockey season: white matter integrity in ice hockey players. Part 3 of 4. *Neurosurg Focus*, **33**, E3: 1-7.
- Konzack, S., Thies, E., Marx, A., Mandelkow, E.M. & Mandelkow, E. (2007) Swimming against the tide: mobility of the microtubule-associated protein tau in neurons. *The Journal of neuroscience: the official journal of the Society for Neuroscience*, **27**, 9916-9927.
- Kopke, E., Tung, Y.C., Shaikh, S., Alonso, A.C., Iqbal, K. & Grundke-Iqbal, I. (1993) Microtubule-associated protein tau. Abnormal phosphorylation of a non-paired helical filament pool in Alzheimer disease. *The Journal of biological chemistry*, **268**, 24374-24384.
- Kordeli, E., Lambert, S. & Bennett, V. (1995) AnkyrinG. A new ankyrin gene with neural-specific isoforms localized at the axonal initial segment and node of Ranvier. *The Journal of biological chemistry*, **270**, 2352-2359.
- Kouri, N., Carlomagno, Y., Baker, M., Liesinger, A.M., Caselli, R.J., Wszolek, Z.K., Petrucelli, L., Boeve, B.F., Parisi, J.E., Josephs, K.A., Uitti, R.J., Ross, O.A., Graff-Radford, N.R.,

- DeTure, M.A., Dickson, D.W. & Rademakers, R. (2014) Novel mutation in MAPT exon 13 (p.N410H) causes corticobasal degeneration. *Acta neuropathologica*, **127**, 271-282.
- Kouri, N., Whitwell, J.L., Josephs, K.A., Rademakers, R. & Dickson, D.W. (2011) Corticobasal degeneration: a pathologically distinct 4R tauopathy. *Nature reviews. Neurology*, **7**, 263-272.
- Kovacs, G.G. (2015) Invited review: Neuropathology of tauopathies: principles and practice. *Neuropathology and applied neurobiology*, **41**, 3-23.
- Kovacs, G.G. (2017) Tauopathies. *Handbook of clinical neurology*, **145**, 355-368.
- Kowall, N.W. & Kosik, K.S. (1987) Axonal disruption and aberrant localization of tau protein characterize the neuropil pathology of Alzheimer's disease. *Annals of neurology*, **22**, 639-643.
- Kraus, M.F., Susmaras, T., Caughlin, B.P., Walker, C.J., Sweeney, J.A. & Little, D.M. (2007) White matter integrity and cognition in chronic traumatic brain injury: a diffusion tensor imaging study. *Brain : a journal of neurology*, **130**, 2508-2519.
- Kuba, H., Adachi, R. & Ohmori, H. (2014) Activity-dependent and activity-independent development of the axon initial segment. *The Journal of neuroscience : the official journal of the Society for Neuroscience*, **34**, 3443-3453.
- Kuznetsov, I.A. & Kuznetsov, A.V. (2017) What mechanisms of tau protein transport could be responsible for the inverted tau concentration gradient in degenerating axons? *Mathematical medicine and biology: a journal of the IMA*, **34**, 125-150.
- Le Bras, B., Freal, A., Czarnecki, A., Legendre, P., Bullier, E., Komada, M., Brophy, P.J., Davenne, M. & Couraud, F. (2014) In vivo assembly of the axon initial segment in motor neurons. *Brain Struct Funct*, **219**, 1433-1450.
- Leterrier, C. (2018) The Axon Initial Segment: An Updated Viewpoint. *The Journal of neuroscience: the official journal of the Society for Neuroscience*, **38**, 2135-2145.
- Leterrier, C. & Dargent, B. (2013) No Pasaran! Role of the axon initial segment in the regulation of protein transport and the maintenance of axonal identity. *Seminars in cell & developmental biology*.
- Leterrier, C. & Dargent, B. (2014) No Pasaran! Role of the axon initial segment in the regulation of protein transport and the maintenance of axonal identity. *Seminars in cell & developmental biology*, **27**, 44-51.
- Leterrier, C., Potier, J., Caillol, G., Debarnot, C., Rueda Boroni, F. & Dargent, B. (2015) Nanoscale Architecture of the Axon Initial Segment Reveals an Organized and Robust Scaffold. *Cell reports*, **13**, 2781-2793.

- Leterrier, C., Vacher, H., Fache, M.P., d'Ortoli, S.A., Castets, F., Autillo-Touati, A. & Dargent, B. (2011) End-binding proteins EB3 and EB1 link microtubules to ankyrin G in the axon initial segment. *Proceedings of the National Academy of Sciences of the United States of America*, **108**, 8826-8831.
- Lewis, J., Dickson, D.W., Lin, W.L., Chisholm, L., Corral, A., Jones, G., Yen, S.H., Sahara, N., Skipper, L., Yager, D., Eckman, C., Hardy, J., Hutton, M. & McGowan, E. (2001) Enhanced neurofibrillary degeneration in transgenic mice expressing mutant tau and APP. *Science*, **293**, 1487-1491.
- Li, X., Kumar, Y., Zempel, H., Mandelkow, E.M., Biernat, J. & Mandelkow, E. (2011) Novel diffusion barrier for axonal retention of Tau in neurons and its failure in neurodegeneration. *The EMBO journal*, **30**, 4825-4837.
- Li, Y., Brown, A. & Jung, P. (2014) Deciphering the axonal transport kinetics of neurofilaments using the fluorescence photoactivation pulse-escape method. *Physical biology*, **11**, 026001.
- Lippa, C.F. (2004) Synaptophysin immunoreactivity in Pick's disease: comparison with Alzheimer's disease and dementia with Lewy bodies. *American journal of Alzheimer's disease and other dementias*, **19**, 341-344.
- Lippa, C.F., Zhukareva, V., Kawarai, T., Uryu, K., Shafiq, M., Nee, L.E., Grafman, J., Liang, Y., St George-Hyslop, P.H., Trojanowski, J.Q. & Lee, V.M. (2000) Frontotemporal dementia with novel tau pathology and a Glu342Val tau mutation. *Annals of neurology*, **48**, 850-858.
- Litvan, I., Agid, Y., Goetz, C., Jankovic, J., Wenning, G.K., Brandel, J.P., Lai, E.C., Verny, M., Ray-Chaudhuri, K., McKee, A., Jellinger, K., Pearce, R.K. & Bartko, J.J. (1997) Accuracy of the clinical diagnosis of corticobasal degeneration: a clinicopathologic study. *Neurology*, **48**, 119-125.
- Liu, Y., Lee, J.W. & Ackerman, S.L. (2015) Mutations in the microtubule-associated protein 1A (Map1a) gene cause Purkinje cell degeneration. *The Journal of neuroscience : the official journal of the Society for Neuroscience*, **35**, 4587-4598.
- Mandelkow, E.M., Biernat, J., Drewes, G., Gustke, N., Trinczek, B. & Mandelkow, E. (1995) Tau domains, phosphorylation, and interactions with microtubules. *Neurobiology of aging*, **16**, 355-362; discussion 362-353.
- Mandell, J.W. & Banker, G.A. (1995) The microtubule cytoskeleton and the development of neuronal polarity. *Neurobiology of aging*, **16**, 229-237; discussion 238.

- Mandell, J.W. & Banker, G.A. (1996a) Microtubule-associated proteins, phosphorylation gradients, and the establishment of neuronal polarity. *Perspectives on developmental neurobiology*, **4**, 125-135.
- Mandell, J.W. & Banker, G.A. (1996b) A spatial gradient of tau protein phosphorylation in nascent axons. *The Journal of neuroscience: the official journal of the Society for Neuroscience*, **16**, 5727-5740.
- Marin, M.A., Ziburkus, J., Jankowsky, J. & Rasband, M.N. (2016) Amyloid-beta plaques disrupt axon initial segments. *Experimental neurology*, **281**, 93-98.
- Masters, C.L., Simms, G., Weinman, N.A., Multhaup, G., McDonald, B.L. & Beyreuther, K. (1985) Amyloid plaque core protein in Alzheimer disease and Down syndrome. *Proc Natl Acad Sci U S A*, **82**, 4245-4249.
- Maxwell, W.L., McCreath, B.J., Graham, D.I. & Gennarelli, T.A. (1995) Cytochemical evidence for redistribution of membrane pump calcium-ATPase and ecto-Ca-ATPase activity, and calcium influx in myelinated nerve fibres of the optic nerve after stretch injury. *Journal of neurocytology*, **24**, 925-942.
- McAllister, T.W., Ford, J.C., Flashman, L.A., Maerlender, A., Greenwald, R.M., Beckwith, J.G., Bolander, R.P., Tosteson, T.D., Turco, J.H., Raman, R. & Jain, S. (2014) Effect of head impacts on diffusivity measures in a cohort of collegiate contact sport athletes. *Neurology*, **82**, 63-69.
- McKee, A.C., Cantu, R.C., Nowinski, C.J., Hedley-Whyte, E.T., Gavett, B.E., Budson, A.E., Santini, V.E., Lee, H.S., Kubilus, C.A. & Stern, R.A. (2009) Chronic traumatic encephalopathy in athletes: progressive tauopathy after repetitive head injury. *Journal of neuropathology and experimental neurology*, **68**, 709-735.
- McKee, A.C., Stein, T.D., Nowinski, C.J., Stern, R.A., Daneshvar, D.H., Alvarez, V.E., Lee, H.S., Hall, G., Wojtowicz, S.M., Baugh, C.M., Riley, D.O., Kubilus, C.A., Cormier, K.A., Jacobs, M.A., Martin, B.R., Abraham, C.R., Ikezu, T., Reichard, R.R., Wolozin, B.L., Budson, A.E., Goldstein, L.E., Kowall, N.W. & Cantu, R.C. (2012) The spectrum of disease in chronic traumatic encephalopathy. *Brain: a journal of neurology*.
- McKee, A.C., Stern, R.A., Nowinski, C.J., Stein, T.D., Alvarez, V.E., Daneshvar, D.H., Lee, H.S., Wojtowicz, S.M., Hall, G., Baugh, C.M., Riley, D.O., Kubilus, C.A., Cormier, K.A., Jacobs, M.A., Martin, B.R., Abraham, C.R., Ikezu, T., Reichard, R.R., Wolozin, B.L., Budson, A.E., Goldstein, L.E., Kowall, N.W. & Cantu, R.C. (2013) The spectrum of disease in chronic traumatic encephalopathy. *Brain : a journal of neurology*, **136**, 43-64.
- Morris, J.C., McKeel, D.W., Jr., Storandt, M., Rubin, E.H., Price, J.L., Grant, E.A., Ball, M.J. & Berg, L. (1991) Very mild Alzheimer's disease: informant-based clinical, psychometric, and pathologic distinction from normal aging. *Neurology*, **41**, 469-478.

- Motulsky, H.J. & Brown, R.E. (2006) Detecting outliers when fitting data with nonlinear regression a new method based on robust nonlinear regression and the false discovery rate. *BMC bioinformatics*, **7**, 123.
- Mufson, E.J., Perez, S.E., Nadeem, M., Mahady, L., Kanaan, N.M., Abrahamson, E.E., Ikonomovic, M.D., Crawford, F., Alvarez, V., Stein, T. & McKee, A.C. (2016) Progression of tau pathology within cholinergic nucleus basalis neurons in chronic traumatic encephalopathy: A chronic effects of neurotrauma consortium study. *Brain injury*, **30**, 1399-1413.
- Murrell, J.R., Spillantini, M.G., Zolo, P., Guazzelli, M., Smith, M.J., Hasegawa, M., Redi, F., Crowther, R.A., Pietrini, P., Ghetti, B. & Goedert, M. (1999) Tau gene mutation G389R causes a tauopathy with abundant pick body-like inclusions and axonal deposits. *Journal of neuropathology and experimental neurology*, **58**, 1207-1226.
- Musiek, E.S. & Holtzman, D.M. (2015) Three dimensions of the amyloid hypothesis: time, space and 'wingmen'. *Nature neuroscience*, **18**, 800-806.
- Nakada, C., Ritchie, K., Oba, Y., Nakamura, M., Hotta, Y., Iino, R., Kasai, R.S., Yamaguchi, K., Fujiwara, T. & Kusumi, A. (2003) Accumulation of anchored proteins forms membrane diffusion barriers during neuronal polarization. *Nature cell biology*, **5**, 626-632.
- Nelson, A.D. & Jenkins, P.M. (2017) Axonal Membranes and Their Domains: Assembly and Function of the Axon Initial Segment and Node of Ranvier. *Frontiers in cellular neuroscience*, **11**, 136.
- Nelson, P.T., Head, E., Schmitt, F.A., Davis, P.R., Neltner, J.H., Jicha, G.A., Abner, E.L., Smith, C.D., Van Eldik, L.J., Kryscio, R.J. & Scheff, S.W. (2011) Alzheimer's disease is not "brain aging": neuropathological, genetic, and epidemiological human studies. *Acta neuropathologica*, **121**, 571-587.
- Nesvizhskii, A.I., Keller, A., Kolker, E. & Aebersold, R. (2003) A statistical model for identifying proteins by tandem mass spectrometry. *Analytical chemistry*, **75**, 4646-4658.
- Nilsen, T.W. (2014) Preparation of cross-linked cellular extracts with formaldehyde. *Cold Spring Harbor protocols*, **2014**, 1001-1003.
- Oikawa, N., Kimura, N. & Yanagisawa, K. (2010) Alzheimer-type tau pathology in advanced aged nonhuman primate brains harboring substantial amyloid deposition. *Brain research*, **1315**, 137-149.
- Padovani, A., Borroni, B., Brambati, S.M., Agosti, C., Broli, M., Alonso, R., Scifo, P., Bellelli, G., Alberici, A., Gasparotti, R. & Perani, D. (2006) Diffusion tensor imaging and voxel based morphometry study in early progressive supranuclear palsy. *Journal of neurology, neurosurgery, and psychiatry*, 77, 457-463.

- Palay, S.L., Sotelo, C., Peters, A. & Orkand, P.M. (1968) The axon hillock and the initial segment. *The Journal of cell biology*, **38**, 193-201.
- Papasozomenos, S.C. & Binder, L.I. (1987) Phosphorylation determines two distinct species of Tau in the central nervous system. *Cell motility and the cytoskeleton*, **8**, 210-226.
- Parhad, I.M., Scott, J.N., Cellars, L.A., Bains, J.S., Krekoski, C.A. & Clark, A.W. (1995) Axonal atrophy in aging is associated with a decline in neurofilament gene expression. *Journal of neuroscience research*, **41**, 355-366.
- Penazzi, L., Bakota, L. & Brandt, R. (2016) Microtubule Dynamics in Neuronal Development, Plasticity, and Neurodegeneration. *International review of cell and molecular biology*, **321**, 89-169.
- Perez, S.E., Raghanti, M.A., Hof, P.R., Kramer, L., Ikonomovic, M.D., Lacor, P.N., Erwin, J.M., Sherwood, C.C. & Mufson, E.J. (2013) Alzheimer's disease pathology in the neocortex and hippocampus of the western lowland gorilla (Gorilla gorilla gorilla). *The Journal of comparative neurology*, **521**, 4318-4338.
- Perrin, R.J., Fagan, A.M. & Holtzman, D.M. (2009) Multimodal techniques for diagnosis and prognosis of Alzheimer's disease. *Nature*, **461**, 916-922.
- Peters, A., Proskauer, C.C. & Kaiserman-Abramof, I.R. (1968) The small pyramidal neuron of the rat cerebral cortex. The axon hillock and initial segment. *The Journal of cell biology*, **39**, 604-619.
- Petersen, R.C., Doody, R., Kurz, A., Mohs, R.C., Morris, J.C., Rabins, P.V., Ritchie, K., Rossor, M., Thal, L. & Winblad, B. (2001) Current concepts in mild cognitive impairment. *Archives of neurology*, **58**, 1985-1992.
- Petrie, E.C., Cross, D.J., Yarnykh, V.L., Richards, T., Martin, N.M., Pagulayan, K., Hoff, D., Hart, K., Mayer, C., Tarabochia, M., Raskind, M.A., Minoshima, S. & Peskind, E.R. (2014) Neuroimaging, behavioral, and psychological sequelae of repetitive combined blast/impact mild traumatic brain injury in Iraq and Afghanistan war veterans. *Journal of neurotrauma*, **31**, 425-436.
- Pigino, G., Morfini, G., Atagi, Y., Deshpande, A., Yu, C., Jungbauer, L., LaDu, M., Busciglio, J. & Brady, S. (2009) Disruption of fast axonal transport is a pathogenic mechanism for intraneuronal amyloid beta. *Proceedings of the National Academy of Sciences of the United States of America*, **106**, 5907-5912.
- Pollock, N.J., Mirra, S.S., Binder, L.I., Hansen, L.A. & Wood, J.G. (1986) Filamentous aggregates in Pick's disease, progressive supranuclear palsy, and Alzheimer's disease share antigenic determinants with microtubule-associated protein, tau. *Lancet*, **2**, 1211.

- Probst, A., Tolnay, M., Langui, D., Goedert, M. & Spillantini, M.G. (1996) Pick's disease: hyperphosphorylated tau protein segregates to the somatoaxonal compartment. *Acta Neuropathol (Berl)*, **92**, 588-596.
- Rapoport, M., Dawson, H.N., Binder, L.I., Vitek, M.P. & Ferreira, A. (2002) Tau is essential to beta -amyloid-induced neurotoxicity. *Proceedings of the National Academy of Sciences of the United States of America*, **99**, 6364-6369.
- Rasband, M.N. (2010) The axon initial segment and the maintenance of neuronal polarity. *Nature reviews. Neuroscience*, **11**, 552-562.
- Rebeiz, J.J., Kolodny, E.H. & Richardson, E.P., Jr. (1968) Corticodentatonigral degeneration with neuronal achromasia. *Archives of neurology*, **18**, 20-33.
- Roberson, E.D., Scearce-Levie, K., Palop, J.J., Yan, F., Cheng, I.H., Wu, T., Gerstein, H., Yu, G.Q. & Mucke, L. (2007) Reducing endogenous tau ameliorates amyloid beta-induced deficits in an Alzheimer's disease mouse model. *Science*, **316**, 750-754.
- Rogaev, E.I., Sherrington, R., Rogaeva, E.A., Levesque, G., Ikeda, M., Liang, Y., Chi, H., Lin, C., Holman, K., Tsuda, T. & et al. (1995) Familial Alzheimer's disease in kindreds with missense mutations in a gene on chromosome 1 related to the Alzheimer's disease type 3 gene. *Nature*, **376**, 775-778.
- Sahara, N., DeTure, M., Ren, Y., Ebrahim, A.S., Kang, D., Knight, J., Volbracht, C., Pedersen, J.T., Dickson, D.W., Yen, S.H. & Lewis, J. (2013) Characteristics of TBS-extractable hyperphosphorylated tau species: aggregation intermediates in rTg4510 mouse brain. *Journal of Alzheimer's disease: JAD*, **33**, 249-263.
- Santuccione, A.C., Merlini, M., Shetty, A., Tackenberg, C., Bali, J., Ferretti, M.T., McAfoose, J., Kulic, L., Bernreuther, C., Welt, T., Grimm, J., Glatzel, M., Rajendran, L., Hock, C. & Nitsch, R.M. (2013) Active vaccination with ankyrin G reduces beta-amyloid pathology in APP transgenic mice. *Molecular psychiatry*, **18**, 358-368.
- Savonenko, A.V., Melnikova, T., Hiatt, A., Li, T., Worley, P.F., Troncoso, J.C., Wong, P.C. & Price, D.L. (2012) Alzheimer's therapeutics: translation of preclinical science to clinical drug development. *Neuropsychopharmacology: official publication of the American College of Neuropsychopharmacology*, **37**, 261-277.
- Selkoe, D.J. (2002) Alzheimer's disease is a synaptic failure. *Science*, **298**, 789-791.
- Shankar, G.M., Bloodgood, B.L., Townsend, M., Walsh, D.M., Selkoe, D.J. & Sabatini, B.L. (2007) Natural oligomers of the Alzheimer amyloid-beta protein induce reversible synapse loss by modulating an NMDA-type glutamate receptor-dependent signaling pathway. *J Neurosci*, **27**, 2866-2875.

- Short, K.M. & Cox, T.C. (2006) Subclassification of the RBCC/TRIM superfamily reveals a novel motif necessary for microtubule binding. *The Journal of biological chemistry*, **281**, 8970-8980.
- Smiley, J.F. & Bleiwas, C. (2012) Embedding matrix for simultaneous processing of multiple histological samples. *Journal of neuroscience methods*, **209**, 195-198.
- Sobotzik, J.M., Sie, J.M., Politi, C., Del Turco, D., Bennett, V., Deller, T. & Schultz, C. (2009) AnkyrinG is required to maintain axo-dendritic polarity in vivo. *Proceedings of the National Academy of Sciences of the United States of America*, **106**, 17564-17569.
- Sohn, P.D., Tracy, T.E., Son, H.I., Zhou, Y., Leite, R.E., Miller, B.L., Seeley, W.W., Grinberg, L.T. & Gan, L. (2016) Acetylated tau destabilizes the cytoskeleton in the axon initial segment and is mislocalized to the somatodendritic compartment. *Molecular neurodegeneration*, **11**, 47.
- Song, A.H., Wang, D., Chen, G., Li, Y., Luo, J., Duan, S. & Poo, M.M. (2009) A selective filter for cytoplasmic transport at the axon initial segment. *Cell*, **136**, 1148-1160.
- Spangler, E.L., Waggie, K.S., Hengemihle, J., Roberts, D., Hess, B. & Ingram, D.K. (1994) Behavioral-Assessment of Aging in Male Fischer-344 and Brown-Norway Rat Strains and Their F(1) Hybrid. *Neurobiology of aging*, **15**, 319-328.
- Spillantini, M.G. & Goedert, M. (2013) Tau pathology and neurodegeneration. *Lancet neurology*, **12**, 609-622.
- Stanley, E.M., Fadel, J.R. & Mott, D.D. (2012) Interneuron loss reduces dendritic inhibition and GABA release in hippocampus of aged rats. *Neurobiology of aging*, **33**, 431 e431-413.
- Stefanoska, K., Volkerling, A., Bertz, J., Poljak, A., Ke, Y.D., Ittner, L.M. & Ittner, A. (2018) An N-terminal motif unique to primate tau enables differential protein-protein interactions. *The Journal of biological chemistry*, **293**, 3710-3719.
- Su, J.H., Cummings, B.J. & Cotman, C.W. (1994) Early phosphorylation of tau in Alzheimer's disease occurs at Ser-202 and is preferentially located within neurites. *Neuroreport*, **5**, 2358-2362.
- Sun, Q. & Gamblin, T.C. (2009) Pseudohyperphosphorylation causing AD-like changes in tau has significant effects on its polymerization. *Biochemistry*, **48**, 6002-6011.
- Sun, X., Wu, Y., Gu, M., Liu, Z., Ma, Y., Li, J. & Zhang, Y. (2014) Selective filtering defect at the axon initial segment in Alzheimer's disease mouse models. *Proceedings of the National Academy of Sciences of the United States of America*, **111**, 14271-14276.

- Tokuda, T., Ikeda, S., Yanagisawa, N., Ihara, Y. & Glenner, G.G. (1991) Re-examination of exboxers' brains using immunohistochemistry with antibodies to amyloid beta-protein and tau protein. *Acta neuropathologica*, **82**, 280-285.
- Torack, R.M. (1978) The pathologic physiology of dementia with indications for diagnosis and treatment. *Monographien aus dem Gesamtgebiete der Psychiatrie*, **20**, 1-150.
- Tortosa, E., Adolfs, Y., Fukata, M., Pasterkamp, R.J., Kapitein, L.C. & Hoogenraad, C.C. (2017) Dynamic Palmitoylation Targets MAP6 to the Axon to Promote Microtubule Stabilization during Neuronal Polarization. *Neuron*, **94**, 809-825 e807.
- Trojanowski, J.Q., Schuck, T., Schmidt, M.L. & Lee, V.M. (1989) Distribution of tau proteins in the normal human central and peripheral nervous system. *The journal of histochemistry and cytochemistry: official journal of the Histochemistry Society*, **37**, 209-215.
- Tsushima, H., Emanuele, M., Polenghi, A., Esposito, A., Vassalli, M., Barberis, A., Difato, F. & Chieregatti, E. (2015) HDAC6 and RhoA are novel players in Abeta-driven disruption of neuronal polarity. *Nature communications*, **6**, 7781.
- Tytell, M., Brady, S.T. & Lasek, R.J. (1984) Axonal transport of a subclass of tau proteins: evidence for the regional differentiation of microtubules in neurons. *Proceedings of the National Academy of Sciences of the United States of America*, **81**, 1570-1574.
- Uchida, A. & Brown, A. (2004) Arrival, reversal, and departure of neurofilaments at the tips of growing axons. *Molecular biology of the cell*, **15**, 4215-4225.
- van Beuningen, S.F., Will, L., Harterink, M., Chazeau, A., van Battum, E.Y., Frias, C.P., Franker, M.A., Katrukha, E.A., Stucchi, R., Vocking, K., Antunes, A.T., Slenders, L., Doulkeridou, S., Sillevis Smitt, P., Altelaar, A.F., Post, J.A., Akhmanova, A., Pasterkamp, R.J., Kapitein, L.C., de Graaff, E. & Hoogenraad, C.C. (2015) TRIM46 Controls Neuronal Polarity and Axon Specification by Driving the Formation of Parallel Microtubule Arrays. *Neuron*, **88**, 1208-1226.
- van Coevorden-Hameete, M.H., van Beuningen, S.F.B., Perrenoud, M., Will, L.M., Hulsenboom, E., Demonet, J.F., Sabater, L., Kros, J.M., Verschuuren, J., Titulaer, M.J., de Graaff, E., Sillevis Smitt, P.A.E. & Hoogenraad, C.C. (2017) Antibodies to TRIM46 are associated with paraneoplastic neurological syndromes. *Annals of clinical and translational neurology*, **4**, 680-686.
- van der Staay, F.J. & Blokland, A. (1996) Behavioral differences between outbred Wistar, inbred Fischer 344, brown Norway, and hybrid Fischer 344 x brown Norway rats. *Physiology & behavior*, **60**, 97-109.
- VanGuilder, H.D., Bixler, G.V., Brucklacher, R.M., Farley, J.A., Yan, H., Warrington, J.P., Sonntag, W.E. & Freeman, W.M. (2011) Concurrent hippocampal induction of MHC II

- pathway components and glial activation with advanced aging is not correlated with cognitive impairment. *Journal of neuroinflammation*, **8**, 138.
- Vasilescu, J., Guo, X. & Kast, J. (2004) Identification of protein-protein interactions using in vivo cross-linking and mass spectrometry. *Proteomics*, **4**, 3845-3854.
- von Bergen, M., Barghorn, S., Biernat, J., Mandelkow, E.M. & Mandelkow, E. (2005) Tau aggregation is driven by a transition from random coil to beta sheet structure. *Biochimica et biophysica acta*, **1739**, 158-166.
- von Bergen, M., Barghorn, S., Li, L., Marx, A., Biernat, J., Mandelkow, E.M. & Mandelkow, E. (2001) Mutations of tau protein in frontotemporal dementia promote aggregation of paired helical filaments by enhancing local beta-structure. *The Journal of biological chemistry*, **276**, 48165-48174.
- Wang, C., Najm, R., Xu, Q., Jeong, D.E., Walker, D., Balestra, M.E., Yoon, S.Y., Yuan, H., Li, G., Miller, Z.A., Miller, B.L., Malloy, M.J. & Huang, Y. (2018) Gain of toxic apolipoprotein E4 effects in human iPSC-derived neurons is ameliorated by a small-molecule structure corrector. *Nature medicine*.
- Wang, L.N., Zhu, M.W., Feng, Y.Q. & Wang, J.H. (2006) Pick's disease with Pick bodies combined with progressive supranuclear palsy without tuft-shaped astrocytes: a clinical, neuroradiologic and pathological study of an autopsied case. *Neuropathology: official journal of the Japanese Society of Neuropathology*, **26**, 222-230.
- Weingarten, M.D., Lockwood, A.H., Hwo, S.Y. & Kirschner, M.W. (1975) A protein factor essential for microtubule assembly. *Proceedings of the National Academy of Sciences of the United States of America*, **72**, 1858-1862.
- West, M.J., Coleman, P.D., Flood, D.G. & Troncoso, J.C. (1994) Differences in the pattern of hippocampal neuronal loss in normal ageing and Alzheimer's disease. *Lancet*, **344**, 769-772.
- West, M.J., Kawas, C.H., Stewart, W.F., Rudow, G.L. & Troncoso, J.C. (2004) Hippocampal neurons in pre-clinical Alzheimer's disease. *Neurobiology of aging*, **25**, 1205-1212.
- Whitwell, J.L., Master, A.V., Avula, R., Kantarci, K., Eggers, S.D., Edmonson, H.A., Jack, C.R., Jr. & Josephs, K.A. (2011) Clinical correlates of white matter tract degeneration in progressive supranuclear palsy. *Archives of neurology*, **68**, 753-760.
- Wilks, S. (1864) Clinical Notes on Atrophy of the Brain. *Journal of Mental Science*, **10**, 11.
- Winckler, B., Forscher, P. & Mellman, I. (1999) A diffusion barrier maintains distribution of membrane proteins in polarized neurons. *Nature*, **397**, 698-701.

- Wischik, C.M., Harrington, C.R., Mukaetova-Ladinska, E.B., Novak, M., Edwards, P.C. & McArthur, F.K. (1992) Molecular characterization and measurement of Alzheimer's disease pathology: implications for genetic and environmental aetiology. *Ciba Foundation symposium*, **169**, 268-293; discussion 293-302.
- Wood, J.G., Mirra, S.S., Pollock, N.J. & Binder, L.I. (1986) Neurofibrillary tangles of Alzheimer disease share antigenic determinants with the axonal microtubule-associated protein tau (tau). *Proceedings of the National Academy of Sciences of the United States of America*, **83**, 4040-4043.
- Yamakawa, K., Takanashi, M., Watanabe, M., Nakamura, N., Kobayashi, T., Hasegawa, M., Mizuno, Y., Tanaka, S. & Mori, H. (2006) Pathological and biochemical studies on a case of Pick disease with severe white matter atrophy. *Neuropathology: official journal of the Japanese Society of Neuropathology*, **26**, 586-591.
- Yoshimura, T. & Rasband, M.N. (2014) Axon initial segments: diverse and dynamic neuronal compartments. *Current opinion in neurobiology*, **27**, 96-102.
- Ypsilanti, A.R., Girao da Cruz, M.T., Burgess, A. & Aubert, I. (2008) The length of hippocampal cholinergic fibers is reduced in the aging brain. *Neurobiology of aging*, **29**, 1666-1679.
- Zempel, H., Dennissen, F.J.A., Kumar, Y., Luedtke, J., Biernat, J., Mandelkow, E.M. & Mandelkow, E. (2017) Axodendritic sorting and pathological missorting of Tau are isoform-specific and determined by axon initial segment architecture. *The Journal of biological chemistry*, **292**, 12192-12207.
- Zempel, H. & Mandelkow, E. (2014) Lost after translation: missorting of Tau protein and consequences for Alzheimer disease. *Trends in neurosciences*, **37**, 721-732.
- Zempel, H., Thies, E., Mandelkow, E. & Mandelkow, E.M. (2010) Abeta oligomers cause localized Ca(2+) elevation, missorting of endogenous Tau into dendrites, Tau phosphorylation, and destruction of microtubules and spines. *The Journal of neuroscience: the official journal of the Society for Neuroscience*, **30**, 11938-11950.
- Zhang, C. & Rasband, M.N. (2016) Cytoskeletal control of axon domain assembly and function. *Current opinion in neurobiology*, **39**, 116-121.
- Zhang, L., Ravdin, L.D., Relkin, N., Zimmerman, R.D., Jordan, B., Lathan, W.E. & Ulug, A.M. (2003) Increased diffusion in the brain of professional boxers: a preclinical sign of traumatic brain injury? *AJNR. American journal of neuroradiology*, **24**, 52-57.
- Zhang, X. & Bennett, V. (1998) Restriction of 480/270-kD ankyrin(G) to axon proximal segments requires multiple ankyrin(G)-specific domains. *Journal of Cell Biology*, **142**, 1571-1581.

- Zhang, Y., Walter, R., Ng, P., Luong, P.N., Dutt, S., Heuer, H., Rojas-Rodriguez, J.C., Tsai, R., Litvan, I., Dickerson, B.C., Tartaglia, M.C., Rabinovici, G., Miller, B.L., Rosen, H.J., Schuff, N. & Boxer, A.L. (2016) Progression of Microstructural Degeneration in Progressive Supranuclear Palsy and Corticobasal Syndrome: A Longitudinal Diffusion Tensor Imaging Study. *PloS one*, **11**, e0157218.
- Zhong, G., He, J., Zhou, R., Lorenzo, D., Babcock, H.P., Bennett, V. & Zhuang, X. (2014) Developmental mechanism of the periodic membrane skeleton in axons. *eLife*, **3**.
- Zhou, D.X., Lambert, S., Malen, P.L., Carpenter, S., Boland, L.M. & Bennett, V. (1998) Ankyrin(G) is required for clustering of voltage-gated Na channels at axon initial segments and for normal action potential firing. *Journal of Cell Biology*, **143**, 1295-1304.